CHEMICAL AND PHYSICAL PROPERTIES OF COMETARY DUST

C. Engrand
IJCLab, Université Paris-Saclay/CNRS-IN2P3, 91405 Orsay Campus, France

J. Lasue
IRAP, Université de Toulouse, CNRS, CNES, 31400 Toulouse, France

D. H. Wooden
NASA Ames Research Center, MS 245-3, Moffett Field, CA 94035-0001, USA

M. E. Zolensky
NASA Johnson Space Center, ARES, X12 2010 NASA Parkway, Houston, TX 77058-3607, USA

Cometary dust particles are best preserved remnants of the matter present at the onset of the formation of the Solar System. In Space missions, telescopic observations and laboratory analyses advanced the knowledge on the properties of cometary dust. the only samples certified with a cometary origin were returned by the *Stardust* space mission from comet 81P/Wild2. The "chondritic porous" (here called "chondritic anhydrous") interplanetary dust particles (CA-IDPs) and micrometeorites (CP-MMs), and the ultracarbonaceous Antarctic MMs (UCAMMs) also show strong evidence for a cometary origin. The elemental composition of cometary dust is generally consistent with the chondritic (CI) composition, with the notable exception of elevated contents in carbon and nitrogen compared with CI. The organic matter of cometary dust is mixed with minor amounts of crystalline (at least 25% of the minerals) and amorphous mineral phases. The most abundant crystalline minerals are ferromagnesian silicates (olivine and low-Ca pyroxenes), but High-Ca pyroxenes, refractory minerals and Low Ni Fe sulfides are also present. The crystalline olivine and low-Ca pyroxene compositions can vary from their Mg-rich end-member (forsterite and enstatite) to relatively Fe-rich compositions. Refractory minerals as well as secondary minerals likeLIME (low-iron, Mn-enriched) olivines, unusual Fe sulfides or mineral aggregates of specific compositions like Kosmochloric high-Ca pyroxene and FeO-rich olivine - KOOL grains) are also found. The presence of carbonates in cometary dust is still debated, but a phyllosilicate-like phase was observed in a UCAMM. The abundance of pyroxene to olivine (in numbers) is larger than in primitive meteorites (e.g. the Px/Ol ratio is usually larger than 1). GEMS phases (glass with embedded metals and sulfides) are abundant in cometary dust, although not systematically found. Some of the organic matter present in cometary dust particle resembles the insoluble organic matter (IOM) present in primitive meteorites, but amorphous carbon and exotic (e.g. N-rich) organic phases are also present. The hydrogen isotopic composition of cometary dust particles (in the organic matter) is usually rich in deuterium, tracing a formation at very low temperatures, either in the protosolar cloud or in the outer regions of the protoplanetary disk. The presolar dust concentration in cometary dust can reach about 1%, which is the most elevated value observed in extraterrestrial samples. The size distribution of cometary dust in comet trails is well represented by a power-law distribution (differential size distribution) with a mean power index N typically ranging from -3 to -4. Polarimetric and light scattering studies of cometary dust suggest mixtures of porous agglomerates of sub-micrometer minerals with organic matter, which is compatible with the in situ analyses of 67P/Churyumov-Gerasimenko by MIDAS (Rosetta) and with the studies of it Stardust samples, CA-IDPs, CP-MMs and UCAMMs. Cometary dust particles have low tensile strength, and low density.

1. COMETARY DUST : FROM SPACE MISSIONS TO GROUND-BASED OBSERVATIONS AND TO THE LABORATORY

Space missions are very powerful in advancing the understanding of comets. However, the cost and timeline of such missions have only permitted the characterization of a limited number of comets so far. Spacecraft flybys of comet 1P/Halley by *Giotto* and *Vega-1&2* with, respectively, the PIA and PUMA 1&2 instruments, comet 81P/Wild 2 (*Stardust*), comet 9P/Tempel 1 (*Deep Impact*), comet 103P/Hartley 2 (*Deep Impact*-Extended) and the long duration rendezvous with comet 67P/Churyumov-Gerasimenko *(Rosetta)* provided key advancements in our understanding about the composition and structure of the

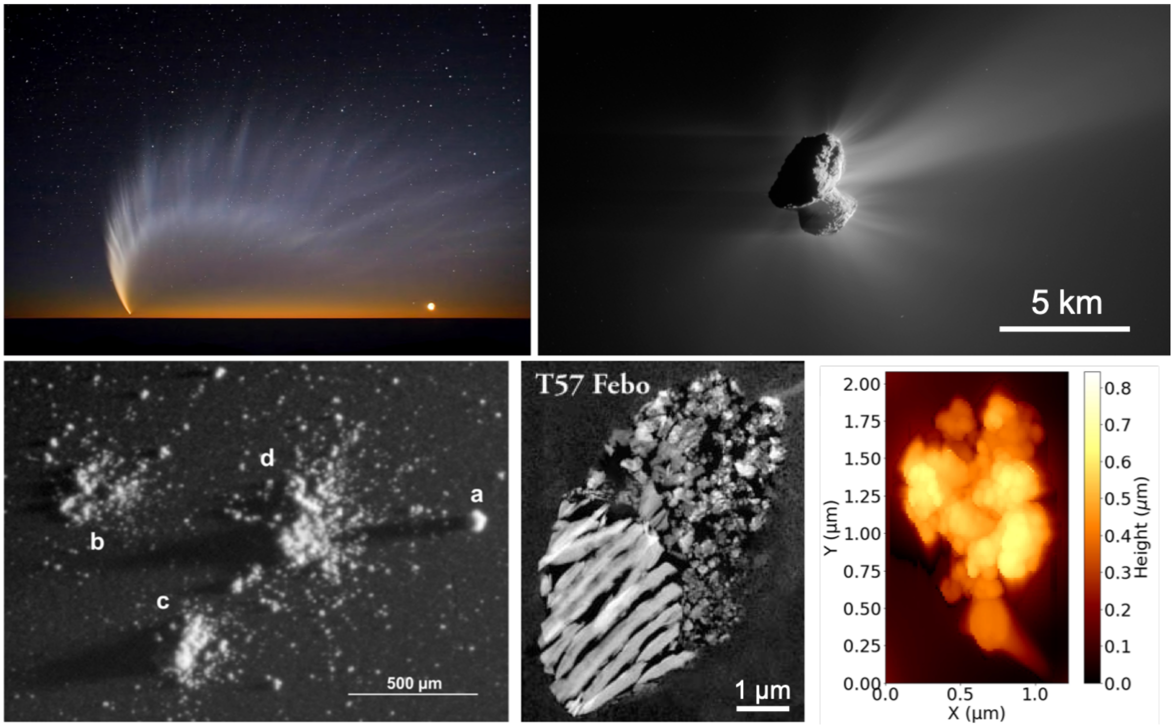

Fig. 1.— *Cometary dust seen at increasing size resolution (from top left to bottom right): Comet C/2006 P1 McNaught observed from Paranal (commons license); comet 67P/Churyumov-Gerasimenko (67P/C-G) by Rosetta (commons license), cometary dust particles of 67P/C-G collected by COSIMA (*Langevin et al. *2016), section of a Stardust particle from 81P/Wild 2 track 57 (*Matrajt et al. *2008), 67P/C-G dust particles collected by MIDAS on Rosetta (*Mannel et al. *2019).*

cometary dust particles, complementing telescopic observations and laboratory work on cometary materials captured in the stratosphere and from polar regions and those returned by the *Stardust* mission to comet 81P/Wild 2.

Ground-based and space-borne observations of comets encompass a wide range of spatial scales, spectral ranges and spectral resolutions. A small perihelion event like with comet C/2006 P1 (McNaught) (Fig. 1) can produce a spectacular release of small to large particles into the coma and dramatic comet tail structures that can be modeled to assess coma particle sizes and modulations in dust production rates.

As the decades advanced from the late 1970s, the instruments and telescopes provided increases in sensitivity and wavelength coverage that allowed multi-epoch studies in the '10 μm window' and limited studies near 20 μm from ground-based telescopes as well as uninterrupted wavelength coverage from $\sim$5–40μm from *ISO SWS*, *SOFIA*, *Spitzer*, and with the majority being single-epoch observations. The James Webb Space Telescope (*JWST*) will provide a greater span of wavelength coverage, which facilitates the simultaneous use of scattered light and thermal emission studies to characterize the dust composition and particle properties in cometary comae. Thus, the decline in the availability in mid- and far-IR instrumentation for photometric and spectroscopic studies of comets on ground-based telescopes is complimented by higher sensitivity and broader wavelength coverage airborne and space-based telescopes. Multi-epoch studies have thus far revealed that the dust composition of the coma of an individual can vary significantly with heliocentric distance, potentially due to changes in seasonal illumination that changes the 'active' areas and/or changes in jet activity. Also, the coma's dust composition can appear to change composition, i.e., increase the relative abundance of crystalline silicates because a decrease in heliocentric distance (r_h) causes increases in solar insolation whereby dust components that are less absorbing of sunlight (e.g., more transparent Mg-rich crystalline silicates that are less optically active) may warm sufficiently to gain spectral contrast with respect to more active species (e.g., amorphous carbon and Mg:Fe amorphous silicates).

NASA has been collecting Interplanetary Dust Particles (IDPs) in the stratosphere (*Warren and Zolensky* 1994), following the pioneering work of Don Brownlee (*Brownlee et al.* 1977). Several lines of evidence point to a cometary origin for chondritic anhydrous (CA) IDPs (*Bradley and Brownlee* 1986; *Bradley* 1994a; *Bradley et al.* 1999) (Fig. 2), including higher atmospheric entry velocities (as determined by noble gas measurements, (*Nier and Schlutter* 1993)), high particle porosity, high bulk carbon content (*Thomas et al.* 1993), anhydrous nature, short solar exposure histories, high presolar grain concentrations (*Rietmeijer* 1998; *Palma et al.* 2005; *Nguyen et al.* 2007; *Busemann et al.* 2009; *Brownlee et al.* 1995; *Bradley et al.* 2014). We chose here to name these IDPs "chondritic anhydrous" whereas they are usually quoted as "chondritic porous" (or "chondritic porous anhydrous") in the literature. This choice was made following the observation that many hydrous IDPs are equally porous (*Zolensky et al.* 1992) so the term 'chondritic porous' is somewhat misleading. Moreover, IDPs having a fluffy-like texture when observed as whole particles are not always showing large porosity when examined in their interior (e.g. by sectioning with ultramicrotomy). In the search for cometary IDPs, timed collections in the stratosphere were performed with the aim of collecting IDPs during dust streams of comet 26P/Grigg-Skjellerup and 21P/Giacobini-Zinner, but the expected fraction of collected particles arising from those particular sources was only a few % (*Busemann et al.* 2009; *Bastien et al.* 2013). Because of limitations of the collection technique, no particular IDP can be unambiguously identified with a specific small body, so the question of their origin(s) is not yet completely resolved. After 50 years of investigation, links between IDPs and comets remain hazy. Nevertheless, a tentative consensus has been formed that the chondritic anhydrous IDPs (CA-IDPs) probably are mainly of cometary origin. Are any of the hydrous chondritic IDPs from comets? The discovery of CAI among 81P/Wild 2 grains could suggest a cometary origin for some refractory IDPs (*Zolensky* 1987; *McKeegan* 1987), which have long been ignored. These IDPs are finer grained than typical meteoritic CAI.

Larger interplanetary dust particles called micrometeorites (MMs) have also been recovered from polar ice and snow. They were originally found by *Maurette et al.* (1986, 1987) in Greenland ice, and later collected at lower temperatures from Antarctic ice, and then snow (e.g. *Maurette et al.* 1991; *Duprat et al.* 2007; *Dobrica et al.* 2009; *Noguchi et al.* 2015). These larger particles are generally more strongly heated during atmospheric entry than IDPs and may be altered in the terrestrial environment, especially by leaching when collected from ice where they can reside for several tens of thousands of years before collection. The samples collected from snow however do not show evidence for extensive aqueous alteration (*Duprat et al.* 2007). Extraterrestrial dust particles in the size range of MMs ($\sim$ 200 μm) constitute the dominant input of extraterrestrial matter on Earth (*Love and Brownlee* 1993; *Rojas et al.* 2021), and they could have played a role in the formation of the terrestrial hydrosphere and the origin of life on Earth (e.g. *Maurette* 2006). Numerical modelling suggests that 80% of micrometeorites could originate from comets (*Carrillo-Sánchez et al.* 2016), but they probably derive from both asteroids and comets. Some MMs have been found to have identical fine-grained components to chondritic-porous IDPs (here called CA-IDPs) and, thus, these "CP-MMs" sample sources that are most likely cometary (*Noguchi et al.* 2015). Ultracarbonaceous Antarctic Micrometeorites (UCAMMs – Fig. 2) constitute a new family of micrometeorites that was recently discovered in the Concordia and Dome Fuji collections (*Nakamura et al.* 2005; *Duprat et al.* 2010; *Yabuta et al.* 2017). They are dominated by organic matter with a variable (but minor) stony component, show large anomalies of their hydrogen isotopic composition, and most probably originate from comets. They contain an unusual N-rich organic matter that could have formed by Galactic cosmic ray irradiation of N-rich ices in the outer regions of the protoplanetary disk (*Dartois et al.* 2013, 2018; *Augé et al.* 2016).

This chapter will describe the chemical and physical properties of cometary dust particles, based on the information recovered from space missions, ground based telescopic observations and analyses in the laboratory of CA-IDPs and UCAMMs.

2. CHEMICAL PROPERTIES

2.1. Elementary composition

The elementary composition of cometary dust particles can be determined from ground-based, space missions and dust samples of very probably cometary origin that are collected on Earth : the chondritic-anhydrous IDPs (CA-IDPs) (*Bradley et al.* 2014) and ultracarbonaceous Antarctic micrometeorites (UCAMMs) (*Duprat et al.* 2010).

Insight into the elemental composition of cometary dust particles was gathered so far for 4 comets visited by space missions (1P/Halley, 9P/Tempel 1, 103/Hartley 2, 67P/Churyumov-Gerasimenko), and from a comet sample return (*Stardust* mission to 81P/Wild2). For comet 1P/Halley, mass spectrometry from *Giotto*, *Vega-1* and *Vega-2*, of cometary dust impacting at high speeds ($\sim$70-75 km.s^{-1}) determined two populations : the "rocky" (elements of Mg, Fe, O, S of approximately solar composition) and the "CHON" particles with elemental abundances enhanced over CI and the Sun (*Jessberger et al.* 1986; *Jessberger* 1999). All particles were in fact, on some level, mixtures of "rocky" and "CHON" materials with about one-quarter being predominantly "rocky", one-quarter predominantly "CHON", and half being mixed with a span of 0.1–10 times CHON/rock elemental ratios (*Fomenkova et al.* 1992; *Lawler and Brownlee* 1992). The very smallest particles had the greatest C abundances (*Lawler and Brownlee* 1992). The bulk composition of Halley dust particles was chondritic within a factor of two, with the exception of carbon, nitrogen and hydrogen, which were enriched with regard to CI by a factor of 11, 8 and 4, respectively (Fig. 3).

The *Stardust Mission* flyby showed that particle streams in the coma resulted from the disintegration (called "autobrecciation") of larger particles released from the nucleus at slower speeds (*Clark et al.* 2004). *Stardust* returned samples revealed the presence of a greater fraction of 'hot inner disk materials' than assessed from Halley, including high temperature CAIs, micro-chondrules (100 μm-size) spanning Mg- to Fe-rich olivine (crystals), plagioclase, nepheline and graphitic carbon, (see section 2.2 for more detail) (*Zolensky et al.* 2006; *Nakamura et al.* 2008; *De Gregorio et al.* 2017).

The impact on comet 9P/Tempel 1, which was created by the *Deep Impact Mission*, released particles into the coma, with coma-gas-accelerated speeds of 200 m/s, that spectrally appeared to be more similar to the submicron-sized silicate-rich and crystal-rich comet Hale-Bopp. In the hours after impact and from ground-based studies of the inner coma, dust compositions varied between highly silicate- and forsterite-rich to poor relative to (what is fitted as) dark carbonaceous species (*Harker et al.* 2005, 2007; *Sugita et al.* 2005). Visible polarization studies revealed the ejection of surface dark carbonaceous particles (*Furusho et al.* 2007). Spectral studies at lower spatial resolution also revealed smaller and more crystal-rich materials were seen in the coma after impact (*Lisse et al.* 2005). The fortuitous explosive release of matter into the coma of 17P/Holmes similarly revealed smaller particles and more crystal-rich compositions that were hitherto thought to be associated with Oort cloud comets like Hale-Bopp (*Reach et al.* 2010).

The flyby over comet 103P/Hartley 2 showed that the two sources of volatile gas 'activity drivers', H_2O and CO_2, produced a different size and composition in the coma whereby, compared to the H_2O rich mid-region, the CO_2-rich end was ejecting ice chunks and organic gases and probably solid state organics (*A'Hearn et al.* 2015; *Feaga et al.* 2021).

The comet 67P/Churyumov-Gerasimenko (hereafter 67P/C-G) was studied in detail during the rendez-vous with the *Rosetta* mission, which orbited the comet from August 2014 to September 2016. The knowledge base about particle structures and compositions was considerably expanded by the *Rosetta* investigations. Cometary dust in 67P/C-G coma consists mainly of mm-size and slow-moving (few km.s^{-1} *Rotundi et al.* (2015)) hierarchical aggregates (*Mannel et al.* 2019) that collapsed to various degrees upon collection (*Langevin et al.* 2016; *Lasue et al.* 2019) (see also section 3.3). The dust mass analyser COSIMA (*Kissel et al.* 2007) collected more than 35,000 particles (*Merouane et al.* 2016), and about 250 of them were analyzed. The composition of $\sim$ 30 particles of these particles was quantified and showed that dust was composed of stony material mixed with a high molecular weight solid state organic (45% by mass) (*Bardyn et al.* 2017; *Fray et al.* 2016). The bulk composition of 67P/C-G dust particles is rather chondritic, except for higher content of C and possibly N (Fig. 3). A carbon to silicon atomic ratio $C/Si = 5.5^{+1.4}_{-1.2}$ was measured in 67P/C-G dust particles (*Bardyn et al.* 2017) (Fig. 4). This value is about one order of magnitude larger than the CI value (0.76 ± 0.10), and close to the protosolar value $(7.19 \pm 0.83$, *Lodders* (2010)). The H/C ratio is 1.04 ± 0.16, which is higher than in IOM extracted from the most primitive meteorites (*Isnard et al.* 2019). The average nitrogen to carbon ratio of 67P/C-G dust particles is $N/C = 0.035 \pm 0.011$ (*Fray et al.* 2017). This value is in turn compatible with the chondritic value $(N/C = 0.04)$ (*Alexander et al.* 2017), but about one order of magnitude lower than the protosolar value $(N/C = 0.3 \pm 0.1$, *Lodders* (2010)). The discovery of ammonium salts in 67P/C-G could account for this missing nitrogen reservoir (*Altwegg et al.* 2020; *Poch et al.* 2020), as these salts would have sublimated before analysis in COSIMA. Phosphorus and fluorine were detected by COSIMA in the dust particles (*Gardner et al.* 2020).

The composition of cometary dust in comet 81P/Wild 2 was measured in samples returned by the *Stardust* mission (*Brownlee et al.* 2006; *Hörz et al.* 2006). Because of the high speed collection of the samples, the light elements could not be quantified, and volatile elements like S probably were redistributed around the tracks (*Ishii et al.* 2008). Other elements show a chondritic composition within a factor of two (*Flynn et al.* 2006; *Ishii et al.* 2008; *Lanzirotti et al.* 2008; *Leroux et al.* 2008; *Stephan* 2008; *Stephan et al.* 2008). The bulk composition of cometary dust as discussed here is displayed in Fig. 3, with the abundances normalized to Fe and to CI. This kind of representation allows comparison with reference values, but should be taken with a hint of caution, as apparent enrichment/depletions could depend on the normalizing element (Fe was chosen here). Na and Si seem systematically enriched in cometary dust. The Na enrichment was indeed used as a tracer in COSIMA elementary maps to pinpoint the location of the dust particles, and was observed during the entry of comet C/2013 A1 (Siding Spring) in the Martian atmosphere (*Benna et al.* 2015).

The composition of CA-IDPs was measured for 24 IDPs (*Thomas et al.* 1993; *Keller et al.* 2004) for all elements displayed in Fig. 3, except for N, K, and Ti. These IDPs show a fairly chondritic composition, with an enrichment in C of about 7 times the CI value, which seems correlated with a mineralogy dominated by pyroxenes (*Thomas et al.* 1993) (see also section 2.4.3). The composition of 10 UCAMMs was measured by electron microprobe and show large ranges of variations, as seen in Fig. 3. Within this large variation range, the compositions are compatible with CI, except for C and N which are markedly enriched in UCAMMs with regard to the CI composition.

Figure 4 displays the C/Si atomic ratio in different kinds of Solar System material, ordered by increasing values. We can note that data available for cometary dust and CA-IDPs are compatible with that of the Sun and of ISM dust. Objects formed in the inner Solar System show lower values than the Sun as noted by *Bergin et al.* (2015). The C/Si atomic ratio of UCAMMs is very high, even higher than that of ISM dust, suggesting a local accumulation process of organics with regard to minerals in the formation regions of UCAMMs (e.g. *Dartois et al.* 2018).

2.2. Organics

Cometary dust particles are rich in organic matter. These organics are present both as volatile compounds mixed with the host ice phase of the dust particles, and as solid organic matter in the dust particles themselves. The organics that are present in the dust particles remain solid when the comet approaches the Sun, and are thus quoted as "refractory" organic matter. They can only be studied in samples in the laboratory, or by in situ analyses.

The volatile organic compounds that have been identi-

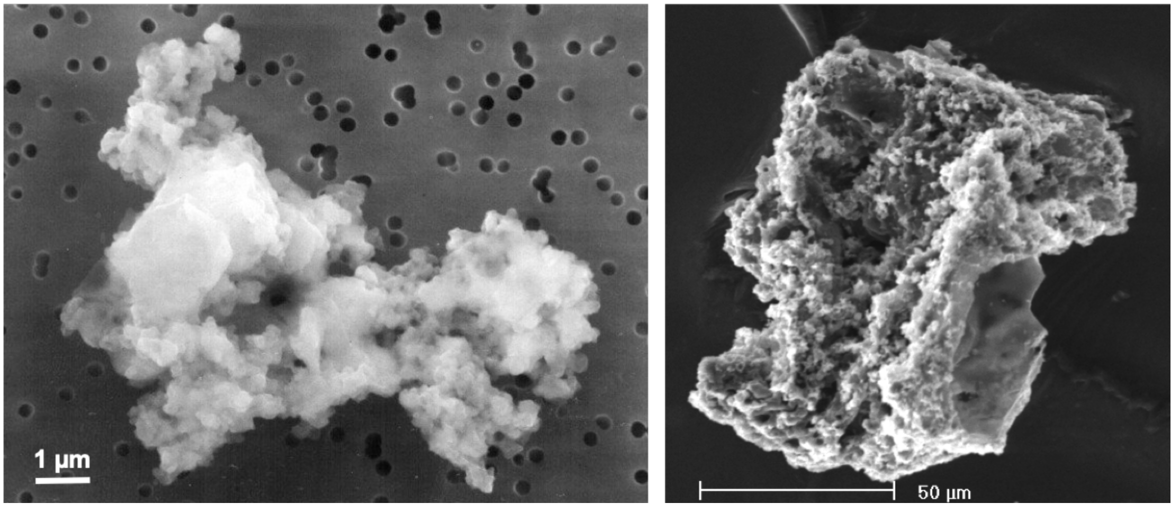

Fig. 2.— *Secondary electron images of dust collected on Earth with a probable cometary origin: a) chondritic anhydrous interplanetary dust particle (CA-IDP) collected in the stratosphere by NASA; b) ultracarbonaceous Antarctic Micrometeorites (UCAMM) from the Concordia collection (*Duprat et al. *2007;* Duprat et al. *2010).*

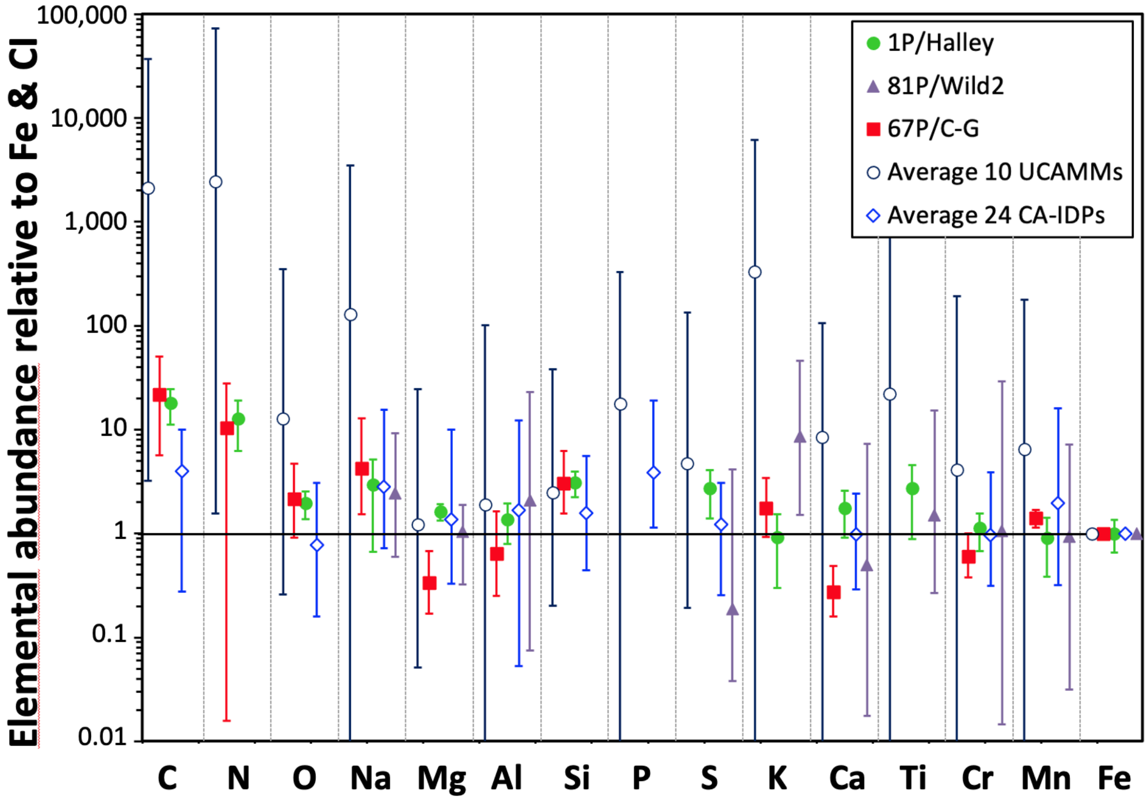

Fig. 3.— *Average elemental ratios relative to Fe and to CI (*Lodders *2010) for dust particles from comets 1P/Halley (*Jessberger et al. *1988), 81P/Wild 2 in aerogel (*Flynn et al. *2006;* Ishii et al. *2008;* Lanzirotti et al. *2008;* Leroux et al. *2008;* Stephan *2008;* Stephan et al. *2008), 67P/Churyumov-Gerasimenko (67P/C-G) (*Bardyn et al. *2017), for 10 ultracarbonaceous Antarctic micrometeorites (UCAMMs) (*Dartois et al. *2018, and unpublished data) and for 24 chondritic anhydrous IDPs (CA-IDPs) (*Thomas et al. *1993;* Keller et al. *2004). Error bars represent the variation of the elemental compositions for the different families of cometary dust particles.*

fied so far in cometary dust particles are associated with ice that sublimates when the comet approached the Sun. The best constraint on their composition was gathered during the *Rosetta* mission around comet 67P/Churyumov-Gerasimenko. They consist mainly in CH(N)O-bearing molecules, with a great variety of CH-, CHN-, CHS-, CHO_2- and CHNO-bearing species, both saturated and unsaturated, and the possible presence of toluene (*Altwegg*

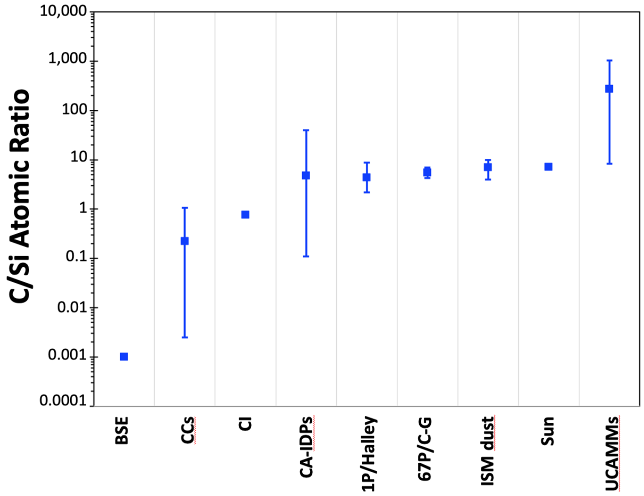

Fig. 4.— *Atomic C/Si ratios for bulk silicate Earth (BSE) (*Bergin et al. *2015), carbonaceous chondrites (CCs) (*Jarosewich *1990), the CI value (*Lodders *2010), the average of 24 CA-IDPs (*Matrajt et al. *2005;* Thomas et al. *1993), comet 1P/Halley (*Jessberger et al. *1988), comet 67P/Churyumov-Gerasimenko (67P/C-G) (*Bardyn et al. *2017), ISM dust (e.g.* Dartois et al. *2018), the Sun (*Lodders *2010) and the average of 10 UCAMMs (*Dartois et al. *2018, and unpublished data).*

et al. 2017). Glycine was identified in the gas phase, with a distribution compatible with the sublimation of ices associated with the cometary dust particles, rather than a direct sublimation of ices from the nucleus (*Altwegg et al.* 2016; *Hadraoui et al.* 2019, 2021). Glycine had also been identified at the surface of Al foil exposed to the coma of 81P/Wild 2 (*Elsila et al.* 2009).

The "refractory" organic matter was identified as being present in comet 1P/Halley, but its nature could not be studied by the *Giotto* and *Vega* mass spectrometers. Spectral evidence for aromatic organic molecules, i.e., PAHs were suggested from UV spectral analyses of comet 1P/Halley (*Moreels et al.* 1994; *Clairemidi et al.* 2008). The very smallest particles had the greatest C abundances (*Lawler and Brownlee* 1992). CHON particles had a range of H, O, and N ratios to C (*Fomenkova et al.* 1992, 1994).

The high speed collection of 81P/Wild 2 cometary dust did not allow a good preservation of the organics (*Brownlee* 2014; *Keller et al.* 2006; *Sandford et al.* 2010). However, some organic matter, including clumps that were 'behind' terminal particles, and therefore somewhat protected from the heat generated by impact during collection, revealed a suite of complex organic bonds including mainly alkenes, aromatic C=C and carboxyl C=O as well as a variety of textures for the organic matter including organic nanoglobules (Fig. 5) (*Matrajt et al.* 2012; *De Gregorio et al.* 2011; *De Gregorio et al.* 2017). The spectral signature of preserved organic matter in *Stardust* samples show similarities with that of insoluble organic matter extracted from meteorites (*De Gregorio et al.* 2011), although a reduced form of carbon as also observed in one *Stardust* sample (*De Gregorio et al.* 2017). The concentration of carbon could not be quantified in 81P/Wild 2 samples due to the collection method in aerogel. The low concentration observed in the samples is interpreted as a consequence of the harsh collection of the samples. It could also represent a collection bias of dust from a portion of the coma which was poor in carbon and not representative of the whole comet (*Westphal et al.* 2017).

The solid organic matter identified in 67P/C-G dust particle also shows similarities with insoluble organic matter extracted from meteorites, although with a higher atomic H/C ratio (1.04 ± 0.16), which suggests less processing and a more primitive origin of the organics present in 67P/C-G (*Fray et al.* 2016, 2017; *Isnard et al.* 2019). The atomic O/C ratio in 67P/C-G is likely higher than in meteoritic IOM (*Bardyn et al.* 2017). The abundance of organic matter in 67P/C-G dust particles was estimated at 45wt%, a value which is compatible with that deduced from the density measurement of the particles by *Fulle et al.* (2016b) of $52 \pm 8\%$ in volume of organic matter. This solid state organic matter is reminiscent of "CHON" in Halley but the techniques available for analyses better reveal the complexity and details of this organic matter. The ROSINA gas mass spectrometer revealed a huge host of complex molecules, including many S species, through the fortuitous impact with a dust particle that occurred during a close flyby of the nucleus (*Altwegg et al.* 2017). Glycine, methylamine and ethylamine, as well as phosphorus, were detected by ROSINA in the gas phase in 67P/C-G (*Altwegg et al.* 2016). The observations of glycine in the coma can be explained by the presence of this amino acid in sublimating water ice in the dust particles (*Hadraoui et al.* 2019, 2021).

Reflectance spectra of the surface of 67P/C-G also suggest a high abundance of organic matter in the surface material, with a darkening material that could be submicrometer sized Fe sulfides (*Quirico et al.* 2016; *Rousseau et al.* 2018; *Capaccioni et al.* 2015).

CA-IDPs, CP-MMs and UCAMMs are enriched in organic matter compared to primitive meteorites. Organic matter in CA-IDPs was studied by Fourier transform infrared microscopy (μFTIR) (*Flynn et al.* 2003; *Keller et al.* 2004; *Matrajt et al.* 2005; *Muñoz Caro et al.* 2006; *Merouane et al.* 2014) and electron energy loss spectroscopy (EELS) (*Flynn et al.* 2003; *Keller et al.* 2004). The organic content of CP-MMs was studied by TEM/EELS, and show the presence of carbonaceous nanoglobules (*Noguchi et al.* 2015). The organic matter of UCAMMs was studied by μFTIR, Raman microscopy and X-Ray absorption microspecroscopy (STXM-XANES). Carbonaceous materials in CA-IDPs range from hydrocarbon nanoglobules (*Wirick et al.* 2009) to completely graphitized carbon (*De Gregorio et al.* 2017), which have been used as thermometers (*Matrajt et al.* 2013). 100 nm-thick coatings of organics observed on some anhydrous crystals and GEMS are proposed to have facilitated grain aggregation (*Flynn et al.* 2003). Figure 5 displays the μFTIR signature of organic matter in a CA-IDP after HF treatment (Fig. 5c) and in UCAMMs without any chemical treatment (Fig. 5b). The signature of the organics in CA-IDPs shows a large abundance of polyaromatic organic matter, with aromatic carbon, ketone (C=O), carbonxyly groups (COOH) and aliphatic C-H contributions. The signature of organic matter in UCAMMs is unusual, with large amounts of N-bearing species (including nitrile), and low signature of C=O and aliphatic C-H (*Dartois et al.* 2013, 2018). STXM-XANES analyses of UCAMMs show that the organics in UCAMM consist in fact of three distinct organic phases, with different spectroscopic signatures and different amount of nitrogen (*Engrand et al.* 2015; *Charon et al.* 2017; *Guérin et al.* 2020; *Dartois et al.* 2018). The first organic phase of UCAMMs is smooth and N-rich, with N/C atomic ratios up to 0.2. This phase has no equivalent in meteorites. The other two organic phases identified in UCAMMs bear similarities with that of chondritic IOM. A carbon-rich clast identified as a cometary xenolith in the LaPaz Icefield 02342 meteorite also shows spectroscopic similarities with meteoritic IOM (*Nittler et al.* 2019). The CH_2/CH_3 ratios measured by µFTIR in aliphatic C-H in CA-IDPs (*Flynn et al.* 2003; *Keller et al.* 2004; *Matrajt et al.* 2005; *Muñoz Caro et al.* 2006; *Merouane et al.* 2014) and in UCAMMs (*Dartois et al.* 2013, 2018) are higher than the value measured in dust from the diffuse interstellar medium, which is around 1 (*Dartois et al.* 2007).

The Raman signature of OM in CA-IDPs, CP-MMs and UCAMMs confirm the polyaromatic nature of the solid organics in these particles, and the low thermal metamorphic grade of their organic matter (*Quirico et al.* 2005; *Bonal et al.* 2006; *Busemann et al.* 2007; *Busemann et al.* 2009; *Brunetto et al.* 2011; *Noguchi et al.* 2015; *Dobrică et al.* 2011; *Dartois et al.* 2013, 2018; *Starkey et al.* 2013). The potential effect of atmospheric entry heating on the degree of disorder of the organic matter cannot be ruled out, but specific experiments would be needed to study these effects in detail.

Organic nanoglobules seem to be ubiquitous in samples of cometary origin. They are found in 81P/Wild 2 samples (*Matrajt et al.* 2008; *De Gregorio et al.* 2010), CA-IDPs (*Matrajt et al.* 2012), CP-MMs (*Noguchi et al.* 2015), and UCAMMs (*Charon et al.* 2017) (and also in chondritic AMMs (*Maurette et al.* 1995), for which models predict a cometary origin for 80% of them (*Carrillo-Sánchez et al.* 2016)).

2.3. Isotopes

The *Giotto* and *Vega* missions during a flyby around comet 1P/Halley led to the rough measurement of carbon isotopes in cometary dust, but most of the data on the isotopic compositions of cometary dust particles were gathered from laboratory analyses of returned cometary samples (*Stardust* mission – 81P/Wild 2 comet), from in-situ analyses (*Rosetta* mission on 67P/Churyumov-Gerasimenko – 67P/C-G) or from the analysis of CA-IDPs, CP-MMs and UCAMMs.

2.3.1. Hydrogen, carbon, nitrogen and sulfur isotopes

The *Giotto* and *Vega* missions to comet Halley allowed the discovery of isotopically light carbon in the dust particles ($^{12}C/^{13}C \sim 5000$), providing a possible link to presolar graphite (*Amari et al.* 1993) or SiC grains, for which a few such light values have been measured (*Hoppe et al.* 2000; *Lin et al.* 2002; *Nittler and Alexander* 2003). The H isotopic composition of cometary dust particles is displayed in Fig. 6. The D/H ratio of samples from comet 81P/Wild 2 (*Stardust* mission) were measured by secondary ion mass spectrometry (*McKeegan et al.* 2006; *De Gregorio et al.* 2010, 2011; *Matrajt et al.* 2008; *Stadermann et al.* 2008). The bulk D/H isotopic ratios of *Stardust* samples vary from the terrestrial D/H value (V-SMOW) of 1.5576×10^{-4} to sub-µm sized hotspots that can reach values up to $\delta D \sim$ 2000 permil, which corresponds to three times V-SMOW. The hydrogen isotopic composition was also measured in dust particles from comet 67P/C-G by COSIMA. The average value measured in the organic matter of 25 cometary particles from 67P/C-G is D/H = $(1.57 \pm 0.54) \times 10^{-3}$ (*Paquette et al.* 2021), which is about one order of magnitude larger than the terrestrial value. The hydrogen isotopic composition of CA-IDPs varies between D/H 10^{-4} and D/H $\sim 4 \times 10^{-3}$ (*Aleon et al.* 2001; *Busemann et al.* 2009; *McKeegan et al.* 1985; *Zinner et al.* 1983). The bulk D/H value measured for eight UCAMMs vary between $\sim 3 \times 10^{-4}$ to 1.5×10^{-3}, with µm-sized regions that reach up to 30 times the terrestrial value (*Duprat et al.* 2010; *Rojas et al.* 2022).

The C isotopic composition of comet Wild2 dust particles in *Stardust* samples varies between $\delta^{13}C \sim$ -20 and $\sim$ -50 permil (*McKeegan et al.* 2006), which are values compatible with that observed in carbonaceous chondrites (*Alexander et al.* 2007) and CA-IDPs (*Messenger et al.* 2003). This value is slightly higher than the solar value determined by the Genesis mission at d $\delta^{13}C = -105 \pm 20$ permil (*Hashizume et al.* 2004). The bulk carbon isotopic composition was measured in three UCAMMs, and vary from 25 permil to $\sim$ -85 permil. A noticeably low isotopic composition at $\sim$ -120 permil is found as a “cold spot” in one UCAMM (*Rojas et al.* 2022).

The nitrogen isotopic composition of *Stardust* samples shows moderately elevated values, with hotspots of submicrometric sizes reaching values up to $\sim$ 500 permil (*McKeegan et al.* 2006), which are compatible with values measured in CA-IDPs (*Messenger et al.* 2003; *Aleon et al.* 2003; *Busemann et al.* 2009). The bulk nitrogen isotopic composition in five UCAMMs vary from $\sim$ -130 permil to $\sim$ 270 permil (*Rojas et al.* 2022) Fig. 7. In most cases, there is no correlation between the nitrogen and hydrogen isotopic compositions.

The sulfur isotopic composition measured in comet 81P/Wild 2 samples is compatible with the solar value, showing an extraterrestrial origin of the impact residue and of the sulfide measured (*Heck et al.* 2012; *Ogliore et al.* 2012a). The sulfur isotopic composition of a cosmic symplectite was analysed in *Stardust* samples, which showed

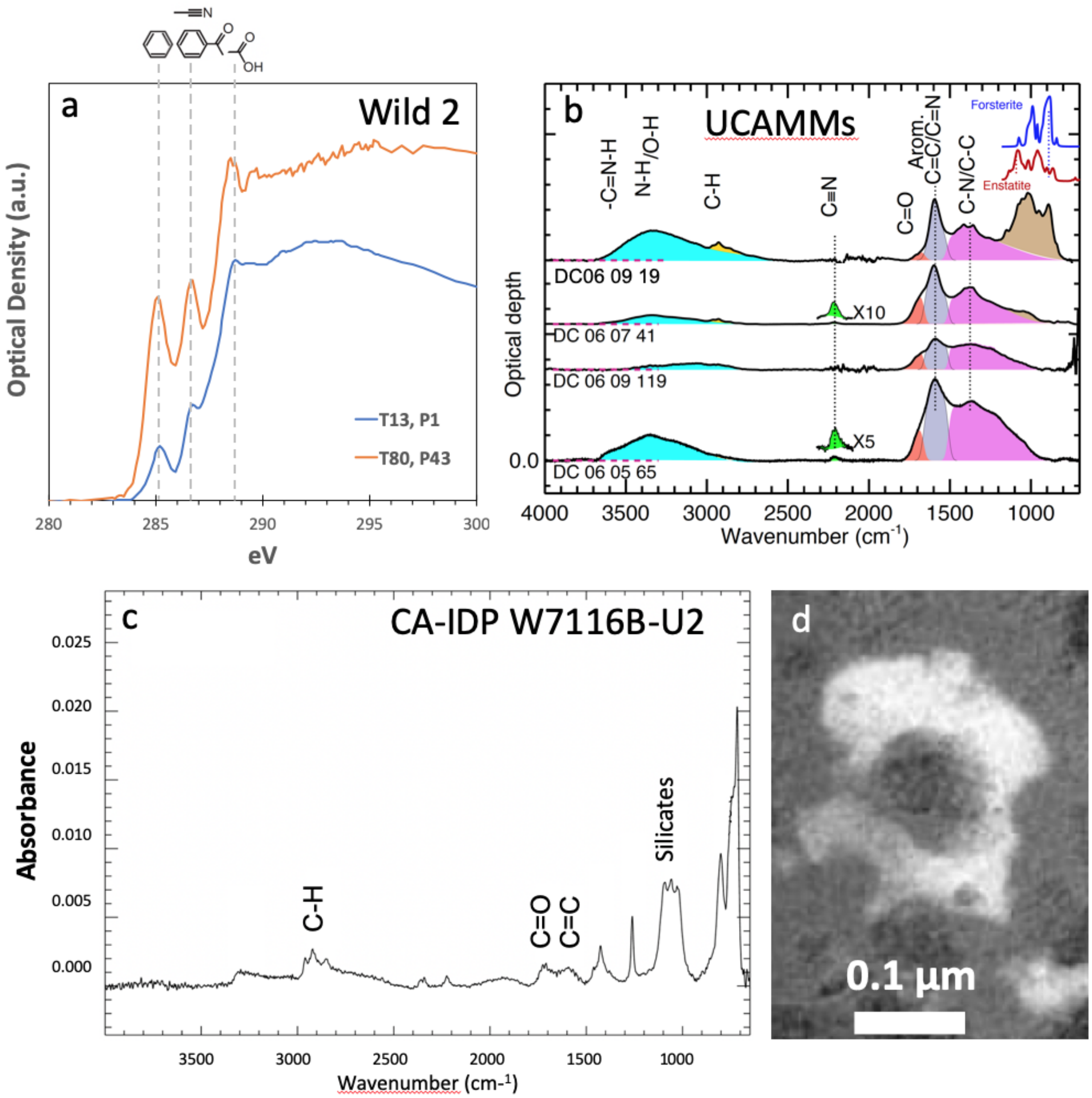

Fig. 5.— *(a) Spectral absorption signatures of organic matter in comet 81P/Wild 2 samples at the carbon K-edge in STXM-XANES (adapted from* De Gregorio et al. *(2011)); (b) µFTIR spectra of 4 representative UCAMMs (*Dartois et al. *2018); (c) µFTIR spectrum of a chondritic anhydrous IDP (*Matrajt et al. *2005). (d) Energy filtered image at the carbon edge of a nanoglobule in comet 81P/Wild 2 samples obtained by transmission electron microscopy (*Matrajt et al. *2008).*

enrichment in ^{33}S (*Nguyen et al.* 2017). This composition could result from photochemical irradiation of solar nebular gas. The sulfur isotopic composition (^{34}S and ^{32}S) of 67P/C-G dust was measured during the *Rosetta* mission by COSIMA, and is compatible with the reference value (*Paquette et al.* 2017). Due to mass interferences, the ^{33}S isotope could not be quantified, so a potential ^{33}S excess could not be ruled-out for 67P/C-G dust particles.

2.3.2. O, Si isotopes

The oxygen isotopic composition in extraterrestrial matter is used as a taxonomic tool, as most meteorite classes own a given (range of) oxygen isotopic composition(s). The oxygen isotopic composition of *Stardust* samples plot on a slope 1 line and show values which are compatible with carbonaceous chondrite signatures, including ^{16}O enrichments for refractory minerals identified in the Wild2 samples (*Nakamura et al.* 2008; *Nakashima et al.* 2012a; *Joswiak et al.* 2014; *Ogliore et al.* 2015; *Defouilloy et al.* 2017; *Zhang et al.* 2021). The oxygen isotopic composition of 81P/Wild 2 samples show a correlation between Δ^{17}O and the Mg content of the analyzed minerals, as in CR chondrites (e.g. *Nakashima et al.* 2012a; *Zhang et al.* 2021, and references therein).

The ^{18}O/^{16}O isotopic ratio could be measured by COSIMA in 67P/C-G dust particles, at ^{18}O/^{16}O = 2.00 × $10^{-3} \pm 1.2 \times 10^{-4}$ (*Paquette et al.* 2018). Given the large error bar associated to this value (due to limitations of measuring isotopic compositions with a ToF-SIMS method), this value is compatible with the terrestrial V-SMOW value, and covers the whole range of values found in meteorites. The oxygen isotopic composition of CA-IDPs is compatible with that of 81P/Wild2 samples (*McKeegan* 1987; *Aléon et al.* 2009; *Nakashima et al.* 2012b; *Zhang et al.* 2021).

The silicon isotopic composition of dust at comet 67P/C-G could be measured by the ROSINA instrument (*Rubin, M. et al.* 2017) and showed a depletion of heavy silicon isotopes ^{29}Si and ^{30}Si compared to the solar value. Such depletions in heavy isotopes are rare, and only found in rare presolar grains identified in meteorites (*Hynes and Gyngard* 2009).

2.3.3. Mg isotopes – ^{26}Al

The magnesium isotopic composition of 81P/Wild2 samples was measured to search for the past presence of ^{26}Al at the time of mineral formation in comet Wild2. No resolvable ^{26}Mg excess resulting from the decay of ^{26}Al was found in Wild2 samples, suggesting a late formation (a few Myr after CAI formation) of minerals in Wild 2 (*Matzel et al.* 2010; *Nakashima et al.* 2015).

The magnesium isotopic composition measured in olivines from *Stardust* samples shows small variations in δ^{26}Mg and δ^{25}Mg values that are compatible with small mass-dependent fractionation from a chondritic reservoir with respect to the Mg isotopes (*Fukuda et al.* 2021).

2.3.4. Presolar grains

Presolar grains are found in minute amounts in interplanetary material. They are grains that were present in the molecular cloud that led to the formation of the solar system and survived in the extraterrestrial samples that can be analyzed in the laboratory. At this time, we can only identify the isotopically anomalous stardust grains that were synthesized in previous generations of stars and got incorporated in the protosolar molecular cloud (*Hynes and Gyngard* 2009; *Stephan et al.* 2020). Stricto sensu, grains that formed in the protosolar molecular cloud before the birth of the Sun are also "presolar", but cannot be identified by isotopic methods, as they carry the solar signature of the initial cloud.

In the recovered samples, the most abundant identified presolar grains are silicates (up to 500 ppm), whereas SiC and graphite were historically the first ones to be identified in the acid residue extracted from meteorites.

As they formed far from the Sun at cold temperatures, comets are expected to have preserved a large abundance of presolar grains. After correction for possible partial destruction during the harsh collection conditions of Wild2 samples, isotopically anomalous grains remain rare among analyzed Wild 2 materials, occurring at initial abundances of $\sim$700 ppm (*Nguyen et al.* 2020; *Stadermann et al.* 2008; *Floss et al.* 2013).

Presolar grains are also found in CA-IDPs and UCAMMs in abundances that can reach up to about 1% (*Busemann et al.* 2009; *Floss et al.* 2012; *Floss and Haenecour* 2016).

2.4. Mineralogy

2.4.1. Comets 1P/Halley and 67P/C-G : hints at their mineralogy

In comet 1P/Halley, the "rocky" particles had a wider range of Mg/Fe but with a narrower range of Mg/Si with similarities to Mg-rich silicates (40%–60% by number of particles), specifically Mg-rich pyroxenes, iron(+nickel) sulfides, with little Fe metal, and $<$1% Fe-oxides (*Schulze et al.* 1997). CAI-like materials were not found in Halley. Few particles could be directly traced to pure mineral grains although the 11.2 μm spectral feature of forsterite was first identified in Halley (*Bregman et al.* 1987; *Campins and Ryan* 1989).

There was no instrument on *Rosetta* that allowed unambiguous identification of minerals in dust from 67P/C-G. The very low reflectance of the nucleus surface suggest the present of opaque minerals, that could be Fe sulfides (*Quirico et al.* 2016; *Rousseau et al.* 2018; *Capaccioni et al.* 2015). The bulk composition and density of 67P/C-G dust particles are also compatible with the presence of silicates, Fe-sulfides and carbon (*Bardyn et al.* 2017; *Fulle et al.* 2016a).

2.4.2. 81P/Wild 2 Mineralogy

To date the only samples that are unambiguously derived from a comet are the 81P/Wild 2 coma dust grains collected by the *Stardust* spacecraft, returned to Earth in 2006. Well-preserved coma grains from comet 81P/Wild 2 are dominated by the coarsest components. Fine-grained materials, representing perhaps 90% of the impacting cometary coma grains, were severely altered or vaporized during high speed (6.1 $km\ sec^{-1}$) capture in the aerogel capture media (*Brownlee et al.* 2006). Fine-grained material was only preserved in a minority of cases, but probably sufficiently well to permit elucidation of its general nature (*Ishii et al.* 2008). It is also possible that the apparent lack of fine-grained amorphous solids could be an artifact of this collection bias. GEMS, frequently abundant in chondritic anhydrous IDPs (*Bradley* 1994a), have not been reliably identified among *Stardust* materials (although there are unverified reports by *Gainsforth et al.* (2016), possibly also due to destruction during collection and compositional and structural similarities to melted silica aerogel.

As expected, in the *Stardust* samples the coarse-grained mineral phases are dominated by olivine, pyroxene and sulfides. The compositions are distinct from meteorites (*Joswiak et al.* 2012; *Frank et al.* 2014; *Joswiak et al.* 2017). Olivines exhibit practically the entire range from forsterite to fayalite, with no significant compositional peak. Some terminal olivines are thought to be "micro chondrules" by their similarity to type II (Fe$>$10%) chondrules in primitive chondrites such as CRs and CMs (*Frank et al.* 2014; *Wooden et al.* 2017). The minor element compositions of *Stardust* olivines link only a subset to LIME olivine

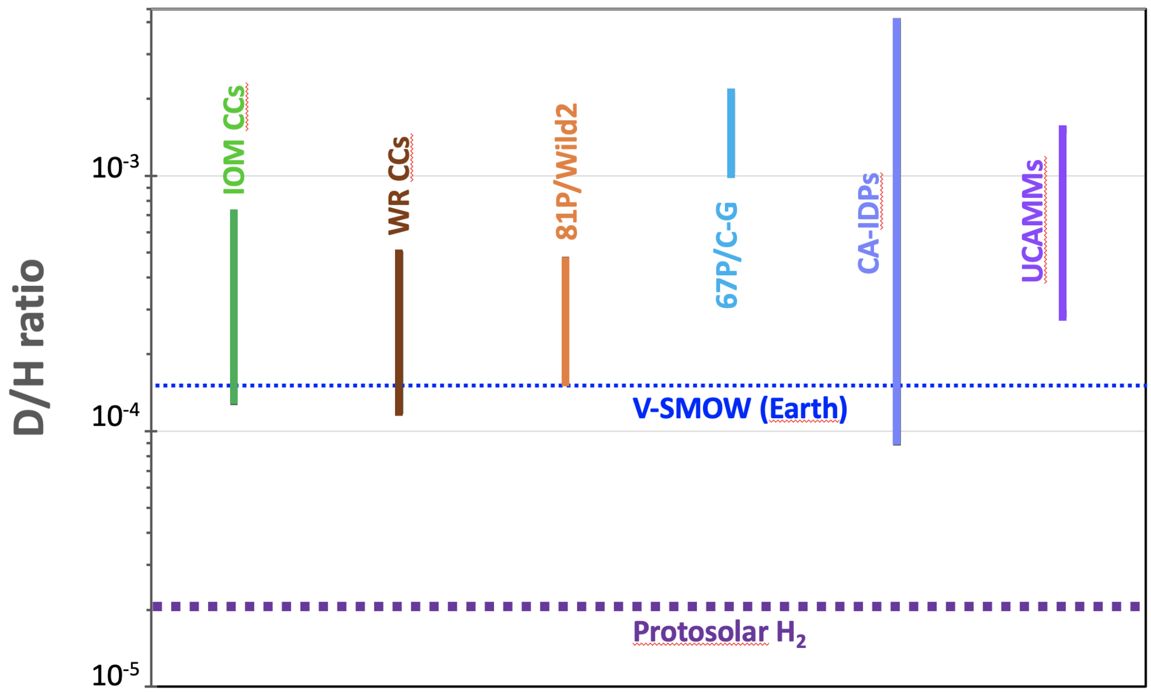

Fig. 6.— *D/H ratio measured in solid phase in cometary dust particles measured in the Stardust samples (81P/Wild 2), in refractory organics by the Rosetta/COSIMA instrument (67P/Churyumov-Gerasimenko– 67P/C-G), in chondritic anhydrous IDPs (CA-IDPs) and UCAMMs. The range of composition of D/H ratios measured in insoluble organic matter extracted from carbonaceous chondrites (IOM CCs) and in whole-rock carbonaceous chondrites (WR CCs), as well as the terrestrial value (V-SMOW, in water) and protosolar value (in H2) are also shown for reference. Data from* Alexander et al. *(2007);* Alexander et al. *(2012);* McKeegan et al. *(2006);* Paquette et al. *(2021);* Zinner et al. *(1983);* McKeegan et al. *(1985);* Messenger *(2000);* Aleon et al. *(2001);* Busemann et al. *(2009);* Duprat et al. *(2010);* Rojas et al. *(2022);* Geiss and Gloeckler *(1998).*

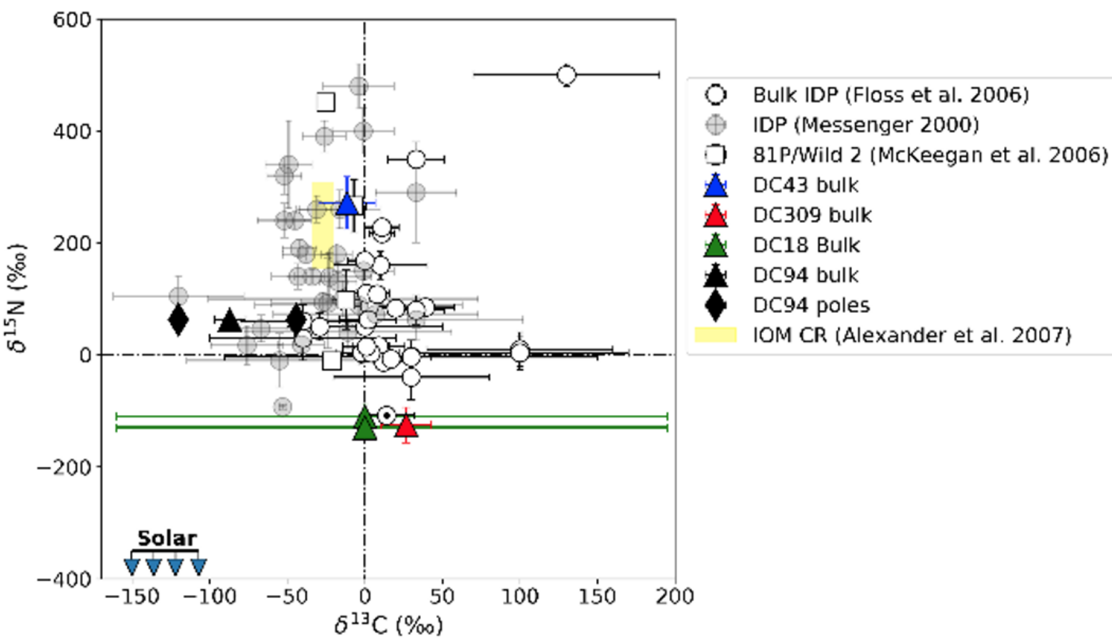

Fig. 7.— *Nitrogen and carbon isotopic compositions of IDPs, 91P/Wild2 samples, UCAMMs (DC43, DC309, DC18, DC94) and IOM extracted from CR chondrites (from* Rojas et al. *(2022))*

(condensates) (*Joswiak et al.* 2017). One *Stardust* micro-chondrule 'Iris' reveals its rapid cooling at high oxygen fugacity and high Na enrichment in the gas phase (*Gainsforth et al.* 2010). The lack of a pronounced compositional peak at forsterite was very unexpected, as this is a hallmark of chondritic IDPs (*Rietmeijer* 1998) and the least equilibrated carbonaceous chondrites (*Frank et al.* 2014). In terms of the olivine and pyroxene compositions, the closest meteoritic analogues are the unequilibrated ordinary chondrites (*Frank et al.* 2014). The high abundance of relatively coarse-grained (>30 μm size) (*Frank et al.* 2014; *Wozniakiewicz et al.* 2015), well-crystalline ferromagnesian silicates, as opposed to amorphous silicates, was also unexpected, given laboratory analogue experiments and interstellar dust spectroscopic studies.

Refractory minerals found in meteoritic calcium aluminium rich inclusions (CAIs) were identified in Wild 2 samples, which contain olivines, pyroxenes, sulfides, and refractory oxides. Mineral assemblages, mineral chemistries and measured bulk particle compositions reveal that these grains are similar to refractory materials in chondrites, with mineral chemistries most similar to CAI from CR2 and CH2 chondrites (*Zolensky et al.* 2006; *Simon et al.* 2008; *Chi et al.* 2009) and Al-rich chondrules (*Bridges et al.* 2012; *Joswiak et al.* 2014).

Chondrule fragments were also found in Wild 2. They are similar to chondrules found in carbonaceous chondrites, but with interesting differences. Few type I chondrules (FeO- and volatile-poor) have been found from Wild 2, though these are the most abundant type in meteorites. To date mainly FeO-, MnO-, volatile-rich type II chondrules have been identified from Wild 2 (*Nakamura et al.* 2008; *Matzel et al.* 2010; *Joswiak et al.* 2012; *Ogliore et al.* 2012b; *Frank et al.* 2014; *Gainsforth et al.* 2015). One Al-rich, ^{16}O rich chondrule fragment has also been identified from Wild 2, as found in carbonaceous chondrites ((*Bridges et al.* 2012).

Minor element compositions of Wild 2 olivine and pyroxenes, particularly Cr and Mn, suggest that Wild 2 experienced mild secondary thermal metamorphism (*Frank et al.* 2014), to approximately 400°C. Some Wild 2 olivines and pyroxenes show compositional similarities to those in L/LL, CH, and aubrite meteorites (Frank et al., submitted). In addition to diverse nebular components associated with multiple chondrite types, Wild 2 apparently incorporated materials that were liberated from evolved, internally heated asteroids.

A mineral assemblage unique to Wild 2 consists of FeO-rich olivines and Na- and Cr-rich clinopyroxenes (typically augites), sometimes with poorly crystallized albite or albitic glass with spinel (*Joswiak et al.* 2009). These assemblages have been named "KOOL" (Kosmochloric high-Ca pyroxene and FeO-rich olivine) grains and are observed in more than half of all *Stardust* tracks. KOOL grains are also observed in CA-IDPs and CP-MMs. The textures and mineral assemblages of KOOL grains are suggestive of formation at relatively high temperatures by igneous or metamorphic processes (its unclear which) and may have formed under relatively high f_{O_2} conditions. KOOL grains have not been observed in chondrites, however the oxygen isotopic composition of a single Wild 2 KOOL grain is similar to some type II (FeO-rich) chondrule olivines from OC, R, and CR chondrites (*Kita et al.* 2011; *Isa et al.* 2011). One type II microchondrule in Wild 2 shows kosmochloric enhancement possibly reinforcing the link between KOOL grains and chondrule forming processes (*Gainsforth et al.* 2015). KOOL grains may represent an important precursor material for FeO-rich chondrules. While no large carbonate grains have been identified among Wild 2 samples, submicron carbonate grains have been reported (*Flynn et al.* 2009), including Mg-Fe-carbonates associated with amorphous silica and iron sulfides (*Mikouchi et al.* 2007). The observation is interesting because carbonates are typically products of aqueous processes. While Ca carbonate could plausibly be a manufacture contaminant in aerogel, Mg carbonates are unlikely (*Mikouchi et al.* 2007). However, in principle carbonates also can be formed without the presence of liquid water, in gas-phase reactions in the nebula (*Toppani et al.* 2005; *Wooden* 2002; *Wooden et al.* 2017), so the presence of carbonates is not an unambiguous signature of cometary aqueous alteration.

Sulfides are abundant in Wild 2, at all sizes (*Zolensky et al.* 2006). These are predominantly pyrrhotite ($Fe_{(1-x)}S$, x = 0 to 0.2), but unusual sulfides are abundant. Some pyrrhotites dominate terminal particles often within assemblages with igneous textures (*Joswiak et al.* 2012; *Gainsforth et al.* 2013; *Gainsforth et al.* 2014). As is generally the case, pyrrhotite often occurs in association with pentlandite $(FeNi)_9S_8$, and Fe-Ni metal (*Joswiak et al.* 2012). ZnS (probably sphalerite) is unusually abundant in Wild 2 as compared to chondrites. A single report of cubanite ($CuFe_2S_3$) has been interpreted as evidence for aqueous processing (*Berger et al.* 2011), however this mineral can form in non-aqueous environments.

The iron oxide magnetite (Fe_3O_4), including a Cr-rich variety, has been identified in a few Wild 2 grains (*Bridges et al.* 2015). Although magnetite in carbonaceous chondrite meteorites is often ascribed to a secondary origin by aqueous alteration (*Kerridge et al.* 1979) more detailed observation of Wild 2 magnetite is necessary in order to reliably assess its origin.

It is clear that carbonates, sulfides and oxides trace a diverse range of formation and processing environments and possibly provide direct evidence for aqueous alteration within Wild 2, although the rarity of these particular phases and the lack of any report of phyllosilicates (*Brownlee and Joswiak* 2017) limits the apparent scope of aqueous alteration.

2.4.3. *Chondritic Anhydrous IDP Mineralogy*

Individual IDPs are under 100 μm in diameter, and consist of tens to hundreds of thousands of grains, with greatly varying mineralogy and composition - non equilibrium phase assemblages. The mineralogy of the anhydrous chondritic IDPs evidences a wide range of protoplanetary disk locations and processes. The most abundant crystalline phases are ferromagnesian silicates, mainly

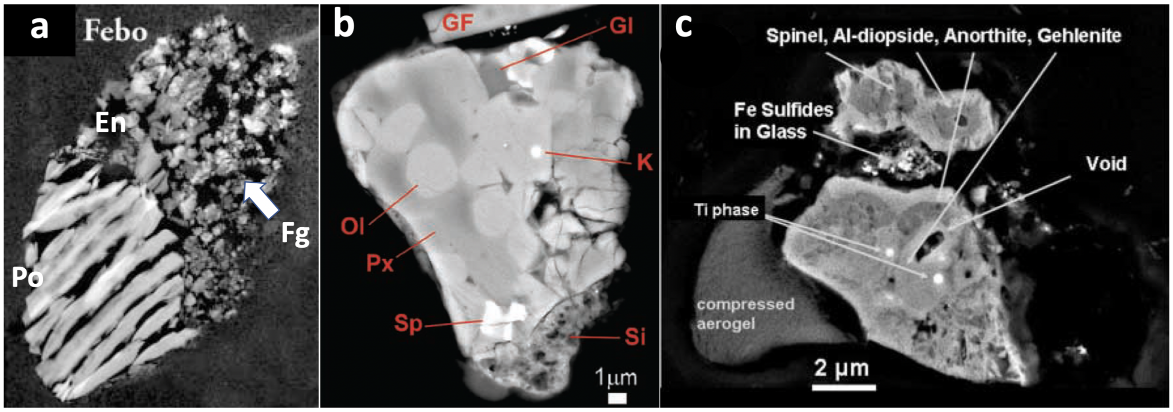

Fig. 8.— *Mineral diversity observed in 81P/Wild 2 samples brought back by the Stardust spatial mission : a) Scanning transmission electron microscopy dark field image of Track 57 terminal grain. Large pyrrhotite (Po) and enstatite (En) crystals are annotated, as well as fine-grained material (Fg). b) Backscattered electron micrograph of a chondrule-like fragment in particle Torajiro, containing olivine (Ol), low-Ca pyroxene (Px), Cr-spinel (Sp), glass (Gl), kamacite (K), silica aerogel from the collector (Si). A glass fiber (GF) holds the sample (*Nakamura et al. *2008). c) Backscattered electron image of a CAI-like particle from track 25 (*Zolensky et al. *2006).*

olivine and low-Ca pyroxene with lesser amounts of high-Ca pyroxene, plagioclase, and Fe-Ni-Zn-sulfides (*Rietmeijer* 1998). The (crystalline) olivine and low-Ca pyroxene compositions range from almost pure forsterite and enstatite to relatively high Fe-compositions. While olivine and low-Ca pyroxene in some IDPs is predominantly Mg-rich, a census of anhydrous and hydrous IDPs shows a slight preponderance of Fe-contents $\sim$60% (*Zolensky et al.* 2008). This is unlike the flat distribution of Fe-contents for terminal olivines ('micro-chondrules') reported for Wild 2 (*Frank et al.* 2014). However additional olivine and pyroxene compositional data for IDPs is required to verify these apparent trends.

Low Fe-, Mn-enriched (LIME) olivines are proposed to be high-temperature nebular condensates (*Klock et al.* 1989). Enstatite whiskers in chondritic IDPs, elongated along the [100] crystallographic axis, are consistent with rapid growth from a vapor phase (*Bradley* 1994). Most anhydrous chondritic IDPs also contain nanoscale beads of glass with embedded metal and sulfides, called "GEMS" (*Bradley* 1994b).

The origins of GEMS is debated, with proposed formation mechanisms including irradiation of crystalline grains (olivine, pyroxene, etc.), formation in the ISM (*Bradley* 2013), or in the protosolar molecular cloud or outer solar nebula (protoplanetary) disk such that GEMS experienced inheritance of 'solar composition' (*Keller and Messenger* 2011), or the formation by cold processes precursor to the aggregation of IDPs (*Ishii et al.* 2018). In meteorites, GEMS-like phases have been reported in few meteorites, for example the Paris CM chondrite (*Leroux et al.* 2015), but this identification is disputed (*Villalon et al.* 2016). Only in the Ningqiang C3 chondrite is a radiation damage origin demonstrated (*Zolensky et al.* 2003). GEMS are therefore believed to be more typical of comets than asteroids. It is therefore very unfortunate that GEMS apparently cannot be reliably recognized in 81P/Wild 2 samples because of their similarity to melted silica aerogel (*Ishii et al.* 2011).

The unanticipated (to say the least) discovery of numerous CAIs among the recovered 81P/Wild 2 grains has refocused attention to refractory IDPs (*Zolensky* 1987; *McKeegan* 1987), which had been ignored as they were erroneously assumed to have purely asteroid origins. These refractory IDPs differ from meteoritic analogues principally in being much finer grained, although they still await detailed characterization.

Through seeking IDPs for comparison to *Stardust* terminal olivine grains or 'micro-chondrules', the Giant IDPs became a focus of state-of-the-art studies because they were found to possess a wide range of Mg:Fe- as well as minor element Mn-, Cr-, and Ca- compositions, potentially similar to the *Stardust* olivines (*Brownlee and Joswiak* 2017) , although additional IDP olivine analyses are still required to demonstrate similarity. As laboratory techniques advanced and focused on Giant IDPs, the studies of anhydrous chondritic IDPs with only high-Mg content olivines were set aside. In order to compare the formation conditions of the olivine and pyroxene in these anhydrous chondritic IDPs, similar studies to the Giant IDPs, at high spatial resolution and sensitivity, e.g. of elemental compositions of individual grains, are hoped for in the future.

2.4.4. UCAMM Mineralogy

The mineral components of UCAMMs consist of isolated minerals or small mineral assemblages embedded in the organic matter (*Dobrică et al.* 2012; *Charon et al.* 2017; *Guérin et al.* 2020; *Yabuta et al.* 2017). Both crystalline and amorphous phases are present. Crystalline minerals consist of low-Ca Mg-rich pyroxenes (with stoichiometry ranging between En_{60} and En_{97}) and Mg-rich olivines (stoichiometry comprised between Fo_{75} and Fo_{99}) with rare Ca-rich pyroxenes and Fe(Ni) sulfides. Several hypocrystalline-like ("chondrule-like") mineral assemblages were identified in several UCAMMs. Low Ni-Fe metal and Fe sulfides are

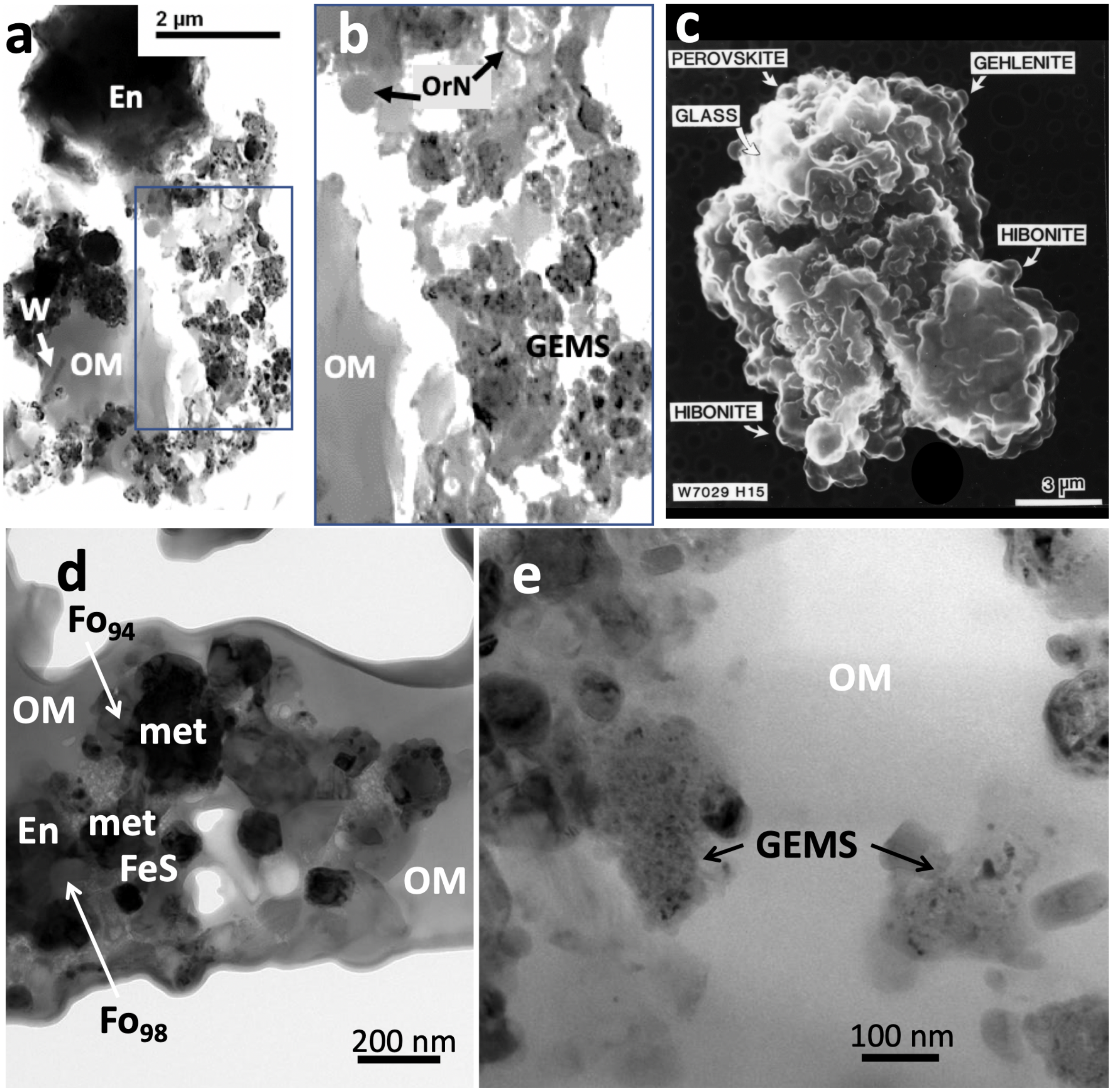

Fig. 9.— *Bright field TEM images (a,b,d,e) ad secondary electron image (c) illustrating the mineral diversity observed in CA-IDPs (a,b,c) and UCAMMs (d,e). (a,b) Anhydrous chondritic IDP U2153 Cluster particle 1; (b) area outlined at in (a). Enstatite (En), an enstatite whisker (W), organic material (OM), GEMS, and two organic nanoglobules (OrN) are indicated (TEM image courtesy of K. Nakamura-Messenger);(c) Refractory IDP W7029 H15, containing perovskite, hibonite, gehlenite and a glass (After (*Zolensky *1987). (d,e) UCAMM DC06-05-94. Mg-rich olivines (Fo94 and Fo98), Enstatite (En), Fe-Ni metal (met), Fe sulfides (FeS), organic material (OM) are indicated (TEM images courtesy of H. Leroux).*

present in mineral assemblages. In several cases, Fe metal inclusions show a rim of Fe sulfide, suggesting the occurrence of an incomplete sulfidization process. Pentlandite is occasionnaly observed. Secondary minerals also include Mn-, Zn-rich sulfide, perryite, as well as small iron oxides, carbonates and phyllosilicate-like phases (*Dobrică et al.* 2012; *Guérin et al.* 2020). Small Na-rich inclusions with stoichiometry close to Na_2S have been observed in the organic matter (*Guérin et al.* 2020). Glassy phases have been found in several UCAMMs (*Charon et al.* 2017; *Guérin et al.* 2020; *Yabuta et al.* 2017) that resemble GEMS found in primitive IDPs (*Keller and Messenger* 2011; *Bradley et al.* 2014). The GEMS-like phases in UCAMMs however tend to lack the metal inclusions of GEMS in IDPs, Fe being mostly in the form of Fe sulfides nano-inclusions. As with the Wild 2 grains, the close association of high-temperature crystalline phases with low-temperature carbonaceous matter in UCAMMs supports the hypothesis of a large-scale radial mixing in the early solar nebula (*Brownlee et al.* 2006). UCAMMs have a low-Ca pyroxene:olivine ratio of approximately 2, similar to anhydrous chondritic IDPs (Zolensky and Berett, 1994). Unlike the situation for Wild2 grains and IDPs, UCAMM olivine and low-Ca pyroxene have compositional peaks at Mg end members. Either Wild 2 ferromagnesian silicates are not typical of comets, or UCAMMs derive from parent bodies different from Wild 2-type comets.

2.5. Cometary dust compositions from astronomical IR spectroscopy

2.5.1. IR spectroscopy

IR spectroscopic spectral energy distributions (SEDs, λF_λ *versus* λ) of dust thermal emission from cometary comae ($\sim$3–40 μm), when fitted with thermal emission models, provides constraints for the composition of the dust particles, their structure (porosity or crystal shape) and their size distribution. The 'grain size distribution' (GSD), or equivalently the dust differential size distribution (DSD), has parameters of power law slope N, and either smallest radii limit a_0 or small particle radii a_p where the DSD peaks before rolling off at yet smaller particle radii (often called the Hanner GSD, *Hanner* (1983)). The particle porosity is often parameterized by a particle fractal dimension D (see Table 1. The particle porosity and DSD slope (D and N) are co-dependent parameters (*Wooden* 2002). With broad wavelength coverage, the mid-IR (MIR, $\lambda\lambda$5–13 μm) and far-IR (FIR,$\lambda\lambda$14–40 μm) resonances can be sought and fitted by thermal models to constrain the dust mineralogies.

From IR SEDs, the dust compositions are better determined for the more numerous smallest particles (in the DSD) and/or hottest particles because smaller particles produce stronger contrast spectral features (referring to $Q_{\lambda,abs}$) and hotter particles produce more relative flux. The more distinct spectral features arise from submicron to micron-sized solid particles ($P = 0\%$) or from up to $\sim$20 μm moderately porous particles ($P = 85\%$), which has some implications for comparisons between IR SEDs and cometary samples. For example, the 20 μm and larger *Stardust* terminal olivine particles would not produce distinct spectral features. Larger extremely porous particles, which are as hot as their small monomers (*Xing and Hanner* 1997), if present in comae even if in smaller mass fractions can produce resonances (*Kolokolova et al.* 2007) and contribute to the SEDs (*Bockelée-Morvan et al.* 2017a) (§ 2.5.7). Particles in the DSD larger than $\sim$20 μm are present in cometary comae because observed FIR SEDs decline more slowly than a single color temperature assessed for the MIR. As a compliment to this, comae do not solely possess large extremely porous particles because the presence of solely porous aggregate particles as warm as their submicron-sized monomers could not explain cometary IR SEDs. Thermal model parameters of composition, which is more sensitive to the properties of the smaller particles, and DSD parameters (P, N, and a_0 or a_p) are constrained by fitting the entire IR SED that extends to particle radii out to which the IR SED is sensitive, e.g., mm-size particles for $\lambda\lambda$7–40 μm. Above mm-size particles, longer wavelengths such as by *Herschel* (*Kiss et al.* 2015) and *ALMA* are required, but the mineralogy is constrained by resonances at MIR-FIR wavelengths discussed here.

Identification of dust compositions may be made by comparison of observed spectral features to laboratory absorption spectra but quantifying the relative abundances requires computing the thermal emission models to predict and compare an emission spectrum of an ensemble of particles to the observed IR SED using standard minimization techniques (χ^2-minimization). A key aspect of determining the dust composition, when feasible, is fitting a broad wavelength SED so that multiple spectral resonances (spectral features) can be fitted from a material's vibrational stretch and vibrational bending modes that span, respectively, MIR to FIR wavelengths.

2.5.2. Five primary dust compositions

The compositions of cometary dust as determined by IR spectral analyses has five primary components that suffice to allow the IR SED to be well-fitted by thermal models for most comets: two Mg:Fe amorphous silicates that produce the broad 10 μm and 20 μm features, two Mg-rich crystalline silicates that produce multiple narrow spectral peaks in the range of $\sim$ 8–33 μm, and a highly absorbing and spectrally featureless and warmer dust component that is ubiquitously observed to dominate the dust's thermal emission in the NIR ($\sim$3–7.5 μm). There is a consensus amongst modelers that this NIR dust emission, sometimes called the NIR dust 'continuum' or 'pseudo-continuum)', is produced by a highly absorbing, carbonaceous dust component. This component is well fitted by the optical properties of amorphous carbon (*Woodward et al.* 2021; *Bockelée-Morvan et al.* 2017a; *Harker et al.* 2022). Aliphatic carbonaceous dust materials are relatively transparent compared to amorphous carbon, and graphitic carbonaceous matter is rare in cometary samples. The potential connections between cometary dust and amorphous carbon, versus other species, e.g. organics dominated by aromatic bonds, by hydrogenated amorphous carbon (HACs), or by graphite, and are discussed in *Wooden et al.* (2017); *Woodward et al.* (2021).

For dielectric materials like silicates, there are spectral features from which we can deduce the mineralogy in combination with modeled radiative equilibrium temperatures and modeled spectral emission features. These four primary siliceous compositions are: Mg:Fe≈50:50 amorphous pyroxene-like $(Mg_{0.5},Fe_{0.5})SiO_3$; Mg:Fe≈50:50 amorphous olivine-like $(Mg_{0.5},Fe_{0.5})_2SiO_4$ (*Dorschner et al.* 1995); Mg-olivine (Forsterite) $(Mg_x,Fe_{(1-x)})_2SiO_4$ for $1.0 \leq x \leq 0.8$, which produces sharp resonances (spectral 'peaks') at or near 11.1–11.2, 19.5, 23.5, 27.5 and 33.5 μm and weaker peaks at 10.5 and 16.5 μm (*Crovisier et al.* 1997; *Hanner and Zolensky* 2010; *Wooden et al.* 2017; *Koike et al.* 2003, 2010); Mg-orthopyroxene (Enstatite) $(Mg_y,Fe_{(1-y)})SiO_3$ for $1.0 \leq y \leq 0.9$ that produces resonances at or near 9.3 and 10.0 μm and with a set of FIR resonances near 20 μm, which is also where Mg:Fe amorphous pyroxene has a broad feature. Depending on the laboratory data and optical constants, the FIR resonances for Mg-pyroxene may be at these sets of wavelengths: (18.5, 19.2, 20.3 μm) for ellipsoidal shapes (in our plots) using optical constants from *Jaeger et al.* (1998), which gives peaks measured at (18.2, 20.6, 21.6 μm); also, laboratory spectra of ortho-enstatite give peaks at (9.3, 10.7, 19.5, 20.7 μm) *Chihara et al.* (2001). Cometary features from Mg-pyroxene are not yet detected at high spectral contrast in the FIR. For a spectrum with strong Mg-pyroxene one may look at FIR *Spitzer* IRS spectrum of Herbig Ae/Be star HD179218 (cf. *Juhász et al.* 2010, Fig. 13). Mg-olivine is a well established cometary dust component by either a peak at 11.1-11.2 μm or by a shoulder on the broad '10 μm' feature, which makes the feature look 'flat-topped'. Also, the FIR peaks for Mg-olivine are well separated from the center of the broad Mg:Fe amorphous olivine '20 μm' feature, whose Mg:Fe composition is established by the radiative equilibrium temperatures (*Harker et al.* 2002). When detected, the mass fraction of Mg-olivine present in the coma is $\gtrsim$20%.

Crystalline silicate feature wavelengths and feature relative intensities depend on composition and crystal shape. Mg-rich (100% – 90% Mg) crystalline Mg-olivine (Forsterite) is tri-refringent (3 optical axes or 3 sets of indices of refraction) and has spectral peaks that can shift to somewhat shorter or longer wavelengths depending on crystal shape (*Koike et al.* 2010; *Lindsay et al.* 2013). The observed spectral features of Forsterite are better fitted by rectangular prisms slightly elongated or flattened along the b-axis (*Lindsay et al.* 2013) or by ellipsoidal shapes flattened also along the b-axis (*Harker et al.* 2002, 2007); note that *Fabian et al.* (2000) shows ellipsoidal shapes and quotes elongation along the b-axis but actually, as computed, these particles are b-axis flattened when the (L_b) parameter used in computing the ellipsoidal particles, as given as by (*Bohren and Huffman* 1983), is larger. The optical constants used for Forsterite (in figures shown here) are from *Steyer* (1974); see *Juhász et al.* (2009) for a comparison of other optical constants. Specific examples of crystal shape are revealed in the absorption spectra of Forsterite powders that are prepared by hand-grinding or ball-grinding, where ball-grinding imparts greater sphericity to the particles (*Koike et al.* 2010; *Lindsay et al.* 2013; *Tamanai et al.* 2009). A long standing discrepancy in lab data was resolved when it was realized that the preparation of the sample as well as the medium in which the ground sample is embedded (KBr *vs.* PE) affects the wavelength positions and relative depths of absorption bands and the degree of sensitivity depends on which spectral features (*Koike et al.* 2010; *Tamanai et al.* 2009; *Lindsay et al.* 2013). With increasing Fe-content, olivine peaks shift to longer wavelengths (*Koike et al.* 2003). The observed range of wavelengths for the cometary 11.1-11.2 μm feature restricts Mg-contents from 100–80% for Mg-olivine.

Silicates, being dielectrics, emit strongly through their MIR vibrational stretching and FIR vibrational bending modes and possess little absorptivity at wavelengths shorter than $\sim$7.5 μm so, we repeat, the thermal emission at shorter wavelengths is likely from a carbonaceous dust component. Iron sulfide (FeS) mineral is dark but not as absorbing as amorphous carbon. FeS has yet to be modeled as a major dust component contributing in the NIR for reasons that include: the optical constants are lacking for the full range of wavelengths and/or are contested and are specifically lacking at 3–10 μm, FeS is not yet firmly detected, and FeS does not yield the correct scattered light color even if held to 6% volume of the particle (*Bockelée-Morvan et al.* 2017a) (§ 2.5.7).

Each of the five dust compositions that dominate SEDs have analogous materials in cometary samples and in anhydrous chondritic IDPs (CA-IDPs). Spectral features are measured in bulk IDPs (*Bradley et al.* 1992; *Wooden et al.* 2000) and in IDP thin sections (*Matrajt et al.* 2005). The amorphous silicates are akin to the GEMS (*Bradley et al.* 1992; *Bradley et al.* 1999; *Bradley* 2013). The Mg-olivine and Mg-pyroxene are spectrally akin to Fo_{100}–Fo_{80} and En_{100}–En_{90}. The amorphous carbon is akin to some phases of disordered carbon and the occasionally quoted amorphous carbon in IDPs. Alternatively, we note that possibly aromatic-bonded carbon (π-bonds or C=C bonds) could produce a significant absorptivity because of its higher UV-VIS cross sections. Laboratory studies find CA-IDPs to not be polyaromatic versus UCAMMs that are polyaromatic. A fraction of particles observed in the *in situ* measurements of 1P/Halley were composed solely of carbon (*Fomenkova et al.* 1994).

Figure 10 shows comet C/1995 O1 (Hale-Bopp), which is the best example of an IR SED of a coma with a plethora of submicron silicate crystals and a higher silicate-to-amorphous carbon ratio (high contrast silicate features relative to the 'featureless' emission from a distribution of porous amorphous carbon particles and distribution of larger porous amorphous silicates). Clear and distinctive spectral peaks from (crystalline) Mg-olivine and (crystalline) Mg-pyroxene provide a benchmark for modeling crystalline silicates (shapes and temperatures). Specifically, the 'hot crystal' model (*Harker et al.* 2002, 2007; *Woodward et al.* 2021; *Harker et al.* 2022) increases the radiative equilibrium temperature of the Mg-olivine by a factor of 1.7 over that predicted using the optical constants in order to fit the Hale-Bopp spectra at 2.75 au. Hale-Bopp's Mg-pyroxene is spectrally discernible by its sharp peaks more so at epochs near perihelion than at r_h =2.75 au, which is attributed to its transparency compared to the other dust compositions (*Wooden et al.* 1999). The same jets are active at the two epochs at r_h= 1.2 and 0.93 au (*Hayward et al.* 2000), and the thermal models fitted to their IR SEDs reveal minor differences in their mineralogy: if the relative strength of the Mg-pyroxene and Mg-olivine features only are attributed to temperature increase at smaller heliocentric distances then Mg-pyroxene would be expected to be enhanced relative to the Mg-olivine peaks at 0.93 au but instead by visual comparison the Mg-pyroxene peaks are enhanced at 1.2 au compared to 0.93 au. Also, shown in Fig. 10 is the distinct contribution of the Mg-pyroxene 9.3 μm peak to the short wavelength shoulders of the broad 10 μm feature from Mg:Fe amorphous pyroxene and Mg:Fe amorphous olivine.

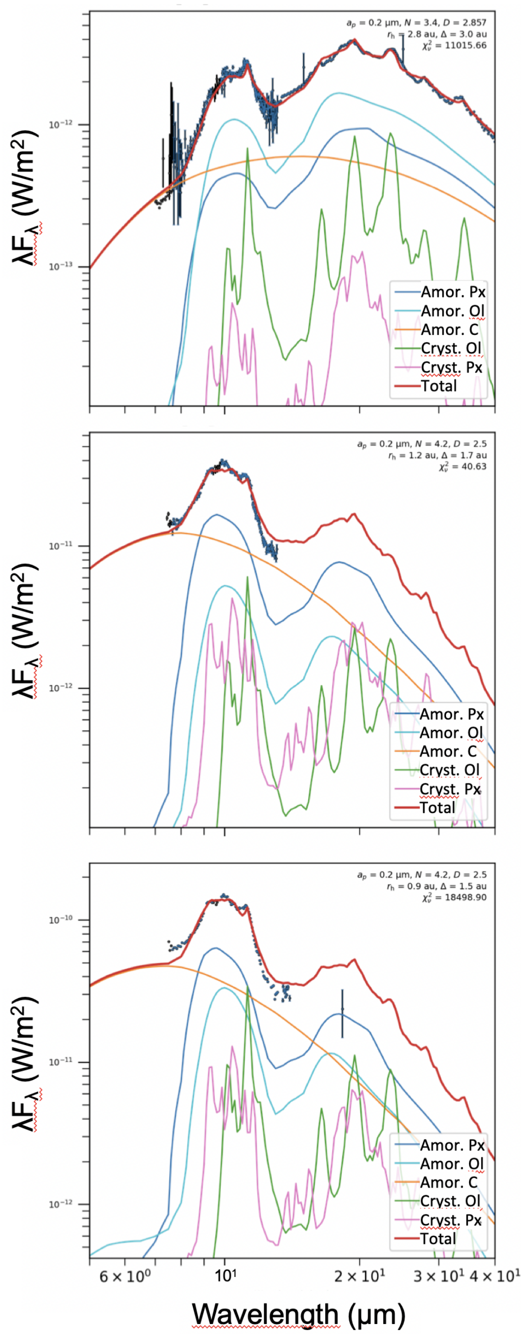

Fig. 10.— Comet C/1995 O1 (Hale-Bopp) at 3 epochs with thermal models (*Woodward et al.* 2021) fitted with 5 compositions, on these UT dates: 19961011 pre-perihelion r_h= 2.75 au from *IRTF*+HIFOGS and *ISO*+SWS (*Crovisier et al.* 1997), *IRTF*+HIFOGS on 19970214 and 19970411 (*Wooden et al.* 1999; *Harker et al.* 2002; *Davies and Barrera* 2004). Mg-olivine (crystalline) has peaks at 10.0, 11.1-11.2, 16.5, 19.5, 23.5, 27.5, and 33.5 μm. Mg-pyroxene (crystalline) has a triple of peaks at 9.3, 10.5, and 11.0-11.3 μm and have modeled far-IR peaks near 19.6 μm, 18.7 μm and $\sim$ 17.9 μm and in λ-vicinity of the FIR Mg:Fe amorphous pyroxene broad feature.

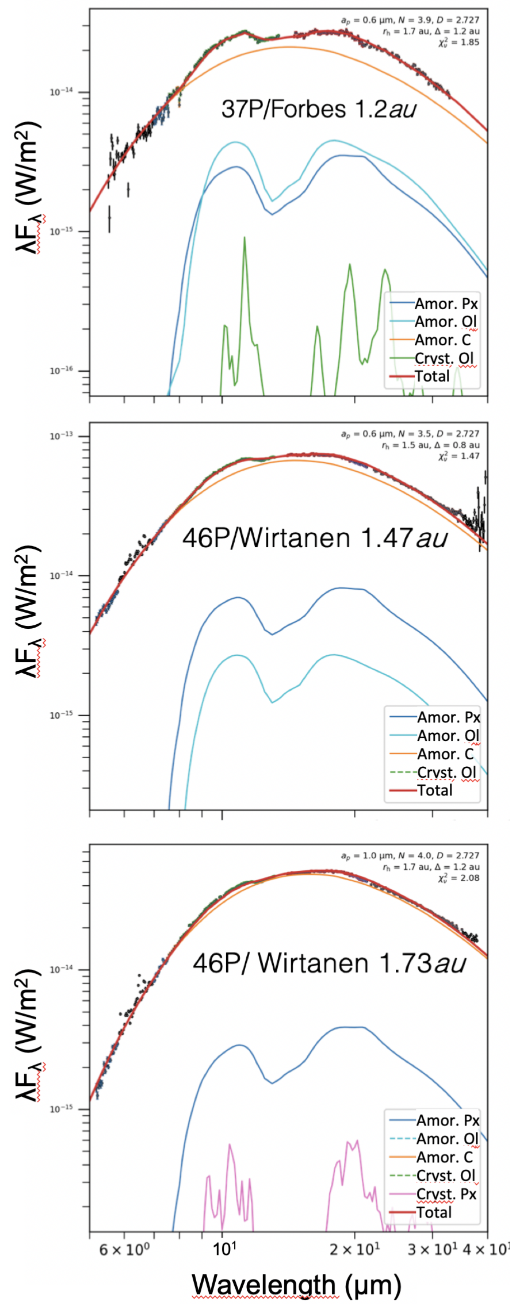

Fig. 11.— *Spitzer*+IRS SEDs of JFCs including 37P, and two epochs of 46P, showing IR SEDs with decreasing ratios of silicate-to-amorphous carbon. IR SEDs are shown with fitted thermal models (*Harker et al.* 2022). Amorphous silicates and no crystalline silicates are constrained in the thermal model fit to 46P at r_h=1.47 au. For comet 46P/Wirtanen at r_h= 1.73 au, weak features from crystalline pyroxene are evident at 9.3, 10.5 μm but more difficult to discern in the far-IR. Multi-epoch spectroscopy is needed to fully ascertain a comet's range of dust compositions. 21P is only fitted through 19 μm because of AOR and calibration challenges at the longer wavelengths (*Kelley et al.* 2021).

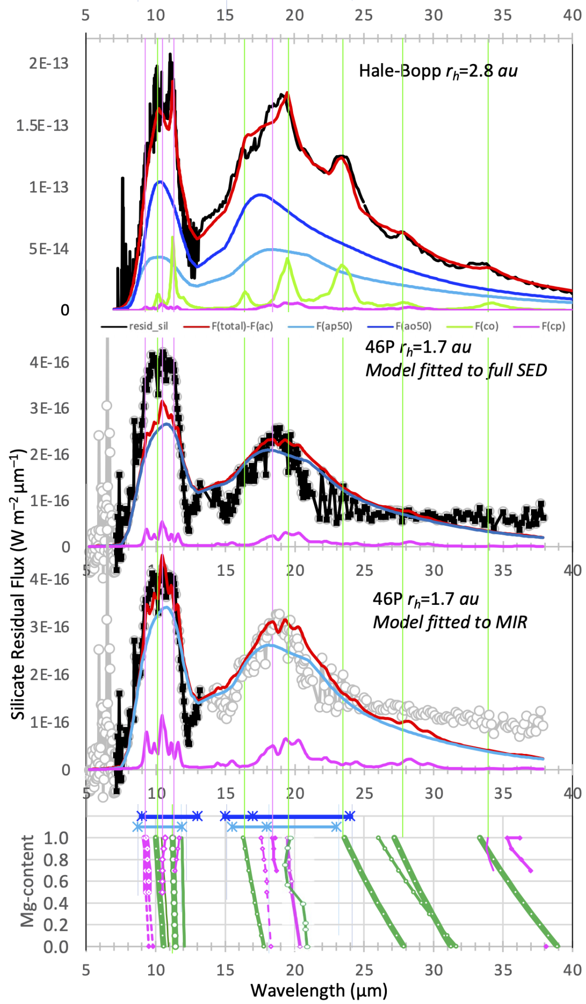

Fig. 12.— Silicate residual flux spectra (*Harker et al.* 2022) shown to highlight the wavelengths of observed crystalline Mg-olivine (co, in *green*) and crystalline Mg-pyroxene (cp, in *magenta*) features and to compare to the wavelength dependencies of the laboratory spectra versus Mg-content=(1 − Fe-content), of the strongest observed features in cometary IR SEDs from *Chihara et al.* (2002); *Koike et al.* (2003). The silicate residual fluxes are the data and model with amorphous carbon (ac) subtracted, i.e., F_{data} - F_{model}(ac) and $F_{model,total}$-F_{model}(ac), respectively, for *top panel* Hale-Bopp at r_h=2.8 au (Fig.10), *middle panel* 46P fitted over the full SED *black points* (as fitted in Fig. 11), and (*residual lower panel*) 46P fitted only over the MIR that shows in an increase in the Mg-pyroxene relative abundance. (*Bottom Panel*) Wavelength dependencies of Mg-olivine and Mg-pyroxene; thickness of lines relates to strengths of observed peaks.

2.5.3. *Degeneracies in compositions derived from thermal models*

Possible degeneracies in dust compositions that can be overcome by fitting multiple spectral peaks include: (a) the 11.1-11.2 μm feature of Mg-olivine and the 11.2 μm PAH emission band; (b) wavelength shifts due to crystal shape (*Koike et al.* 2010; *Lindsay et al.* 2013) or increasing Fe-contents (*Koike et al.* 2003) because the 23.5 μm FIR feature of Mg-olivine is more sensitive to shape and above 40% Fe the entire FIR spectrum changes morphology (*Koike et al.* 2003); (c) at $r_h \gtrsim$ 3–3.5 au, the MIR short wavelength shoulder can be fitted with Mg:Fe amorphous pyroxene or by the warm featureless emission from amorphous carbon but fitting the FIR pyroxene band removes this degeneracy; (d) the Mg-pyroxene 9.3 μm peak and the short wavelength shoulder of the Mg:Fe amorphous pyroxene feature occur at 9.3 μm but sufficent SNR to detect the Mg-pyroxene 10.5 μm peak as well as measuring the far-IR resonances can distinguish between these two compositions. If we contrast Mg-pyroxene with Mg-olivine, Mg-olivine may be assessed even when the 11.1-11.2 μm peak is not clearly discernible against the broad Mg:Fe amorphous olivine or Mg:Fe amorphous pyroxene features because Mg-olivine's primary peak in the MIR occurs at the longer wavelength side of the broad '10 μm silicate feature' so that if a broad silicate feature appears to not be declining at 11-12.5 μm but instead appears 'flat-topped' then Mg-olivine is the candidate. The FIR the peaks from Mg-olivine are at distinctly different wavelengths than the Mg:Fe amorphous olivine feature, thereby allowing for Mg-olivine peaks to not compete with Mg:Fe amorphous olivine in the χ^2-minimization between the model and the data, and the effect is that Mg-olivine peaks are spectrally discernible even when the peaks are weak.

In contrast, the FIR sharp peaks from Mg-pyroxene and the FIR broad feature of Mg:Fe amorphous pyroxene are at nearly the same wavelengths. Moreover, there are some variations in the predicted wavelengths for the Mg-pyroxene FIR peaks partly because of there are variations in the optical constants, the peaks depend on shapes of the crystals, and laboratory measurements of feature wavelengths depend on the embedding medium (*Tamanai et al.* 2009). We have yet to observe a cometary IR SED that has strong Mg-pyroxene peaks in the FIR to confirm the choice of optical constants and crystal shapes in the models. We show for comet 46P/Wirtanen at r_h= 1.94 au, the coincidence of Mg-pyroxene and Mg:Fe amorphous pyroxene in the FIR (see Fig. 11(c) and Fig. 12(b)). In observed cometary IR SEDs, Mg-pyroxene peaks appear more discernible at MIR wavelengths than in the FIR, and this may contribute to Mg-pyroxene having lower relative abundance relative to the other dust components when the MIR and FIR are fitted compared to when only the MIR is fitted (see Fig.12 and compare middle panel with model fitted to full SED with next lower panel with model fitted only to MIR for 46P at 1.7 au). This aspect of thermal models seems contrary to the aim of fitting multiple resonances over the fullest wavelength range (compare Fig. 12(b) and (c)). When weak Mg-pyroxene features are modeled then there is a significant relative mass fraction ($\gtrsim$30%) of this dust component because of its lower absorptivity (Q_{abs}) (*Harker et al.* 2022) and cooler temperatures and hence lower fluxes relative to warmer dust components (*Wooden et al.* 1999). Mg-pyroxene FIR peaks may or may not be fitted by χ^2-minimization of models to the data when the stronger broad feature from Mg:Fe amorphous pyroxene broad feature dominates the flux. These factors need to be considered when contrasting the relatively low number of cometary IR SEDs fitted with Mg-pyroxene compared to the frequent identification of Mg-pyroxene in cometary samples.

Comet 46P at r_h=1.47 au has a weak silicate feature (Fig. 11 (b)). The fitted thermal model has a DSD that peaks at a_p=0.6 μm so submicron particles are present in the coma, which can produce distinct features when composed of silicates. The weak silicate feature thus is modeled by a high relative mass fraction of amorphous carbon compared to the amorphous silicates whose resonances also are fitted. This epoch of comet 46P is similar to comet C/2017 US_{10} (Catalina) that has a high wt% amorphous carbon. The elemental C/Si ratio for comet C/2017 US_{10} (Catalina) is similar to comet 67P/C-G, which has organic IOM-like matter, and both of which have C/Si ratios close to the ISM value (*Woodward et al.* 2021).

2.5.4. *Dust compositions not yet firmly detected in IR SEDs*

As stated above, the five dominant compositions assessed from IR SEDs have analog dust species in cometary IDPs, in *Stardust* samples, and in *in situ* compsitional studies of 1P/Halley and 67P/C-G particles but the contrary is not true: there are dust compositions in cometary samples that are not detected in IR SEDs that include inorganics and organics. The inorganic materials found in samples include Fe-olivine, FeS, Mg-carbonates (*Fomenkova and Mendis* 1992; *Wooden et al.* 2017; *Flynn et al.* 2020), and minor phyllosilicates (10 vol% smectite) in 'hybrid IDPs' that otherwise contain anhydrous minerals Mg-olivine and Mg-pyroxene (*Nakamura-Messenger et al.* 2011), and amorphous Mg-Al-Na, Si-rich mesostasis (glass) in *Stardust* tracks (*Nakamura-Messenger et al.* 2012). Organic materials found in cometary samples include aliphatic carbon and also the relatively rare aromatic carbon such as the three *Stardust* aromatic nano-globules (*De Gregorio et al.* 2010, 2011). In contrast, UCAMMs have abundant aromatic organics.

Fe-olivine. (Fayalitic crystalline olivine). Fe-olivine are abundant in *Stardust* samples as Type II 'micro-chondrules', are similar to CR chondrites' Type II chondrules, and have counterparts in Giant IDPs (*Frank et al.* 2014; *Wooden et al.* 2017; *Brownlee and Joswiak* 2017). As the Fe-content of olivine increases from 20% to 40%, the MIR peak shifts from 11.2 – 11.4 μm (*Koike et al.* 2010) but this wavelength also depends on crystal shape (*Lindsay et al.* 2013). Detections of peaks in the 16–27 μm FIR region are required to discern Mg:Fe≈60:40 (see Fig. 12 and *Koike et al.* (2003)). Due to the enhanced $Q_{abs,UVIS}$ of Fe-olivine, thermal models also will need to demonstrate increased raditative equilibrium temperatures of Fe-olivine in contrast to Mg-olivine.

FeS. FeS is present and abundant in many cometary samples and UCAMMs. FeS may be identified through a very broad 23 μm feature, which is much broader compared to Mg-olivine 23.5 μm feature, and only is expected for submicron FeS grains (*Keller et al.* 2000). However, different measurements produce different predictions for $Q_{abs,IR}$ that range from strong FIR resonances (*Begemann et al.* 1994; *Henning and Mutschke* 1997) to no FIR resonances (*Hofmeister and Speck* 2003). A single reference suggests a 3.63 μm feature in the NIR (*Tamanai et al.* 2003), and dirth of FeS data in the NIR is represented by a dashed line in the *Pollack et al.* (1994)'s protoplanetary disk opacities. If FeS has a spectral feature near 3 μm then FeS could not provide the opacity needed to explain the ubiquitous featureless thermal emission (NIR 'pseudo-continuum) from warm particles, which currently is ascribed to a highly absorbing cabonaceous component and well-fitted by amorphous carbon.

Phyllosilicates. The MIR spectral features of phyllosilicates overlap with the 10 μm features of anhydrous amorphous silicates, e.g. Mg:Fe amorphous olivine and Mg:Fe amorphous pyroxene, but the 20 μm features from phyllosilicates are significantly different (*Wooden et al.* 1999). Phyllosilicates including Montmorillonite (*Wooden et al.* 1999), smectite and serpentine are abundant in hydrated chondritic IDPs (*Bradley et al.* 1989). At most 5% Montmorillonite may be present in the coma of C/1995 O1 (Hale-Bopp) (*Wooden et al.* 1999). The spectral features of phyllosilicates (smectite nontronite) are claimed for 9P/Tempel 1 at +45 *min* post-*Deep Impact* (*Lisse et al.* 2007), as well as for comet C/1995 O1 (Hale-Bopp) but other well-fitted thermal models are without phyllosilicates (*Harker et al.* 2002; *Harker and Desch* 2002; *Min* 2005) (Fig. 10). Laboratory efforts to hydrate Mg-olivine into serpentine has a low yield (*Nakamura-Messenger et al.* 2011). Phyllosilicates are not detected in *Stardust* samples (*Brownlee and Joswiak* 2017).

Carbonates Mg-carbonates are relatively rare in cometary samples (§2.4) and are not definitively detected in cometary IR SEDs. Carbonates (siderite and magnesite) are discussed for comet 9P/Tempel 1 (*Lisse et al.* 2007) but the simultaneous occurrence of water vapor emission lines in the overlapping wavelength region, when modeled, yields a marginal detection of the 7.00 μm carbonate feature and an abundance that is 2 to 3 times lower (*Crovisier and Bockelée-Morvan* 2008). Water vapor lines must be modeled concurrently with the dust thermal emission, and the 5–8 μm spectral region calls for higher SNR studies such as will be available from *JWST*.

Aromatic organics, PAHs. In a micron-sized organic *Stardust* particle, 2- and 3-ring PAHs and NPAHs were identitied via mass spectrometry and these authors suggest photoprocessing may have occurred to the aromatic matter within the organic particle (*Clemett et al.* 2010). Absorption features from the aromatic C=C bonds (near 1600 cm^{-1})

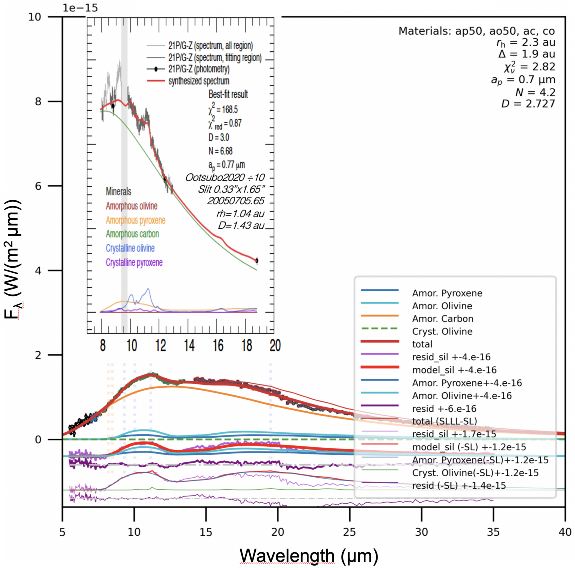

Fig. 13.— Comet 21P/Giacobini-Zinner (21P/G-Z) at 2 epochs with thermal models (*Harker et al.* 2022) fitted with 5 compositions, Near perihelion and at higher spatial resolution for the inner coma, the discovery of organic emission features are shown by the gray points that cannot be fitted by the 5 compositions. These organics likely are related to PAH emission because of their wavelengths and widths of the emission bands (*Ootsubo et al.* 2020).

are rarely observed in CA-IDPs. Aromatic organics are observed in the IR spectra of UCAMMs (see §2.2, Fig. 5). The spectral features sought are their skeletal vibration bands in the 5–8 μm wavelength region and by their peripherial C-H bonds near 3.28 μm and at longer wavelengths where the skeletal structure affects the feature locations. PAHs are discussed for comet 9P/Tempel 1 (*Lisse et al.* 2007). However, thermal models of the same IR SED that simultaneously model the water vapor emission lines and the PAHs in the 5.25–8.5 μm wavelength region produce lower abundances of PAHs by at least 2–3 times (*Crovisier and Bockelée-Morvan* 2008).

Distinct resonances from PAH-like organics contribute to features at $\sim$8.5 μm and $\sim$11.2 μm and possibly aliphatic hydrocarbons at $\sim$9.2 μm (Fig. 13) in the inner coma of comet 21P/Giacobini-Zinner at r_h=1.04 au (*Ootsubo et al.* 2020) as well as Mg-rich amorphous silicates and Mg-silicates. However, the organic bands are not detected in the coma of 21P post-perihelion by lower spatial resolution *Spitzer*+IRS at the larger heliocentric distance of r_h= 2.292 au (*Harker et al.* 2022) (Fig. 13).

Aromatic macromolecules or PAHs are efficient emitters of IR photons and their spectra can be predicted (`https://astrochem.org/`). Unlike the free-flying PAH macromolecules, we are asking: what are the excitation mechanisms that could produce emission features from aromatic-bonded carbon within organic-rich particles? Can photoprocessing of PAHs, which can alter their size distribution, occur within organic-rich particles (*Clemett et al.* 2010)? Currently, we rely on computing emission spectra of particles using optical constants that have been determined for a limited number of organic residues (tholin-like materials). Measurements of absorption spectra are more numerous than the suite of available optical constants (n, k) from which we can compute $Q_{abs,UVIS}$ and $Q_{abs,IR}$ for thermal emission models. UCAMMs offer the best template for IR spectral features because UCAMMs have so much organic material that their absorption spectra can be obtained without acid dissolution of the silicates, which is done for meteoritic IOM and that is known to alter some of the organic fraction (e.g., see *Matrajt et al.* 2005).

Aliphatic organics, the 3.4 μm Diffuse ISM feature. Organics with aliphatic bonds may produce a 3.4 μm emission feature such as seen in CA-IDPs (*Matrajt et al.* 2005) and in some *Stardust* particles (*Matrajt et al.* 2008) and are suggested for comet 103P/Hartley 2 (*Feaga et al.* 2021; *Wooden et al.* 2011) as well as other comets by *Bockelée-Morvan et al.* (1995) who noted a strong correlation with CH_3OH production rates. Lines of sight through the diffuse ISM, e.g, towards the Galactic Center, reveal the 3.4 μm feature. By comparison of the two primary components of this feature from $-CH_3$ ($\sim$2960 cm^{-1}, 3.38 μm) and $-CH_2$ ($\sim$2930 cm^{-1}, 3.41 μm), the diffuse ISM has shorter chains and is more processed than in cometary matter (*Matrajt et al.* 2013).

This solid state emission feature from organics is in the same spectral region as gaseous emission lines from ethane C_2H_6 and methanol CH_3OH that are observed at high spectral resolution and for which modeling is a challenge (*Bonev et al.* 2021, Fig. 5) so a method that combines observing or modeling the emission lines of the gaseous species (*Feaga et al.* 2021, as mentioned in) with modeling the solid state material that typically has multiple resonances from $-CH_2$ and $-CH_3$ bonds is required to further assess the presence of this aliphatic carbon component. Absorption features from aliphatic bonds are common in CA-IDPs (§2.2). The difference between laboratory studies of IDP absorption spectra and cometary IR spectra is that the 3.4 μm features arising from dust in comae are expected to be in emission. Predicting the emission spectra is at the forefront of thermal modeling developments and we note that optical constants are lacking for carbonaceous materials dominated by aliphatic bonds as opposed to rich in aromatic bonds.

To date, most organics that have measured optical constants are dominated by aromatic bonds (the 3.28 μm PAH feature and features in the 5–9 μm region) and for modeling comets we need organic residues that are rich in aliphatic bonds, if we use CA-IDPs as our guide. The temperatures of the organic-bearing particles that produce the 3.4 μm emission feature and its relative abundance will determine the strength or contrast of the feature relative to the strong NIR 'continuum' emission from highly absorbing carbonaceous matter that is modeled by optical constants of amorphous carbon.

2.5.5. *Discrete materials or mixed material aggregates?*

There are compelling reasons to treat cometary particles as aggregates of mixed materials. CA-IDPs show that particles are mixtures, i.e., unequilibrated aggregates of amorphous silicates (GEMS), crystalline silicates, organics of varying compositions (§ 2.2), and iron sulfides. Some CA-IDPs are dominated by carbonaceous matter (*Thomas et al.* 1993) while others like the Giant IDPs are intimate mixtures of mini-chondrules of Fe-olivine with minor Mg-olivine, as well as sulfides and GEMS (*Brownlee and Joswiak* 2017). Alternatively, there are some observations that strongly motivate our thinking that the carbonaceous materials and the siliceous materials may be discrete components in cometary comae or at least they vary in their relative abundance ratios depending on what part of the nucleus is active. Some examples are: (a) comet C/2001 Q4 (NEAT) revealed a significant drop in the silicate feature contrast in about a hour, which is the jet crossing time for the observing aperture (*Wooden et al.* 2004), (b) comet C/2017 US_{10} (Catalina) had an increase in the amorphous carbon-to-silicate ratio between two epochs separated by about 6 weeks of time (*Woodward et al.* 2021), (c & d) the inner coma studies of 9P/Tempel 1 post-*Deep Impact* by *Gemini*+Michelle spectroscopy show rapidly changing compositions (*Harker et al.* 2007) and by *Subaru*+COMICS narrow band imaging show Mg-olivine, then amorphous carbon, and then Mg-olivine in the few hours following the *Deep Impact* event, (e) the outburst of comet 17P/Holmes showed crystalline-rich material that then changed composition well after outburst (*Reach et al.* 2010), and (f) multi-epoch *Spitzer*+IRS spectra of a handful of comets show variable compositions for multi-epochs (*Harker et al.* 2022). Complimenting remote sensing results, the *in situ* measurements of cometary particles indicate from 1P/Halley revealed that particles were siliceous-only, carbonaceous-only, and mixed particles (*Schulze et al.* 1997; *Fomenkova et al.* 1992; *Lawler and Brownlee* 1992) and that carbonaceous-only particles dominated within 9000 km of the nucleus (*Fomenkova and Chang* 1994).

2.5.6. *Thermal emission models, Dust Equations*

Computing the scattered light component and the thermal emission component (typically starting at 3 μm for r_h<2.5 au) of the flux observed from a cometary coma requires a set of equations (Table 1) and a set of suppositions: suppose a single DSD, a chosen porosity P and an ensemble of compositions represent the dust in the coma and then the models are assessed against the observations using standard minimization (χ^2-minimization) techniques.

The emergent flux is a sum over the particle size distribution of the thermally emitted fluxes per particle of varying compositions and/or particle structures. Per particle, the thermal flux is set by the particles' dust temperature (T_d) that results from radiative equilibrium between absorbed sunlight and emitted thermal radiation. Both the dust temperature and dust flux depend upon the product of the particle's absorptivity ($Q_{abs,IR}$) and its cross sectional area $G(a)$. The particle's wavelength-dependent absorptivity ($Q_{\lambda,abs}$) depends on composition, radius (a), shape and porosity.

The optical properties are called the absorptivity $Q_{abs,IR}$ and scattering efficiency $Q_{\lambda,sca}$, which are computed from the real and imaginary optical constants, n and k, using various methods. Porous aggregates of mixed compositions, such as amorphous silicates, amorphous carbon and FeS, can be well modeled by 'mixing' optical constants and vacuum such as when Mie Theory is combined with Effective Medium Theory (EMT) or Brugemann Mixing Theory (BM); or by layering such as in Distribution of Hollow Spheres (DHS) (*Min* 2005); or Rayleigh-Gans-Debye (*Bockelée-Morvan et al.* 2017a,b). However, Mg-olivine cannot be well modeled by mixing optical constants with vacuum; the predicted spectral features do not come close to observed spectra or laboratory spectra. This presents the challenge of computing the optical properties of mixed material porous aggregates with crystal monomers with edges and faces, and some progress has been made using the Discrete Dipole Approximation with the DDSCAT code (*Moreno et al.* 2003; *Wooden et al.* 2021). Scattering efficiencies ($Q_{\lambda,sca}$) have been computed using DDSCAT or T-Matrix because aggregates scatter differently than spheres (*Kimura et al.* 2016; *Kolokolova et al.* 2022).

More absorbing particles are warmer and smaller particles are warmer, and the co-dependencies between these dust properties is mitigated by the assessment of the relative fluxes and wavelengths of spectral resonances or spectral 'features'. Spectral features only arise from particles composed of dielectric materials that are smaller than about 1–3 μm-radii for solid (0% porosity, fractal dimension $D = 3$) particles and for $\lesssim$ 10–20 μm-diameter moderately porous particles (~65–85% porosity, $D \sim 2.86 - -2.7$, *Harker et al.* (2002)). For particles of the same composition, the dust temperature depends more weakly on effective radius than on heliocentric distance from the Sun (r_h). When of the same composition, smaller particles are hotter simply because quantum mechanically smaller particles are less efficient emitters of photons at wavelengths larger than their cross sections ($G(a)$); historically, this effect has been called *Superheat* (*Gehrz and Ney* 1992). Cometary SEDs do not reveal a single color temperature (Planck function fitted to wavelengths outside resonant features); the color temperature is warmer at shorter NIR wavelengths and cooler at FIR wavelengths. For a color temperature $T_{color}(r_h)$ fitted to ~7.5 μm and ~13 μm, a longstanding relationship versus heliocentric distance (r_h) is given in the Table 1.

For particles of the same effective radius and r_h, there is strong dependence of dust temperature on the dust composition through significant variations in the absorptivity $Q_{abs,UVIS}$ at wavelengths where sunlight is absorbed. To achieve the highest temperatures observed for comae particles (e.g., § 2.5.7), small and highly absorbing particles are required or large extremely porous aggregates that are composed of mainly highly absorbing materials and whose large particle temperatures are equivalent to the temperatures of their submicron monomers.

Crystalline materials in the DSD are often are limited to radii of less than 1 μm to a few micron because predicted resonances of larger crystals do not fit observed spectral features (e.g., see *Lindsay et al.* 2013). Relative mass fractions are quoted for the up-to 1 μm portion of the DSD. The emission spectra of silicate particles or of amorphous carbon particles of increasing larger radii than these 3 μm and 20 μm radii, respectively for solid and for moderately porous particles, have increasingly broader as well as significantly weaker contrast resonances (with respect to wavelengths outside of their resonances). Thermal model parameters are co-dependent but are not degenerate when dielectric materials like silicates are present in comae because, in practice, varying the composition, DSD, and particle porosities produces thermal models that are distinguishable when fitted against the observed SEDs with good signal-to-noise ratios using minimization metrics (χ^2-minimization).

There are three albedos of interest for assessing comae particle properties: the particle albedo, the geometric albedo, and the bolometric albedo.

The geometric albedo is, by definition, assessed at zero degrees phase angle ($\alpha = 0°$ in the observer's frame) (*Hanner et al.* 1981; *Bockelée-Morvan et al.* 2017a) ($\alpha = 0°$ translates to $\theta = 180°$ or opposition, where θ is the angle between incident sunlight and scattered ray in the particle's frame). The geometric albedo at non-zero phase angles may be extrapolated from comae observations of $A_p(\alpha) = A_p(\alpha = 0°) \times j(\alpha)$ using the "phase curve" $j(\alpha)$ and $A_p(\alpha)$ can be compared to $A_p(\alpha)$ computed for spheres (Mie) and for porous aggregate particles of varying composition and porosity (*Hanner et al.* 1981; *Kimura et al.* 2016; *Kimura et al.* 2006, 2003).

Alternatively, to calculate at the observed phase angle ($A_p(\alpha)$), one can use the thermal model fitting parameters that include the product $G(a)\mathrm{Q}_{\lambda,abs}$ to derive the dust effective area by assuming $Q_{abs} = 1$:

$$\text{dust effective area} = \mathrm{K} \int_{\mathrm{a_{min}}}^{\mathrm{a_{max}}} \mathrm{G(a)\ n(a)\ da}$$

Then the geometric albedo is the scattered light flux density divided by the dust effective area $G(a)$ (*Hanner et al.* 1981; *Tokunaga et al.* 1986) at the observer's phase angle α. $G(a)$ can be calculated from either the Wein side of the thermal emission in the NIR or by thermal models fitted to a broader wavelength IR SED. This technique of calculating the geometric albedo, which was popular when the dust emission was studied with narrow band filter photometry, avoids having to measure or assume knowledge of the dusty coma phase curve $j(\alpha)$.

Finally, the bolometric albedo (*Gehrz and Ney* 1992) enables an empirical assessment of the particle properties in the comae of many comets at different phase angles (*Woodward et al.* 2015, 2021). The bolometric albedo $A(\alpha)_{bolo}$ is an approximate measure of the scattered to total incident energy (sunlight) (*Woodward et al.* 2015), where the total incident energy is assessed by the sum of the thermal (re-emitted) and scattered energies ($\lambda\ F_\lambda$), each measured at the wavelengths of their maximum energy output (Table 1). The opportunity to tie the scattered light to the thermal emission potentially offers additional insights into dust properties and compositions for two reasons: the scattered light may be contributed to by higher albedo (and potentially cooler) dust components such as ice grains or organics, and particle structure affects scattering and thermal in distinct ways (*Tokunaga et al.* 1986) (§ 2.5.7, 2.5.8).

2.5.7. Dust composition and DSD from combined scattered & NIR thermal: 67P/C-G outbursts

The *Rosetta*+VIRTIS-H spectra of the quiescent coma and of two short duration outbursts (20150913T13.645 and 20150914T18.828 UT) from comet 67P/C-G provide an excellent example of how constraints on the dust parameters arise from the analyses of scattered light and the NIR thermal IR as presented by *Bockelée-Morvan et al.* (2017a,b). Better constraints on dust composition and grain size distribution are possible if the visible through NIR wavelengths are measured to reveal the scattered light color and the onset (Wein side) of the thermal emission. Specifically, the dust composition, porosity and coupled DSD parameters of a_0 and N can be constrained when the spectra provide the three metrics of dust scattered light color slope S', NIR color temperature $T_{d,color}$ from the thermal emission, and either the bolometric albedo $A_\lambda(\theta)_{bolo}$ or the geometric albedo A_p.

The scattered light color (S') (whether the color is 'blue', 'neutral' or 'red' relative to reflected sunlight) provides information about the composition of the dust particles (*Storrs et al.* 1992; *Zubko et al.* 2015; *Hyland et al.* 2019; *Kulyk et al.* 2021; *Li et al.* 2014). The bolometric albedo is an approximate measure of the scattered to total incident energy (sunlight) (*Woodward et al.* 2015) and is assessed at the observers phase angle α = 180°–θ = 108°, 99° for the two dates given above. The geometric albedo $A_p(\alpha)$ requires the dust effective area be calculated from dust thermal models fitted to the IR (*Hanner et al.* 1981, 1985; *Tokunaga et al.* 1986). The dust color temperature represents either the DSD-weighted temperatures of the warmest particles, i.e., the smallest and/or most highly absorbing ones, or the DSD-weighted temperatures of aggregate mixed particles, or a combination thereof.

First, we summarize the properties of the quiescent coma of 67P/C-G on the two dates prior to the coma outbursts. The quiescent coma presents a NIR 'red' color slope of S'_{color}=2.6±0.3%/100 nm, 2.3±0.4%/100 nm for λ_{ref}, λ =2.0 μm, 2.5 μm on the two respective dates. The visible wavelength scattered light spectra on these same dates show the quiescent coma has a steeper color slope in the visible of 15–18±3%/100 nm with λ_{ref}, λ=0.45–0.8 μm compared to the NIR (*Rinaldi et al.* 2017), which is typical of cometary comae. The quiescent coma has an estimated bolometric albedo of $A_\lambda(\theta)_{bolo} = 0.13 \pm 0.2$,

Dust Equations	Designation	Notes
$P = 1 - f,$ given fractional filled volume $f = (a/a_0)^{D-3}$	Porosity, fractal dimension D for $1.7 \lesssim D \leq 3$	(*Harker et al.* 2002; *Woodward et al.* 2021; *Lasue et al.* 2019)
Q_{abs}, Q_{sca}	Absorptivity, Scattering efficiency	
$C_{abs} = G(a)\, Q_{abs}, C_{sca} = G(a)\, Q_{sca}$	Absorption, Scattering Cross Sections	
$Q_{ext} = (Q_{abs} + Q_{sca})$	Extinction efficiency	
$F_{emiss}(\lambda) = \frac{1}{1} K \int_{a_{min}}^{a_{max}} G(a) Q_{\lambda,abs}(a)\, \pi B_\lambda(T_d(a))\, n(a)\, da$	thermal flux density	$G(a) = \pi a^2$ for sphere
$\pi B_\lambda(T_d(a) = 2hc^2 \lambda^{-5} \left(exp^{hc/\lambda k T_d} - 1\right)^{-1}$	Planck Function	
$n(a) = \left(1 - \frac{a_0}{a}\right)^M \left(\frac{a}{a_0}\right)^N$	differential grain size distribution (DSD, GSD)	Hanner GSD: $a_p = \frac{(M+N)}{N}$
$K = \frac{N_{dust}(a_0)}{4\pi(\Delta\ [cm])^2}$ or $K = \frac{N_{dust}(a_p)}{4\pi(\Delta\ [cm])^2}$ for HGSD	flux scaler, at a_0 (DSD) or at a_p (HGSD, $M \neq 0$)	
$F_{sca}(\lambda, \alpha) = \frac{F_\lambda(T_\odot)}{(r_h\ [au])^2} K \int_{a_{min}}^{a_{max}} G(a) Q_{\lambda,sca}(a)\, p_{\lambda,sca}(a, \alpha)\, n(a)\, da$	scattered	$F_\lambda(T_\odot)$ solar flux at 1 au
$\theta(\deg)$	angle from incoming to outgoing ray	
$\alpha = 180° - \theta$	phase angle betw. incident sunlight and observer	
$\int_{4\pi} p_{\lambda,sca}\, d\Omega = 1 = \frac{1}{C_{\lambda,sca}(a)} \int_{4\pi} \frac{d(C_{\lambda,sca}(a;\theta,\phi))}{d\Omega} d\Omega$	"phase function" $p_{\lambda,sca}$, normalized differential scattering cross section	$C = G(a)Q$
$j_\lambda(a, \alpha') = \frac{p_\lambda(a, \theta=180°-\alpha')}{p_\lambda(\theta=180°)} = \frac{p_\lambda(a,180°-\alpha')}{p_\lambda(\alpha'=0°)}$	"phase curve", phase fn normalized at backscattering angle θ=180°	(*Hanner et al.* 1981) α'=0≡θ=180° ref
A=Q_{sca}/Q_{ext}	Albedo of particle	
$A_p(\alpha') = A_p(\alpha = 0°) \frac{p_\lambda(a,180°-\alpha')}{p_\lambda(a,180°)} \equiv A_p(0) j(\alpha')$	geometric albedo, ratio of energy *backscattered* to that of Lambertian surface of equal area	phase angle $\alpha' \equiv 180° - \theta$
$A_\lambda(\theta)_{bolo} = \frac{f(\theta)}{(1+f(\theta))},\ f(\theta) = \frac{[\lambda F_{sca}(\lambda,\alpha)]\ \|_{\lambda=\lambda_{max,sca}}}{[\lambda F_{abs}(\lambda)]\ \|_{\lambda=\lambda_{max,abs}}}$	bolometric albedo, ratio of scattered to sum of scat. & thermal energy at $\lambda_{max,sca}$ & $\lambda_{max,emiss}$	(*Woodward et al.* 2015)
$\int_0^{\inf} F_{\lambda_{VIS},abs}(Q_{\lambda_{VIS},abs})\, d\lambda = \int_0^{\inf} F_{\lambda_{IR},emis}(Q_{\lambda_{IR},abs}, T_d)\, d\lambda$	Radiative Equilibrium (absorption = emission)	rad eq temp T_d
$\int_{\lambda_{min}}^{\lambda_{max}} F_{\lambda_{VIS},abs}(Q_{\lambda_{VIS},abs})\, d\lambda = \int_{\lambda_{min}}^{\lambda_{max}} \frac{F_\lambda(T_\odot)}{r_h^2} G(a) Q_{\lambda,abs}(a) d\lambda$	Sunlight absorbed (L)	
$\int_{\lambda_{min}}^{\lambda_{max}} F_{\lambda_{IR},emis}(Q_{\lambda_{IR},abs}, T_d)\, d\lambda = \int_{\lambda_{min}}^{\lambda_{max}} \pi B_\lambda(T_d)\, G(a) Q_{\lambda,abs}(a) d\lambda$	Thermal emitted (R)	
$g_{col}(\lambda) \equiv \left(\frac{\lambda}{\lambda_{ref}}\right)^{-p_{col}} \propto \int G(a)\, Q_{\lambda,sca}(a)\, p_{\lambda,sca}(a, \alpha)\, n(a)\, da$	scat. light color g_{col}	power p_{col}
$S'_{color} = \frac{2}{(\lambda_{ref}-\lambda)[nm]} \frac{g_{col}(\lambda)-g_{col}(\lambda_{ref})}{g_{col}(\lambda)+g_{col}(\lambda_{ref})}$	color gradient (slope) [%/100 nm]	
$T_{d,color} \approx 1.1 \times 278\ [K](r_h/[au])^{-0.5}$	dust color temperature, typical behavior	(*Hanner et al.* 1997)

Table 1: *Table of equations including dust thermally emitted and scattered fluxes, and parameters that quantify observed dust properties.*

and a dust color temperature of $T_{d,color} \approx 300\ K$ derived from fitting a scaled Planck function to the 2–5 μm dust continuum measurements.

Models for the dust scattering and thermal emission predict S'_{color}, $T_{d,color}$ and $A(\theta)_{bolo}$. The four parameters that the dust models constrain, via χ^2-minimization against the metrics derived from the spectra, are: two DSD parameters (smallest particle radius a_0 and DSD slope N), the particle porosity P that is parameterized by a fractal dimension D, and the dust composition quantified by q_{frac} where q^3_{frac} is the volume fraction of inclusions of lesser opaque material within a matrix of more highly opaque material. *Bockelée-Morvan et al.* (2017a,b) first models the particles as amorphous, porous spheres using effective medium theory (EMT).

For the quiescent coma, and for a DSD of porous spheres of 2-compositions of Mg:Fe amorphous olivine in a matrix of amorphous carbon the ranges of parameters include (a_0, N,q_{frac}, D, P) = (0.3μm, 2.5, 0.7, 2.5, $\leq$0.5) and (0.9μm, 3.0, 0.7, 2.5, $\leq$0.5) with constraints $N \leq 3$ and forcing $P \leq 0.5$ (*Mannel et al.* 2016, MIDAS 'compact particles'), and for q_{frac}=0.7 that translates to 66 vol% amorphous carbon and 34 vol% amorphous olivine. Note that a fractal dimension for the porous spheres of $D = 2.5$ yields the following radii-dependent porosity values of P(0.4 μm)=0.5, P(1 μm)=0.68, P(3 μm)=0.82. The model forces $P \leq 0.5$ so this forces particles bigger than 0.4 μm to have the porosity that is lower that the porosity equation (Table 1) and independent of radii a, unlike if D was applied over the full DSD. Similar DSD parameters and porosity prescription also allow compositions of pure carbon, carbon and a lower q_{frac} of more transparent Mg-rich amorphous pyroxene or Mg-olivine (Forsterite). For pure silicate grains or silicates mixed with 6 vol% FeS (consistent with *Fulle et al.* (2016c)), DSD parameters sufficient to produce the measured $T_{d,color}$ yield NIR neutral colors (as opposed to the observed NIR red colors) and bolometric albedos higher than measured. Thus, for the quiescent coma particles with carbon or carbon with silicates are necessary to fit the parameters derived from the spectra of $A(\theta)_{bolo}$, S'_{color} and $T_{d,color}$.

The quiescent coma also is modeled with a portion (25% by number) of extremely porous aggregate particles (D=1.7). Extremely porous aggregate particles provide less than 1.5 per cent of the albedo at 2 μm as well as provide thermal emission (*Bockelée-Morvan et al.* 2017a) and the quiescent coma dust properties still have the same dust composition as cited for lower porous particles (D=2.5, $P \leq 0.4$) but have a steeper size distribution $N \geq 3$ (*Bockelée-Morvan et al.* 2017b). This DSD slope is more commensurate with GIADA and OSIRIS studies of 67P/C-G's dust *Fulle et al.* (2016c). Also, a subpopulation ($\sim$25% by number) of extremely porous particles (fractal dimension D=1.7–1.8) (*Lasue et al.* 2019) is supported by *in situ* studies by GIADA (*Fulle et al.* 2015), by MIDAS (*Mannel et al.* 2016; *Bentley et al.* 2016a), and by particle topologies (*Langevin et al.* 2016).

Extremely porous aggregate particles, which are often referred to as ('fluffy' or dendritic) Ballistic Cluster Cluster Aggregates (BCCA) (*Kimura et al.* 2016) , with D=1.7 (P >0.95 for 1 μm and >0.999 for 20 μm effective radii) behave significantly differently than highly porous particles (P=85% for $a \gtrsim 100$ μm with D=2.727) or moderately porous particles (P=65% for $a \gtrsim 200$ μm with D=2.86) (e.g. *Harker et al.* 2002) because BCCA have radiative equilibrium temperatures that are similar to their submicron monomers and, practically speaking, have temperatures independent of their size (*Bockelée-Morvan et al.* 2017a; *Tazaki et al.* 2016; *Kimura et al.* 2016). Also, BCCA have spectral features similar to their monomers (*Kolokolova et al.* 2007), and their relative contributions to the scattered light albedo is extremely minimal (*Kimura et al.* 2006). For the quiescent comae, Rayleigh-Gans-Debye (RGD) computations of extremely porous aggregates demonstrate T_{color} is practically independent of a_0 for range [0.1μm,6μm] (*Bockelée-Morvan et al.* 2017a).

In contrast to the quiescent coma, the outbursting coma has hotter particles, has a bluer NIR scattered light color, and higher bolometric albedo, where all three properties change with time as the outbursts evolve. During outbursts, the dust colors in the visible remained in ranges of 10–15%/100 nm and 6–12 %/100 nm, for the respective two dates (*Rinaldi et al.* 2018). The particles are moving relatively fast compared to dust nominal speeds for 67P/C-G, $v(a$ <10 μm)$\geq$ 30 $m\ s^{-1}$, so subsequent *VIRTIS-H* spectra sampled different sets of particles. The outbursts are characterized by sudden increase in dust thermal emission that peaks in a few minutes and then decays towards nominal comae levels in about 30 minutes. The changes in the NIR during the outbursts of 67P/C-G are related to changes in the properties of the dust (composition, smallest particle size, and DSD slope) in the outburst materials, which evolve over the course of the outburst events.

At the onset of the outbursts on the two consecutive days, the particles are significantly hotter $T_{d,color} = 550\ K, 640\ K$, with blue colors (extreme values of $S'_{color} =$ –10%/100 nm with modeled color slope power of $p_{col} =$ 2.30) and a higher bolometric albedo $A_\lambda(\theta)_{bolo} = 0.6$. In the first outburst, all three metrics trend together and follow the light curve but during the second outburst $A(\theta)_{bolo}$ remains high (and increasing) as the light curve and $T_{d,color}$ and S'_{color} decay towards quiescent coma values.

Particles ejected in the outburst, as modeled, are higher in carbon (smaller q_{frac}), and have smaller minimum particle radii as well as having a steeper DSD slope (a_0, N). Two of three metrics, which are S'_{color} and $T_{d,color}$ are fitted but the $A(\theta)_{bolo}$ is too low to be fitted by dust parameters. A water ice band cannot be more than $\sim$10% in depth so ice particles are not likely driving the high bolometric albedo. The higher $A(\theta)_{bolo}$ is in contrast to the dramatic increase in the numbers of dark (carbonaceous) and smaller particles because the "high color temperatures and blue colors imply the presence of Rayleigh-type scatterers in the ejecta, i.e. either very small grains or BCCA type agglomerates"

(*Bockelée-Morvan et al.* 2017a). Moderately porous particles require steep slopes 4$\leq N \leq 5$, which means submicron a_0=0.1 μm dominate with a mean radius of $a_{mean} \sim$ 0.1 μm. In summary, particles ejected in the outburst are so hot and the color less red so the ejected grain population was dominated very small carbon grains (a_{mean}=0.1 μm).

As stated above, the high bolometric albedo of $\sim$0.6 is not explained by submicron carbonaceous (dark and hot) particles. Somewhat larger moderately porous particles ($a_0 \sim 0.5\mu$m) are in second outburst but the highest values of the bolometric albedo also are not explained. Pure and submicron Mg:Fe olivine grains can account for the bolometric albedo but the modeled compact (P=0) olivine spheres have a color temperature of $<$530 K that is too low to match the observed color temperatures ($>$600 K). If 6 vol% FeS is mixed with Mg:Fe amorphous olivine then the color temperatures increase to 575 K, however the S'_{color} cannot be fitted. BCCA may explain the high color temperatures but certainly not the high albedos during outburst.

Alternatively, there could be two distinct compositions of submicron grains in the outbursts, one that is cold and bright complimented by dark and hot; however, any potential 3 μm ice band cannot be more than 10% band depth from the observations. *Bockelée-Morvan et al.* (2017a) also suggest some limited lifetime organics are mixed with the submicron Mg:Fe amorphous olivine and the rapid degeneration of hypothesized organics may contribute to the enhanced temperatures and enhanced albedos observed during outburst, especially at the onset of the first outburst and the sustained albedo during the second outburst. Next, we discuss other evidence from scattered light data for albedo contributions from limited lifetime organics.

2.5.8. *Scattered light, limited lifetime distributed sources*

Scattered light observations at UV through NIR wavelengths provides constraints on the structure of dust particles. Polarization (*Kolokolova et al.* 2022), the scattered light color, and the surface brightness spatial distribution can provide insights into dust composition for those dust components that contribute to scattered light. Here are some examples that do not involve polarization measurements. Limited-lifetime organic species were discovered following outburst of C/2000 WM1 (LINEAR) and the *Deep Impact* impact of 9P/Tempel 1 because they produce wavelength-dependent scattered light 'colors' (slope in %/nm) akin to a combination of organics created in the laboratory by irradiating ice mixtures (*Jenniskens et al.* 1993). (Limited lifetime species associated with the dust, or 'extended sources' or 'distributed sources' also are known to occur in some comae by the molecular production rates having more extended spatial distributions than the water vapor and these molecules may include CO, formaldehyde (H_2CO), NH_3, and recently discovered C_2H_2 (*Dello Russo et al.* 2021).)

Another metric is the total scattering cross section (SA), related to the number and intrinsic color of the dust particles:

$$\mathrm{SA} = \int (\Sigma\ \mathrm{A}_\lambda(\alpha)\ \mathrm{f})\, \mathrm{d}\rho$$

Tozzi et al. (2004) and *Tozzi et al.* (2015) used this approach to assess limited lifetime dust that contributed the changes in the scattered light for comets C/2000 WM1 (LINEAR) and 9P/Tempel 1. The significant difference between the two comets is that C/2000 WM1 (LINEAR) has a sublimating component that scatters in the visible and 9P/Tempel 1 does not, so nature of the sublimating grains are different between the two comets.

For C/2000 WM1 (LINEAR) at r_h=1.2 au, scalelengths for column densities of limited lifetime organics are assessed for two components with 12250$\pm$1625km and 940$\pm$150km, and adopting a dust velocity $v_{dust} \approx 0.2\ km\ s^{-1}$ implies 1.7 hr and 17 hr coma lifetimes, respectively (*Tozzi et al.* 2004). The scattered light colors were similar to minimally irradiated and long-exposure irradiated organic residues that may be similar to the UV-irradiated residues created on NASA's orbiting Skylab (EURECA (*Li and Greenberg* 1997). An impulsive event offers a better opportunity to assess the changes in surface brightness distribution and color, that then can be used to determine lifetimes in the coma.

Prior to the *Deep Impact* event, 9P/Tempel 1 has a non-sublimating component and sublimating component (with scale length of 6300 km, assuming $v_{dust} \approx 0.2\ km\ s^{-1}$ implies 11 hr at r_h=1.5 au) and these 2 components differ in their IR colors with the sublimating component being redder from J to K_s band but both being inefficient scatterers at visible wavelengths ($\lesssim 0.8\mu$m). Details about post-*Deep Impact* observations include that the color was neutral from J to H band but increases by 25% from H to K_s. Three hours later, the scattering efficiency increases by 84% between J and K_s so the reddening increased but the total brightness declined. Also, there was no correlation in the quiescent coma versus *Deep Impact* ejecta cloud.

One may wish to consider the "quiescent" coma of comet 9P/Tempel 1 with the post*Deep Impact* coma. In the hours following the *Deep Impact* encounter, polarization images uniquely reveal an expanding front of polarizing particles that are not detected in non-polarized images so these particles are submicron-size (from their ejected velocities) and 'dark' carbonaceous grains (*Kadono et al.* 2007). Spatial imaging via IR photometry as well as scattered light colors and structures in the coma reveal properties about the dust but with more degeneracies in the derived dust composition than with IR spectroscopy thermal modeling because of the IR spectral resonances directly probe the composition of the dust particles contributing to the thermal emission for those compositions that have resonances.

3. PHYSICAL PROPERTIES

3.1. Sizes and size distribution

Cometary dust is ejected from the active cometary nuclei and expand in space following initially a quasi-spherical shell within about 10,000 km from the nucleus, named the coma, and further creating an expanding tail in the direction opposite to the Sun as illustrated in Fig. 1 (see e.g. *Finson and Probstein* 1968a). The striae visible in the solar direction of the impressive comet C/2006 P1 McNaught (Fig. 1), named synchrones, represent dust ejected at different times along the orbit of the comet, and that disperse in space due to the effect of the β parameter representing the ratio of the forces of radiation and gravity acting on the dust particles.

$$\beta = \frac{3L_\circ}{16\pi c G M_\circ} \frac{Q_{pr}}{\rho s} \tag{1}$$

where $L_\circ$ and $M_\circ$ are the luminosity and the mass of the Sun, c is the speed of light, G the gravitational constant and Q_{pr} the radiation pressure efficiency of the dust grain having bulk density ρ and an effective radius s. β therefore depends on the dust grain's composition, shape, structure and size but is generally proportional to $\frac{1}{\rho s}$, the small grains being easily pushed away by the radiation pressure, while the largest grains, typically 1 micrometer in size and above, will tend to follow the orbit of the cometary nucleus around the Sun (*Burns et al.* 1979).

The extent of cometary trails is evidence that cometary dust grains present a large range of sizes. Cometary dust size distributions are traditionally estimated by inverting the cometary tails (see e.g. *Finson and Probstein* 1968a). While cometary dust size distributions are typically inverted bin size by bin size, they are canonically represented by a simpler power-law distribution as it represents well the properties of the observed clouds of dust. This is represented as a *Differential Size Distribution* (DSD) with power index, N (also called α). N is related to γ, the power index of the mass distribution of particles by $N = -3\gamma - 1$, assuming a constant density for the particles. If $N > -3$, both the mass and brightness depend on the largest ejected grains. Brightness and mass become decoupled if $-4 < N < -3$ in which case the dust mass depends on the largest ejected grains, while the brightness depends on the micrometer-sized grains (*Fulle* 2004). Typical values for the mean power index, N, range from about -3 to about -4 (See table 1 in *Fulle* 2004, for a review of ground-based derived DSD). But one has to recognize that the actual dust size distributions in comets are more complex and can be quite variable with time and space due to outburst and activity (*Fulle* 1987).

With the advent of space missions to active cometary nuclei, the ground-based observations and models of cometary dust size distributions of the coma are now complemented by direct measurements close to the nucleus, or laboratory measurements from returned samples (see Table 2). However, those measurements cannot directly be compared as their relationship is complicated by fragmentation of particles, sublimation of volatiles, differential speed of ejection, and surface inhomogeneous activity (see *Agarwal et al.* 2007, and references therein).

In situ data on the dust mass distribution was obtained for 1P/Halley by the *Vega 1*, *Vega 2* and *Giotto* missionsin 1986 (*Divine and Newburn* 1988). *McDonnell et al.* (1987) used the dust impact detection system (DIDSY) onboard *Giotto* to derive a double size distribution at the nucleus of 1P/Halley with $N = -4.06$ for small particles ($m < 10^{-8}$ kg) and $N = -3.13$ for larger particles ($m > 10^{-8}$ kg). The average DSD prior to close approach was estimated at the nucleus to be $N = -3.49 \pm 0.15$ (*McDonnell et al.* 1986). *Fulle et al.* (1995) developed a model of 1P/Halley dust emissions to fit the DIDSY fluences and obtained a constant DSD index of $N = -3.5 \pm 0.2$ for grains larger than 20 μm. Later combined models of optical and impact measurements resulted in a value of $N = -2.6 \pm 0.2$ (*Fulle et al.* 2000). The interpretation of Halley data did not lead to a general agreement regarding the dust size distribution at the nucleus of the comet, however it is generally admitted that the coma is dominated by millimetre-sized and larger particles (*Agarwal et al.* 2007). The *Giotto* space mission continued its exploration of comets with a close flyby of comet 26P/Grigg–Skjellerup in 1992. The dust distribution detected in that case corresponds to $N = -1.81$ for particles with mass larger than $m > 10^{-9}$ kg indicating for this comet a coma dominated by large particles (*McDonnell et al.* 1993).

In 2005, the Deep Impact mission collided with comet 9P/Tempel 1, excavating a crater about 150 m large and several 10s of meters deep, which helped decipher the composition and low strength of the near subsurface layers of cometary nuclei. The impact generated a strong ejection of fresh ice and dust particles that was akin to a cometary activity outburst (*A'Hearn et al.* 2005). Similarly, the DSD index measured in the coma after the impact ($N = -4.5 \pm 0.2$ (*Lisse et al.* 2006)) demonstrates a strong increase in the DSD slope as compared to the pre-impact coma value ($N = -3.0 \pm 0.45$ (*Lisse et al.* 2005)) corresponding to a sharp increase in the number of small particles present in the coma liberated by the impact. Evidence from the changes in activity, in gas composition, and in dust particles DSD were used to argue that pristine cometary material was present a few 10s of meters below the surface of cometary nuclei (*A'Hearn et al.* 2005). The Deep Impact mission was then diverted towards comet 103P/Hartley 2. This very active small comet nucleus ejects very large particles, some of which are made of pure water ice (*A'Hearn et al.* 2011). Observations from the ground indicated relatively steep DSD indices, from -3.2 ± 0.1 (*Epifani et al.* 2001) to -3.91 ± 0.3 (*Bauer et al.* 2011). The in situ dust size distribution obtained by the space probe was even steeper with a value ranging from -6.6 to -4.7, but applicable to the largest dust particles sizes detected by photometry, from 1 cm to 20 cm in the case of icy particles (*Kelley et al.* 2013).

In 2006, the *Stardust* mission delivered samples from comet 81P/Wild 2 to Earth for laboratory analysis (*Brownlee et al.* 2006). During the comet fly-by, the Dust Flux Monitor Instrument (DFMI) monitored the dust impacts with a high temporal resolution and gave evidence of fragmentation of dust particles within the coma. The size distributions detected by the probe are quite variable with a best fit value of -3.25 for particle masses lower than 10^{-8} kg at around closest approach, but with values as high as -1.99 and as low as -4.39 depending on the coma region probed (*Tuzzolino et al.* 2004; *Green et al.* 2004). However, additional information could be retrieved from the laboratory analyses of the tracks in the aerogel and the craters on the aluminum foils of the return capsule, using calibrations made on Earth by impacting with analog compact particles. The resulting DSD index corresponds to -2.71 (*Hörz et al.* 2006). Further recalibration on the ground taking into account impacts by aggregates of silica particles slightly revised this value to a lower one of $N = -2.89$ for particles larger than 10 microns, more compatible with the average value given by DFMI (*Price et al.* 2010).

Finally, the *Rosetta* space mission was the only cometary space probe that could survey a comet nucleus over a major part of its orbital trajectory (*Glassmeier et al.* 2007) for a period spanning 2 years and a half. The ground-based size distribution of comet 67P/Churyumov-Gerasimenko was determined to be $N = -3.4 \pm 0.2$ from an average of previous observations since its discovery (*Fulle* 2004, and references therein). During the *Rosetta* mission survey, the dust size distribution showed a strong time-evolution, with the optical cross-section dominated by the largest ejected dust far from perihelion with $N \approx -3$, while the smallest ejected dust dominate around perihelion with $N \approx -3.9$ (*Moreno et al.* 2017).

The *Rosetta* space mission also used its many dust analysis instruments (GIADA, COSIMA, Osiris, ROLIS) to determine the dust size distribution in many complementary size ranges from 1 μm to 1 m. Fig. 14 summarizes the results obtained for all these different measurements before the 2015 equinox, around the perihelion time in August 2015 and the size distribution of boulders on the surface of 2 landing areas studied for Philae. Overall the DSD index measured by *Rosetta* is consistent with an average value around -4, with variations due to the timings of measurements with smaller particles typically ejected around perihelion time.

In addition, over the last five years, the Solar System was visited by 2 interstellar objects (1I/Oumuamua and 2I/Borisov). Fortunately, interstellar comet 2I/Borisov was active enough that its coma and tail could be studied by telescopic observations. In that case, the DSD is also ranging from -3.7 to -4 (see Table 2) which is consistent with most active comets and also 'fresh' comets such as C/1995 O1 (Hale-Bopp) or C/1996 B2 (Hyakutake) (*Fulle* 2004, and references therein)

In summary, cometary dust size distributions usually correspond well to power laws, with typical indices ranging from -3 to -4. However large variations are detected depending on the activity of the nucleus, the timing of measurements and the techniques used. The consistency of all measurements made so far are certainly consistent with probing the DSD of primordial building blocks of comets as the DSD index for active comets is consistent over all types of comets, including 'fresh' ones and even interstellar comet 2I/Borisov.

Further analysis of cometary dust ejected at different times will certainly improve our knowledge of the dust size properties and how they may relate to primordial solar nebula materials.

3.2. Optical and thermal properties

Light scattering has historically been the main provider of information on the physical properties of cometary dust through telescopic studies (for more details see *Kolokolova* 2015; *Kolokolova et al.* 2022) The observations made in several domains have been useful in constraining the size, size distribution, structure and optical indices of the dust particles. The observations in the visible domain have been used to model the extension of the coma and tail of comets (*Haser et al.* 2020; *Finson and Probstein* 1968a,b) and deduce from it the surface activity of the nucleus. In the case of the dust particles in the coma of comet 67P/C-G, they present a specific scattering phase function with a u-shape and minimum at intermediate phase angles. This is different from the phase function that was usually considered for cometary dust (*Kolokolova et al.* 2004). The color is consistent with the average of the nucleus surface below 30° of phase angles. There is negligible phase reddening at phase angles $< 90°$ indicating a coma dominated by single scattering (*Bertini et al.* 2017). Such a phase curve shape may be consistent with crushed primitive meteorites, but even more with analogues developed to simulated the scattering properties of interplanetary dust particles (*Levasseur-Regourd et al.* 2019). Photometric studies of single grains with the OSIRIS camera filters from 535 to 882 nm indicate slopes covering the ranges of slopes detected over the reddest to bluest regions of the nucleus (*Frattin et al.* 2017). Assuming that the majority of dust particles in the zodiacal cloud come from comets, their average geometric albedo towards the Gegenschein has been determined to be 0.06 ± 0.01, similar to the low albedo detected for cometary nuclei (*Ishiguro et al.* 2013).

The coma and tails of comets are astronomical objects that present some of the largest polarization detected in the solar system (for more details see *Kolokolova* 2015; *Kolokolova et al.* 2022). Polarimetric observations of comets give complementary information to the scattering properties of the dust particles, in particular on their optical indices and morphologies. Initial polarimetric observations of comet Halley combined with Mie light scattering simulations and laboratory work comparisons already indicated that the scattering particles were likely large, rough with a low albedo, and it was shown that material from the Orgueil meteorite was a good scattering analogue (*Kikuchi*

Comet	Instrument	DSD index N	Reference
1P/Halley	DIDSY	-3.49 ± 0.15 (avg)	*McDonnell et al.* (1986)
1P/Halley	DIDSY	$-4.06(< 10^{-8}\ kg)$	*McDonnell et al.* (1987)
1P/Halley	DIDSY	$-3.13(> 10^{-8}\ kg)$	*McDonnell et al.* (1987)
1P/Halley	DIDSY	$-3.5 \pm 0.2(> 20\ \mu m)$	*Fulle et al.* (1995)
1P/Halley	OPE + DID	$-2.6 \pm 0.2(> 10^{-12}\ kg)$	*Fulle et al.* (2000)
9P/Tempel 1	IRAS	-3.0 ± 0.45 (pre-impact)	*Lisse et al.* (2005)
9P/Tempel 1	Spitzer	-4.5 ± 0.2 (post-impact)	*Lisse et al.* (2006)
26P/Grigg-Skjellerup	Ground-based	$-4.0 < N < -3.0$	*Fulle* (2004, and references therein)
26P/Grigg-Skjellerup	DIDSY	$-1.81^{+0.39}_{-0.6}$	*McDonnell et al.* (1993)
67P/Churyumov-Gerasimenko	Ground-based	-3.4 ± 0.2 (avg)	*Fulle* (2004, and references therein)
67P/Churyumov-Gerasimenko (far from perihelion)	Ground-based (tail)	-3	*Moreno et al.* (2017)
67P/Churyumov-Gerasimenko (around perihelion)	Ground-based (tail)	$-3.7 < N < -4.3$	*Moreno et al.* (2017)
67P/Churyumov-Gerasimenko	Ground-based (trail)	$-3.6 < N < -4.1$	*Moreno et al.* (2017)
81P/Wild 2	DFMI	-3.25 (closest approach)	*Tuzzolino et al.* (2004); *Green et al.* (2004)
81P/Wild 2	DFMI	$-1.99 < N < -4.39$	*Tuzzolino et al.* (2004); *Green et al.* (2004)
81P/Wild 2	laboratory analysis	$-2.72; -2.89$	*Hörz et al.* (2006); *Price et al.* (2010)
103P/Hartley 2	ISOCAM	-3.2 ± 0.1	*Epifani et al.* (2001)
103P/Hartley 2	WISE/NEOWISE	-3.91 ± 0.3	*Bauer et al.* (2011)
103P/Hartley 2	Deep Impact photometry	$-6.6 < N < -4.7$	*Kelley et al.* (2013)
2I/Borisov	Ground-based	-3.7 ± 1.8	*Guzik et al.* (2020)
2I/Borisov	Ground-based	-4.0 ± 0.3	*Cremonese et al.* (2020)

Table 2: *Summary table of cometary dust size distribution indices N retrieved by space missions and ground-based observations. A full table of N values determined from ground-based observations (range and averages) and models is available in* Fulle *(2004).*

et al. 1988; *Mukai et al.* 1988; *Dollfus* 1989). It was also recognized that polarimetric properties of dust particles were significantly changed during outbursts (*Dollfus et al.* 1988) and varied related to jet structures in the coma when the *Giotto* mission crossed them (*Levasseur-Regourd et al.* 1999). Since then, improved models of cometary dust particles have been developed that may include a diversity of material mixtures (silicates, organics, ices, etc.) and morphologies, such as hollow spheres, irregular particles, spheroids and aggregates thereof (see e.g. *Hanner* 2003; *Min* 2005; *Lasue et al.* 2009; *Kolokolova and Kimura* 2010; *Zubko et al.* 2015, and references therein).

Polarimetric observations of 67P/C-G have been performed during both 2008 and 2015 perihelion passages (*Hadamcik et al.* 2010, 2016; *Rosenbush et al.* 2017). Agglomerates of sub-micrometer-sized grains best fit the higher polarization observed in cometary jets and after fragmentation or disruption events, while a mixture of porous agglomerates of submicrometer-sized Mg-silicates, Fe-silicates, and carbon black grains mixed with compact Mg-silicates grains is generally needed to fit whole comae observations (*Hadamcik et al.* 2006, 2007). Simple geometric shapes of dust particles are generally poor fits to the observational cometary data (*Kolokolova et al.* 2004). Numerical simulations strongly suggest that cometary dust is a mixture of (possibly fractal) agglomerates and of compact particles of both non-absorbing silicate-type materials and more absorbing organic-type materials (see e.g. *Lasue et al.* 2009; *Kiselev et al.* 2015). The variety, structure and size distribution of agglomerates and grains is consistent with the general description of dust particles detected at 67P-C-G by *Rosetta* (*Güttler et al.* 2019; *Mannel et al.* 2019).

Observations in the infrared and thermal wavelength ranges give specific information on the dust particle size distribution and their spatial distribution and dynamics in the cometary coma and tail (*Agarwal et al.* 2007). In the particular case of 67P/C-G, VIRTIS observations of the dust in the coma from 2 to 5 μm, generally show a temperature a few per cents above the equilibrium, but it increases 3 to 4 fold during outbursts. This may be related to the ejection of much smaller dust particles during outbursts (size $<$ 100nm) (*Bockelée-Morvan et al.* 2017a). Such small particles are not detected by other *Rosetta* instruments, indicating a collecting bias or a dearth of such particles in the cometary environment.

A general model of light scattering and emission by dust particles consistent with all the observed constraints remains to be elaborated.

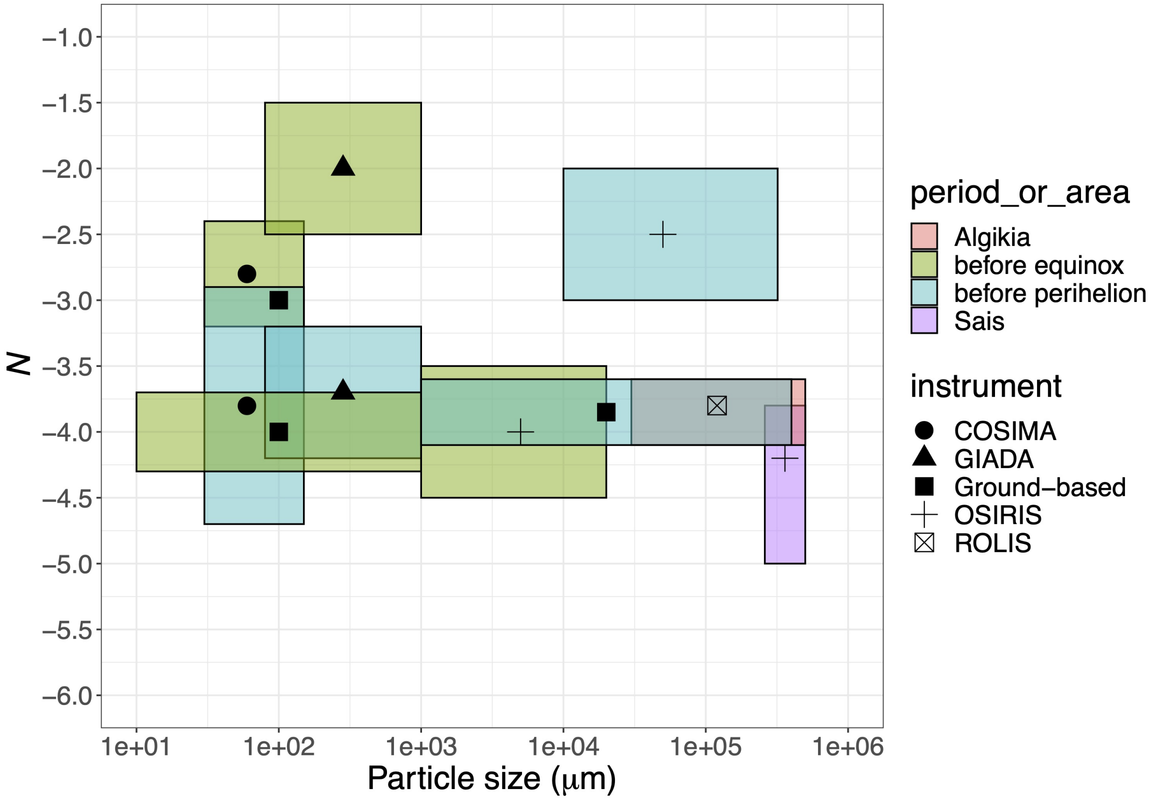

Fig. 14.— *Power index of the differential size distribution of 67P/C-G. Blue rectangles: power index before the 2015 equinox. Green rectangles: power index around the 2015 perihelion. The ranges along the x axis show the instrument size range sensitivity, the ranges along the y axis are given by the uncertainty of the power index. (Data taken from* Merouane et al. *(2017);* Rotundi et al. *(2015);* Fulle et al. *(2016a);* Ott et al. *(2017);* Pajola et al. *(2017);* Moreno et al. *(2017). Figure adapted from* Levasseur-Regourd et al. *(2018)). Agilkia was the initial landing site of Philae, and Sais was the final landing site of the Rosetta spacecraft.*

3.3. Morphology

The morphology of dust particles corresponds to the spatial arrangement of their constituting components and is often described by parameters such as the porosity, which indicates the ratio of voids to occupied volume, or the fractal dimension, a measure of the self-similarity at different scales of the assemblages. It is critical to study the morphology of cometary dust particles as these properties are essential to better understand the physical properties of the dust, such as strength, thermal and light scattering properties of the dust, but may also be witness to the primitive aggregation processes in the primordial nebula. Initially, polarimetric observations of comets have suggested that the basic morphology of cometary dust particles was best explained by including a combination of porous aggregates and more compact dust particles (see e.g. *Lasue et al.* 2009; *Kolokolova* 2015; *Kolokolova et al.* 2022) As the *Stardust* samples were analyzed in the laboratory, the impacts on the aluminium foils and the aerogel demonstrated the presence of both compact and porous, easily fragmented dust particles (*Brownlee* 2014). However, the samples were altered by the speed of collection reaching about 6 m.s^{-1}. IDPs collected from the stratosphere also indicate a diversity of morphologies including very porous fragile aggregates as well as more compact particles, however, the effect of atmospheric traverse, collection by plane and unknown specific origin of the particles makes it difficult to relate their precise morphologies to a particular Solar System body or physics phenomenon (see e.g. *Brownlee* 2016).

To date, the microscopes on-board the *Rosetta* space mission have provided the best in situ morphological analysis of cometary dust particles collected at low speeds of 1 to 15 m.s^{-1} (*Fulle et al.* 2015) and distances from the nucleus lower than 500 km. The scale ranges accessible to both the atomic force microscope MIDAS and the microscope and mass spectrometer COSIMA were < 1 μm to 1 mm with topographic information also available (*Bentley et al.* 2016b; *Mannel et al.* 2019; *Hilchenbach et al.* 2016). These scales also correspond to the smallest (1 μm, *Bentley et al.* (2016b); *Mannel et al.* (2019)) and largest (350 μm, *Langevin et al.* (2016)) particles detected. All particles present textural substructures identified as aggregated monomers which classifies them generally as "compact aggregates" (*Güttler et al.* 2019). Additionally, it has been shown that collected particles have a tendency to breakup as they impact the plates and produce clusters of fragments with a variety of morphologies ranging from shattered, flattened particles to rubble piles (*Langevin et al.* 2016). Such a diverse set of morphologies can originate from a single type of aggregates and be related to different incoming velocities and tensile strength of the particles (*Hornung et al.* 2016; *Ellerbroek et al.* 2017, 2019; *Lasue et al.* 2019). In fact, many compact aggregates analyzed by COSIMA fragmented into smaller constituents during analysis due to electrostatic forces (*Hilchenbach et al.* 2017), demonstrating the relationship between the fragments and their parent compact aggregate particles. Similar fragmentation upon collection have been shown to occur for MIDAS as well (*Bentley et al.* 2016b). The surface features detected by the two microscopes on-board at their respective scales are reminiscent of those found in chondritic porous interplanetary dust particles as illustrated in Fig. 1.

The extension of the morphological analysis to the lowest scales accessible by MIDAS have shown that the smallest aggregate dust particles units are down to 8 nm in size with most of the dust particles being fragile agglomerated dust particles and small micrometer-sized dust particles also formed of those subunits (*Mannel et al.* 2019). A fragile agglomerate was also determined to have a fractal dimension of about 1.7 (*Mannel et al.* 2016) consistent with very fluffy dust particles measured by the impact GIADA instrument (*Fulle et al.* 2015). Even though they do not present a significant fraction of the mass of the cometary nucleus, such fragile particles would not survive most impacts of the early solar system accretion phase and their detection favors an accretion of planetesimals under the gravitational collapse of pebble model (*Fulle and Blum* 2017; *Blum et al.* 2017).

In summary, we find that the cometary dust particles present an apparent scale invariance of properties similar to those that would result from a fractal aggregation process, consistent with the one that would be expected to be at work during the early stages of the planetary formation in the early Solar System (see e.g. *Blum* 2018). The results the microscopes obtained on dust collected from 67P/C-G together with many other in situ measurements by the *Rosetta* space mission provide the first view of the hierarchical structure of dust in comets as reviewed in *Güttler et al.* (2019).

3.4. Tensile strength

Laboratory simulations of macroscopic agglomerates of small silica dust particles (diameters ranging from 0.1 to 10 μm) by ballistic deposition were realized to simulate early aggregation of dust particles similar to the ones forming comets. The tensile strength of such resulting aggregates, the size of which may reach several centimeters, range from 1 to 6 kPa (*Blum and Schräpler* 2004; *Güttler et al.* 2009; *Meisner et al.* 2012). A more realistic set of simulations using silica dust particles and water ice particles under low temperatures ($\approx$ 150 K) showed that the tensile strength decreases linearly with the particles diameter, ranging from 4kPa to 18kPa in agreement with previous estimates (*Gundlach et al.* 2018). Additionally, the experiments demonstrated that under low temperatures, the tensile strength of water ice aggregates was comparable to the data for the silica spheres. This means that at low temperatures water ice presents a specific surface energy similar to the one of silica, which was not expected. Perhaps at temperatures above 150 K, the surface energy of water ice increases steeply, or sintering effects take place. Few direct measurements of the ejected solid material of comets are available, however, the tensile strength of dust particles ejected from 67P/C-G was estimated to be of the order of ≈ 1 kPa from the study of the fragments distribution observed with the COSIMA experiment on-board *Rosetta* (*Hornung et al.* 2016). Similarly, the meteor showers breakup observed in the Earth atmosphere can give estimates of cometary dust tensile strengths since they are associated with parent comets (*Jenniskens and Jenniskens* 2006). The derived tensile strengths are again extremely low, and of the same order of magnitude of the other estimates depending on the parent comet: from 40 to 1000 Pa in *Trigo-Rodríguez and Llorca* (2006) and from 0.4 to 150 kPa as presented in Table 2 of *Blum et al.* (2014). A more detailed synthesis of tensile strength values for cometary materials at different scales of the cometary nucleus can be found in Fig. 10 of *Groussin et al.* (2019).

3.5. Density

The density of cometary dust particles is closely related to their morphology and their porosity, defined as 1 minus the volume filling factor of the particle. As described in §3.3, two main morphological types of dust particles have been detected from cometary ejection: compact dust particles and very fluffy aggregated dust particles following the classification made by *Güttler et al.* (2019). This was seen first by the *Stardust* samples brought back to Earth, where high-speed impacts of 81P/Wild 2 particles generated carrot-like aerogel tracks for compact particles (65% of tracks) and bulbous tracks consistent with the disruption of fluffy aggregates (35% of tracks) (*Brownlee* 2014; *Burchell et al.* 2008; *Trigo-Rodriguez et al.* 2008)

These observations are consistent with the particle detections of GIADA for which compact and fluffy dust particles are detected (*Della Corte et al.* 2015). The strength of the compact particles is consistent with a microporosity ranging from 34% to 85% (*Levasseur-Regourd et al.* 2018). Dust showers observed by GIADA can only be explained by fractal aggregates with dimensions lower than 2 getting fragmented a few meters from the spacecraft (*Fulle et al.* 2015), this represents about 30% of the dust detected (*Fulle and Blum* 2017). MIDAS also detected an extremely porous particle with fractal dimension $D_f = 1.7 \pm 0.1$ which would translate to a porosity around 99% (*Mannel et al.* 2016; *Mannel et al.* 2019; *Fulle and Blum* 2017). Following *Güttler et al.* (2019), fluffy aggregated particles are expected to have a microporosity $> 90\%$. Studies of the mean free path of light through particles fragments detected by COSIMA have also indicated a microporosity $> 50\%$ (*Langevin et al.* 2017).

The GIADA measurements combine both the geometric cross section of the particles and the momentum of impact, which allows to retrieve the average density of the particles. The value obtained over 271 compact particles detections gives $\rho = 785^{+520}_{-115}$ kg m^{-3}, at 1σ confidence level (*Fulle et al.* 2017). With a dust microporosity estimated to be $59 \pm 8\%$, this corresponds to a bulk density of compacted and dried dust of 1925^{+2030}_{-560} kg m^{-3}, at 1σ (*Fulle et al.* 2017). Additionally, a significant fraction of dust particles detected by GIADA has a bulk density larger than 4000 kg m^{-3}. Those are interpreted as single grain minerals similar to single mineral tracks in *Stardust* (*Burchell et al.* 2008).

3.6. Electrical properties

As dust particles are ejected from a comet, they get exposed to space plasma and UV radiations and become electrically charged, which influences their motion (*Horányi* 1996). While there were evidence of particle charging in the coma of 1P/Halley from the calculations of particles trajectories (*Ellis and Neff* 1991), the *Rosetta* mission provided the first direct evidence of electrically charged nanodust particles in a cometary coma (*Burch et al.* 2015; *LLera et al.* 2020). It is typically estimated that a 10^{-19} kg dust particle will be disrupted by its charging if its tensile strength is less than about 0.5 MPa (*Mendis and Horányi* 2013).

The dust showers detected by GIADA have been modelled in terms of mm-sized fluffy dust aggregates charged by the flux of secondary electrons from the spacecraft decreasing their electric potential by 7 to 15V (*Fulle et al.* 2015). The particles are disrupted by their interaction with the electric field of the spacecraft, their deceleration provides the appropriate kinetic energy to explain the RPC/IES charged nanodust detections of 0.2 to 20keV (*Fulle et al.* 2016b). The predicted fractal dimension of such fluffy aggregates is about 2, consistent with the fractal dimensions measured by MIDAS on some particles (*Mannel et al.* 2016; *Mannel et al.* 2019, $D_f = 1.7 \pm 0.1$).

4. DISCUSSION

Analysis of the 81P/Wild 2 coma grains in particular has revealed how similar inorganic comet solids are to some asteroidal materials, at least for comet Wild 2. The observation of crystalline silicates in Hale-Bopp, and the presence in the coma of comet Wild 2 of a significant fraction of coarse-grained inorganic mineral grains, including very refractory materials, was largely unexpected, and has profoundly influenced models of early solar system dynamics. The apparent lack of a significant fraction of amorphous and presolar materials in Wild 2 was another surprise, although the collection process in aerogel may have significantly destroyed these materials. The nature of cometary organics was not a major goal of the *Stardust* mission, and thus great uncertainty remains for this topic. The *Rosetta* mission contributed to the analysis of cometary organics, confirming that cometary particles can contain a large proportion of organics (as first seen in the CHON grains in comet Halley), and that this organic matter bears some similarities with the refractory organics present in carbonaceous chondrites. The organic matter present in CA-IDPs also bear similarities with that of carbonaceous chondrites, as for two of the three organic phases identified in UCAMMs. The formation of the N-rich organic phase in UCAMMs could have been made by irradiation of N-rich ices in the outer regions of the protoplanetary disk, by Galactic cosmic rays. The timing of the mineral incorporation in the ices/organic matter of cometary dust is however not fully understood yet. Cometary dust (or the ice that initially contained it) also carry soluble organics like amino acids. Cometary dust thus probably significantly contributed to the input of prebiotic matter on the early Earth. The presence of a "continuum" between asteroidal and cometary matter is now considered seriously, asteroidal components being found in cometary material, and cometary activity being observed in asteroids (main-belt comets). The formation and incorporation mechanisms of mineral and organic components in comets are not yet fully understood. Thus, despite great recent progress in our understanding of comets, critical gaps remain concerning the formation and processing of organics, condensation of inorganic volatiles, nature and role of presolar dust in the evolution of early nebular solids, timing and location of condensation and processing of cometary materials, possible role of radiogenic nuclides including ^{26}Al. In particular the dream of a cryogenic sample return from a comet nucleus remains just that - a dream.

Acknowledgments

The micrometeorite collections are performed thanks to the logistic support of IPEV and PNRA. C. E. ackowledges the support in France of ANR COMETOR (ANR -18-CE31-0011-0), CNRS, LabEx P2IO, DIM-ACAV+ and CNES. M.E.Z. thanks NASA for support of astromaterials research and curation, and the Cosmic Dust Program and *Stardust* Mission.

REFERENCES

Agarwal J., Müller M., and Grün E. (2007) *Dust environment modelling of comet 67p/churyumov-gerasimenko*, *Space Science Reviews*, *128*, 79–131.

A'Hearn M. F., Belton M. J. S., Delamere W. A., Feaga L. M., Hampton D., Kissel J., Klaasen K. P., McFadden L. A., Meech K. J., Melosh H. J., Schultz P. H., Sunshine J. M., Thomas P. C., Veverka J., Wellnitz D. D., Yeomans D. K., Besse S., Bodewits D., Bowling T. J., Carcich B. T., Collins S. M., Farnham T. L., Groussin O., Hermalyn B., Kelley M. S., Kelley M. S., Li J.-Y., Lindler D. J., Lisse C. M., McLaughlin S. A., Merlin F., Protopapa S., Richardson J. E., and Williams J. L. (2011) *EPOXI at Comet Hartley 2*, *Science*, *332*, 1396.

A'Hearn M. F., Belton M. J. S., Delamere W. A., Kissel J., Klaasen K. P., McFadden L. A., Meech K. J., Melosh H. J., Schultz P. H., Sunshine J. M., Thomas P. C., Veverka J., Yeomans D. K., Baca M. W., Busko I., Crockett C. J., Collins S. M., Desnoyer M., Eberhardy C. A., Ernst C. M., Farnham

T. L., Feaga L., Groussin O., Hampton D., Ipatov S. I., Li J.-Y., Lindler D., Lisse C. M., Mastrodemos N., Owen W. M., Richardson J. E., Wellnitz D. D., and White R. L. (2005) *Deep Impact: Excavating Comet Tempel 1*, *Science*, *310*, 258–264.

A'Hearn M. F., Bodewits D., La Forgia F., Lara L. M., Agarwal J., Bertaux J.-L., Cremonese G., Davidsson B., Fornasier S., Güttler C., Knollenberg J., Lazzarin M., Leyrat C., Lin Z.-Y., Magrin S., Naletto G., Sierks H., Snodgrass C., Thomas N., Tubiana C., and Vincent J.-B. (2015) *Rotational Variation of Outgassing Morphology in 67P/Churyumov-Gerasimenko*, *IAU General Assembly*, *22*, 57858.

Aléon J., Engrand C., Leshin L. A., and McKeegan K. D. (2009) *Oxygen isotopic composition of chondritic interplanetary dust particles: A genetic link between carbonaceous chondrites and comets*, *Geochimica et Cosmochimica Acta*, *73*, 4558–4575.

Aleon J., Engrand C., Robert F., and Chaussidon M. (2001) *Clues to the origin of interplanetary dust particles from the isotopic study of their hydrogen-bearing phases*, *Geochimica et Cosmochimica Acta*, *65*, 4399–4412.

Aleon J., Robert F., Chaussidon M., and Marty B. (2003) *Nitrogen isotopic composition of macromolecular organic matter in interplanetary dust particles*, *Geochimica et Cosmochimica Acta*, *67*, 3773–3783.

Alexander C. M. O., Bowden R., Fogel M. L., Howard K. T., Herd C. D. K., and Nittler L. R. (2012) *The provenances of asteroids, and their contributions to the volatile inventories of the terrestrial planets*, *Science*, *337*, 721–723.

Alexander C. M. O. D., Cody G. D., De Gregorio B. T., Nittler L. R., and Stroud R. M. (2017) *The nature, origin and modification of insoluble organic matter in chondrites, the major source of Earth's C and N*, *Chemie der Erde / Geochemistry*, *77*, 227–256.

Alexander C. M. O. D., Fogel M., Yabuta H., and Cody G. D. (2007) *The origin and evolution of chondrites recorded in the elemental and isotopic compositions of their macromolecular organic matter*, *Geochim. Cosmochim. Acta*, *71*, 4380–4403.

Altwegg K., Balsiger H., Bar-Nun A., Berthelier J.-J., Bieler A., Bochsler P., Briois C., Calmonte U., Combi M. R., Cottin H., Keyser J. D., Dhooghe F., Fiethe B., Fuselier S. A., Gasc S., Gombosi T. I., Hansen K. C., Haessig M., Jäckel A., Kopp E., Korth A., Roy L. L., Mall U., Marty B., Mousis O., Owen T., Rème H., Rubin M., Sémon T., Tzou C.-Y., Waite J. H., and Wurz P. (2016) *Prebiotic chemicals – amino acid and phosphorus – in the coma of comet 67P/Churyumov-Gerasimenko*, *Science Advances*, *2*, e1600285.

Altwegg K., Balsiger H., Berthelier J., Bieler A., Calmonte U., Fuselier S., Goesmann F., Gasc S., Gombosi T. I., Le Roy L., de Keyser J., Morse A., Rubin M., Schuhmann M., Taylor M. G. G. T., Tzou C.-Y., and Wright I. (2017) *Organics in comet 67P – a first comparative analysis of mass spectra from ROSINA–DFMS, COSAC and Ptolemy*, *Monthly Notices of the Royal Astronomical Society*, *469*, S130–S141.

Altwegg K., Balsiger H., Hänni N., Rubin M., Schuhmann M., Schroeder I., Sémon T., Wampfler S., Berthelier J.-J., Briois C., Combi M., Gombosi T. I., Cottin H., De Keyser J., Dhooghe F., Fiethe B., and Fuselier S. A. (2020) *Evidence of ammonium salts in comet 67P as explanation for the nitrogen depletion in cometary comae*, *Nature Astronomy*.

Amari S., Hoppe P., Zinner E., and Lewis R. S. (1993) *The isotopic compositions and stellar sources of meteoritic graphite grains*, *Nature*, *365*, 806–809.

Augé B., Dartois E., Engrand C., Duprat J., Godard M., Delauche L., Bardin N., Mejía C., Martinez R., Muniz G., Domaracka A., Boduch P., and Rothard H. (2016) *Irradiation of nitrogen-rich ices by swift heavy ions - clues for the formation of ultracarbonaceous micrometeorites*, *Astronomy & Astrophysics*, *592*, A99.

Bardyn A., Baklouti D., Cottin H., Fray N., Briois C., Paquette J., Stenzel O., Engrand C., Fischer H., Hornung K., Isnard R., Langevin Y., Lehto H., Le Roy L., Ligier N., Merouane S., Modica P., Orthous-Daunay F.-R., Rynö J., Schulz R., Silén J., Thirkell L., Varmuza K., Zaprudin B., Kissel J., and Hilchenbach M. (2017) *Carbon-rich dust in comet 67P/Churyumov-Gerasimenko measured by COSIMA/Rosetta*, *Monthly Notices of the Royal Astronomical Society*, *469*, S712–S722.

Bastien R., Broce S., Brown P., Burkett P. J., Campbell-Brown M., Frank D., Gearheart D., Kapitzke M., Moes T., Rodriguez M., Steel D., Williams T., and Zolensky M. E. (2013) in *44th Annual Lunar and Planetary Science Conference*, Lunar and Planetary Science Conference, p. 1622.

Bauer J. M., Walker R. G., Mainzer A. K., Masiero J. R., Grav T., Dailey J. W., McMillan R. S., Lisse C. M., Fernández Y. R., Meech K. J., Pittichova J., Blauvelt E. K., Masci F. J., A'Hearn M. F., Cutri R. M., Scotti J. V., Tholen D. J., DeBaun E., Wilkins A., Hand E., and and E. L. W. (2011) *WISE/NEOWISE Observations of Comet 103P/Hartley 2*, *The Astrophysical Journal*, *738*, 171.

Begemann B., Dorschner J., Henning T., Mutschke H., and Thamm E. (1994) *A Laboratory Approach to the Interstellar Sulfide Dust Problem*, *Astrophysical Journal Letters*, *423*, L71.

Benna M., Mahaffy P. R., Grebowsky J. M., Plane J. M. C., Yelle R. V., and Jakosky B. M. (2015) *Metallic ions in the upper atmosphere of mars from the passage of comet c/2013 a1 (siding spring)*, *Geophysical Research Letters*, *42*, 4670–4675.

Bentley M. S., Arends H., Butler B., Gavira J., Jeszenszky H., Mannel T., Romstedt J., Schmied R., and Torkar K. (2016a) *MIDAS: Lessons learned from the first spaceborne atomic force microscope*, *Acta Astronautica*, *125*, 11 – 21.

Bentley M. S., Schmied R., Mannel T., Torkar K., Jeszenszky H., Romstedt J., Levasseur-Regourd A.-C., Weber I., Jessberger E. K., and Ehrenfreund P. (2016b) *Aggregate dust particles at comet 67P/Churyumov–Gerasimenko*, *Nature*, *537*, 73–75.

Berger E. L., Zega T. J., Keller L. P., and Lauretta D. S. (2011) *Evidence for aqueous activity on comet 81P/Wild 2 from sulfide mineral assemblages in Stardust samples and CI chondrites*, *Geochimica et Cosmochimica Acta*, *75*, 3501–3513.

Bergin E. A., Blake G. A., Ciesla F., Hirschmann M. M., and Li J. (2015) *Tracing the ingredients for a habitable earth from interstellar space through planet formation*, *Proceedings of the National Academy of Science*, *112*, 8965–8970.

Bertini I., La Forgia F., Tubiana C., Güttler C., Fulle M., Moreno F., Frattin E., Kovacs G., Pajola M., Sierks H., Barbieri C., Lamy P., Rodrigo R., Koschny D., Rickman H., Keller H. U., Agarwal J., A'Hearn M. F., Barucci M. A., Bertaux J.-L., Bodewits D., Cremonese G., Da Deppo V., Davidsson B., Debei S., De Cecco M., Drolshagen E., Ferrari S., Ferri F., Fornasier S., Gicquel A., Groussin O., Gutierrez P. J., Hasselmann P. H., Hviid S. F., Ip W.-H., Jorda L., Knollenberg J., Kramm J. R., Kührt E., Küppers M., Lara L. M., Lazzarin M., Lin Z.-Y., Moreno J. J. L., Lucchetti A., Marzari F., Massironi M., Mottola S., Naletto G., Oklay N., Ott T., Penasa L., Thomas N., and Vincent J.-B. (2017) *The scattering phase function of comet 67P/Churyumov–Gerasimenko coma as seen from the Rosetta/OSIRIS instrument*, *Monthly Notices of the Royal As-*

tronomical Society, *469*, S404–S415.

Blum J. (2018) *Dust evolution in protoplanetary discs and the formation of planetesimals*, *Space Science Reviews*, *214*, 52.

Blum J., Gundlach B., Krause M., Fulle M., Johansen A., Agarwal J., Von Borstel I., Shi X., Hu X., and Bentley M. S. (2017) *Evidence for the formation of comet 67P/Churyumov-Gerasimenko through gravitational collapse of a bound clump of pebbles*, *Monthly Notices of the Royal Astronomical Society*, *469*, S755–S773.

Blum J., Gundlach B., Mühle S., and Trigo-Rodriguez J. M. (2014) *Comets formed in solar-nebula instabilities!–An experimental and modeling attempt to relate the activity of comets to their formation process*, *Icarus*, *235*, 156–169.

Blum J. and Schräpler R. (2004) *Structure and mechanical properties of high-porosity macroscopic agglomerates formed by random ballistic deposition*, *Physical review letters*, *93*, 115503.

Bockelée-Morvan D., Brooke T. Y., and Crovisier J. (1995) *On the origin of the 3.2 to 3.6-micron emission features in comets.*, *Icarus*, *116*, 18–39.

Bockelée-Morvan D., Rinaldi G., Erard S., Leyrat C., Capaccioni F., Drossart P., Filacchione G., Migliorini A., Quirico E., Mottola S., Tozzi G., Arnold G., Biver N., Combes M., Crovisier J., Longobardo A., Blecka M., and Capria M. T. (2017a) *Comet 67P outbursts and quiescent coma at 1.3 au from the Sun: dust properties from Rosetta/VIRTIS-H observations*, *Mon. Not. R. Astron. Soc.*, *469*, S443–S458.

Bockelée-Morvan D., Rinaldi G., Erard S., Leyrat C., Capaccioni F., Drossart P., Filacchione G., Migliorini A., Quirico E., Mottola S., Tozzi G., Arnold G., Biver N., Combes M., Crovisier J., Longobardo A., Blecka M., and Capria M. T. (2017b) *Erratum: Comet 67P outbursts and quiescent coma at 1.3 AU from the Sun: dust properties from Rosetta/VIRTIS-H observations*, *Mon. Not. R. Astron. Soc.*, *469*, S842–S843.

Bohren C. F. and Huffman D. R. (1983) *Absorption and scattering of light by small particles*, New York: Wiley.

Bonal L., Quirico E., Montagnac G., and Reynard B. (2006) *Interplanetary dust particles: Organic matter studied by raman spectroscopy and laser induced fluorescence*, *37th Annual Lunar and Planetary Science Conference*, *37*, 2271.

Bonev B. P., Dello Russo N., DiSanti M. A., Martin E. C., Doppmann G., Vervack J., Ronald J., Villanueva G. L., Kawakita H., Gibb E. L., Combi M. R., Roth N. X., Saki M., McKay A. J., Cordiner M. A., Bodewits D., Crovisier J., Biver N., Cochran A. L., Shou Y., Khan Y., and Venkataramani K. (2021) *First Comet Observations with NIRSPEC-2 at Keck: Outgassing Sources of Parent Volatiles and Abundances Based on Alternative Taxonomic Compositional Baselines in 46P/Wirtanen*, *Planetary Science Journal*, *2*, 45.

Bradley J. (1994a) in *Analysis of Interplanetary Dust, AIP Conf. Proc.* (M. Zolensky, T. Wilson, F. Rietmeijer, and G. J. Flynn, eds.), vol. 310, pp. 89–104, Amer. Inst. Physics Press, New York.

Bradley J. P. (1994b) *Chemically anomalous preaccretionally irradiated grains in interplanetary dust from comets*, *Science*, *265*, 925–929.

Bradley J. P. (1994) *Nanometer-scale mineralogy and petrography of fine-grained aggregates in anhydrous interplanetary dust particles*, *Geochim. Cosmochim. Acta*, *58*, 2123–2134.

Bradley J. P. (2013) *How and where did GEMS form?*, *Geochim. Cosmochim. Acta*, *107*, 336–340.

Bradley J. P. and Brownlee D. E. (1986) *Cometary particles - thin sectioning and electron beam analysis*, *Science*, *231*, 1542–1544.

Bradley J. P., Germani M. S., and Brownlee D. E. (1989) *Automated thin-film analyses of anhydrous interplanetary dust particles in the analytical electron microscope*, *EPSL*, *93*, 1–13.

Bradley J. P., Holland H. D., and Turekian K. K. (2014) *1.8 - Early Solar Nebula Grains –Interplanetary Dust Particles*, pp. 287–308, Elsevier, Oxford.

Bradley J. P., Humecki H. J., and Germani M. S. (1992) *Combined infrared and analytical electron microscope studies of interplanetary dust particles*, *Astrophys. J.*, *394*, 643–651.

Bradley J. P., Keller L. P., Snow T. P., Hanner M. S., Flynn G. J., Gezo J. C., Clemett S. J., Brownlee D. E., and Bowey J. E. (1999) *An infrared spectral match between gems and interstellar grains*, *Science*, *285*, 1716–1718.

Bregman J. D., Witteborn F. C., Allamandola L. J., Campins H., Wooden D. H., Rank D. M., Cohen M., and Tielens A. G. G. M. (1987) *Airborne and groundbased spectrophotometry of comet P/Halley from 5-13 micrometers*, *Astron. Astrophys.*, *187*, 616–620.

Bridges J. C., Changela H. G., Nayakshin S., Starkey N. A., and Franchi I. A. (2012) *Chondrule fragments from comet wild2: Evidence for high temperature processing in the outer solar system*, *Earth and Planetary Science Letters*, *341–344*, 186–194.

Bridges J. C., Hicks L. J., MacArthur J. L., Price M. C., Burchell M. J., Franchi I. A., and Gurman S. J. (2015) in *European Planetary Science Congress*, pp. EPSC2015–866.

Brownlee D. (2014) *The Stardust Mission: Analyzing Samples from the Edge of the Solar System*, *Annual Review of Earth and Planetary Sciences*, *42*, 179–205.

Brownlee D., Joswiak D., Schlutter D., Pepin R., Bradley J., and Love S. (1995) in *Lunar and Planetary Science Conference*, vol. 26.

Brownlee D., Tsou P., Aléon J., Alexander C. M. O., Araki T., Bajt S., Baratta G. A., Bastien R., Bland P., Bleuet P., Borg J., Bradley J. P., Brearley A., Brenker F., Brennan S., Bridges J. C., Browning N. D., Brucato J. R., Bullock E., Burchell M. J., Busemann H., Butterworth A., Chaussidon M., Cheuvront A., Chi M., Cintala M. J., Clark B. C., Clemett S. J., Cody G., Colangeli L., Cooper G., Cordier P., Daghlian C., Dai Z., D'Hendecourt L., Djouadi Z., Dominguez G., Duxbury T., Dworkin J. P., Ebel D. S., Economou T. E., Fakra S., Fairey S. A. J., Fallon S., Ferrini G., Ferroir T., Fleckenstein H., Floss C., Flynn G., Franchi I. A., Fries M., Gainsforth Z., Gallien J.-P., Genge M., Gilles M. K., Gillet P., Gilmour J., Glavin D. P., Gounelle M., Grady M. M., Graham G. A., Grant P. G., Green S. F., Grossemy F., Grossman L., Grossman J. N., Guan Y., Hagiya K., Harvey R., Heck P., Herzog G. F., Hoppe P., Hörz F., Huth J., Hutcheon I. D., Ignatyev K., Ishii H., Ito M., Jacob D., Jacobsen C., Jacobsen S., Jones S., Joswiak D., Jurewicz A., Kearsley A. T., Keller L. P., Khodja H., Kilcoyne A. D., Kissel J., Krot A., Langenhorst F., Lanzirotti A., Le L., Leshin L. A., Leitner J., Lemelle L., Leroux H., Liu M.-C., Luening K., Lyon I., MacPherson G., Marcus M. A., Marhas K., Marty B., Matrajt G., McKeegan K., Meibom A., Mennella V., Messenger K., Messenger S., Mikouchi T., Mostefaoui S., Nakamura T., Nakano T., Newville M., Nittler L. R., Ohnishi I., Ohsumi K., Okudaira K., Papanastassiou D. A., Palma R., Palumbo M. E., Pepin R. O., Perkins D., Perronnet M., Pianetta P., Rao W., Rietmeijer F. J. M., Robert F., Rost D., Rotundi A., Ryan R., Sandford S. A., Schwandt C. S., See T. H., Schlutter D., Sheffield-Parker J., Simionovici A., Simon S., Sitnitsky

I., Snead C. J., Spencer M. K., Stadermann F. J., Steele A., Stephan T., Stroud R., Susini J., Sutton S. R., Suzuki Y., Taheri M., Taylor S., Teslich N., Tomeoka K., Tomioka N., Toppani A., Trigo-Rodríguez J. M., Troadec D., Tsuchiyama A., Tuzzolino A. J., Tyliszczak T., Uesugi K., Velbel M., Vellenga J., Vicenzi E., Vincze L., Warren J., Weber I., Weisberg M., Westphal A. J., Wirick S., Wooden D., Wopenka B., Wozniakiewicz P., Wright I., Yabuta H., Yano H., Young E. D., Zare R. N., Zega T., Ziegler K., Zimmerman L., Zinner E., and Zolensky M. (2006) *Comet 81P/Wild 2 Under a Microscope*, *Science*, *314*, 1711–1716.

Brownlee D. E. (2016) *Cosmic Dust: Building Blocks of Planets Falling from the Sky*, *Elements*, *12*, 165–170.

Brownlee D. E. and Joswiak D. J. (2017) *Diversity of the initial rocky planetary building materials at the edge of the solar system*, *Meteoritics and Planetary Science*, *52*, 471–478.

Brownlee D. E., Tomandl D. A., and Olszewski E. (1977) *Interplanetary dust - a new source of extraterrestrial material for laboratory studies*, *Lunar and Planetary Science Conference Proceedings*, *8*, 149–160.

Brunetto R., Borg J., Dartois E., Rietmeijer F. J. M., Grossemy F., Sandt C., Le Sergeant d'Hendecourt L., Rotundi A., Dumas P., Djouadi Z., and Jamme F. (2011) *Mid-IR, Far-IR, Raman micro-spectroscopy, and FESEM-EDX study of IDP L2021C5: Clues to its origin*, *Icarus*, *212*, 896–910.

Burch J. L., Gombosi T. I., Clark G., Mokashi P., and Goldstein R. (2015) *Observation of charged nanograins at comet 67P/Churyumov-Gerasimenko*, *Geophysical Research Letters*, *42*, 6575–6581.

Burchell M. J., Fairey S. A. J., Wozniakiewicz P., Brownlee D. E., Hoerz F., Kearsley A. T., See T. H., Tsou P., Westphal A., Green S. F., Trigo-Rodriguez J. M., and Dominguez G. (2008) *Characteristics of cometary dust tracks in stardust aerogel and laboratory calibrations*, *Meteoritics and Planetary Science*, *43*, 23–40.

Burns J. A., Lamy P. L., and Soter S. (1979) *Radiation forces on small particles in the solar system*, *Icarus*, *40*, 1–48.

Busemann H., Alexander C. M. O., and Nittler L. R. (2007) *Characterization of insoluble organic matter in primitive meteorites by microraman spectroscopy*, *Meteoritics and Planetary Science*, *42*, 1387–1416.

Busemann H., Nguyen A. N., Cody G. D., Hoppe P., Kilcoyne A. L. D., Stroud R. M., Zega T. J., and Nittler L. R. (2009) *Ultra-primitive interplanetary dust particles from the comet 26P/Grigg-Skjellerup dust stream collection*, *Earth and Planetary Science Letters*, *288*, 44–57.

Campins H. and Ryan E. V. (1989) *The identification of crystalline olivine in cometary silicates*, *Astrophys. J.*, *341*, 1059–1066.

Capaccioni F., Coradini A., Filacchione G., Erard S., Arnold G., Drossart P., Sanctis M. C. D., Bockelee-Morvan D., Capria M. T., Tosi F., Leyrat C., Schmitt B., Quirico E., Cerroni P., Mennella V., Raponi A., Ciarniello M., McCord T., Moroz L., Palomba E., Ammannito E., Barucci M. A., Bellucci G., Benkhoff J., Bibring J. P., Blanco A., Blecka M., Carlson R., Carsenty U., Colangeli L., Combes M., Combi M., Crovisier J., Encrenaz T., Federico C., Fink U., Fonti S., Ip W. H., Irwin P., Jaumann R., Kuehrt E., Langevin Y., Magni G., Mottola S., Orofino V., Palumbo P., Piccioni G., Schade U., Taylor F., Tiphene D., Tozzi G. P., Beck P., Biver N., Bonal L., Combe J.-P., Despan D., Flamini E., Fornasier S., Frigeri A., Grassi D., Gudipati M., Longobardo A., Markus K., Merlin F., Orosei R., Rinaldi G., Stephan K., Cartacci M., Cicchetti A., Giuppi S., Hello Y., Henry F., Jacquinod S., Noschese R., Peter G., Politi R., Reess J. M., and Semery A. (2015) *The organic-rich surface of comet 67P/Churyumov-Gerasimenko as seen by VIRTIS/Rosetta*, *Science*, *347*, aaa0628.

Carrillo-Sánchez J. D., Nesvorný D., Pokorný P., Janches D., and Plane J. M. C. (2016) *Sources of cosmic dust in the earth's atmosphere*, *Geophysical Research Letters*, *43*, 11,979–11,986.

Charon E., Engrand C., Benzerara K., Leroux H., Swaraj S., Belkhou R., Duprat J., Dartois E., Godard M., and Delauche L. (2017) in *48th Annual Lunar and Planetary Science Conference*, Lunar and Planetary Science Conference, p. 2085.

Chi M., Ishii H. A., Simon S. B., Bradley J. P., Dai Z., Joswiak D., Browning N. D., and Matrajt G. (2009) *The origin of refractory minerals in comet 81P/Wild 2*, *Geochimica et Cosmochimica Acta*, *73*, 7150–7161.

Chihara H., Koike C., and Tsuchiyama A. (2001) *Low-Temperature Optical Properties of Silicate Particles in the Far-Infrared Region*, *Publications of the Astronomical Society of Japan*, *53*, 243–250.

Chihara H., Koike C., Tsuchiyama A., Tachibana S., and Sakamoto D. (2002) *Compositional dependence of infrared absorption spectra of crystalline silicates. I. Mg-Fe pyroxenes*, *Astron. Astrophys.*, *391*, 267–273.

Clairemidi J., Moreels G., Mousis O., and Bréchignac P. (2008) *Identification of anthracene in Comet 1P/Halley*, *Astronomy & Astrophysics*, *492*, 245–250.

Clark B. C., Green S. F., Economou T. E., Sandford S. A., Zolensky M. E., McBride N., and Brownlee D. E. (2004) *Release and fragmentation of aggregates to produce heterogeneous, lumpy coma streams*, *Journal of Geophysical Research (Planets)*, *109*, E12S03.

Clemett S. J., Sandford S. A., Nakamura-Messenger K., Hörz F., and McKay D. S. (2010) *Complex aromatic hydrocarbons in Stardust samples collected from comet 81P/Wild 2*, *Meteoritics and Planetary Science*, *45*, 701–722.

Cremonese G., Fulle M., Cambianica P., Munaretto G., Capria M. T., Forgia F. L., Lazzarin M., Migliorini A., Boschin W., Milani G., Aletti A., Arlic G., Bacci P., Bacci R., Bryssinck E., Carosati D., Castellano D., Buzzi L., Rubbo S. D., Facchini M., Guido E., Kugel F., Ligustri R., Maestripieri M., Mantero A., Nicolas J., Ochner P., Perrella C., Trabatti R., and Valvasori A. (2020) *Dust Environment Model of the Interstellar Comet 2I/Borisov*, *The Astrophysical Journal*, *893*, L12.

Crovisier J. and Bockelée-Morvan D. (2008) *Comment on "Comparison of the composition of the Tempel 1 ejecta to the dust in Comet C/Hale Bopp 1995 O1 and YSO HD 100546" by C.M. Lisse, K.E. Kraemer, J.A. Nuth III, A. Li, D. Joswiak [2007. Icarus 187, 69 86]*, *Icarus*, *195*, 938–940.

Crovisier J., Leech K., Bockelee-Morvan D., Brooke T. Y., Hanner M. S., Altieri B., Keller H. U., and Lellouch E. (1997) *The spectrum of comet Hale-Bopp (C/1995 O1) observed with the infrared space observatory at 2.9 astronomical units from the sun.*, *Science*, *275*, 1904–1907.

Dartois E., Engrand C., Brunetto R., Duprat J., Pino T., Quirico E., Remusat L., Bardin N., Briani G., Mostefaoui S., Morinaud G., Crane B., Szwec N., Delauche L., Jamme F., Sandt C., and Dumas P. (2013) *UltraCarbonaceous Antarctic micrometeorites, probing the Solar System beyond the nitrogen snow-line*, *Icarus*, *224*, 243–252.

Dartois E., Engrand C., Duprat J., Godard M., Charon E., Delauche L., Sandt C., and Borondics F. (2018) *Dome C ultracarbonaceous Antarctic micrometeorites. Infrared and Raman fin-*

gerprints, *Astronomy & Astrophysics*, *609*, A65.

Dartois E., Geballe T. R., Pino T., Cao A.-T., Jones A., Deboffle D., Guerrini V., Bréchignac P., and D'Hendecourt L. (2007) *IRAS 08572+3915: constraining the aromatic versus aliphatic content of interstellar HACs*, *Astron. Astrophys.*, *463*, 635–640.

Davies J. K. and Barrera L. H. (2004) *The first decadal review of the Edgeworth-Kuiper Belt*, vol. 92.

De Gregorio B. T., Stroud R. M., Cody G. D., Nittler L. R., David Kilcoyne A. L., and Wirick S. (2011) *Correlated microanalysis of cometary organic grains returned by stardust*, *Meteoritics and Planetary Science*, *46*, 1376–1396.

De Gregorio B. T., Stroud R. M., Nittler L. R., Alexander C. M. O., Kilcoyne A. L. D., and Zega T. J. (2010) *Isotopic anomalies in organic nanoglobules from comet 81p/wild 2: Comparison to murchison nanoglobules and isotopic anomalies induced in terrestrial organics by electron irradiation*, *Geochimica et Cosmochimica Acta*, *74*, 4454–4470.

De Gregorio B. T., Stroud R. M., Nittler L. R., and Kilcoyne A. L. D. (2017) *Evidence for Reduced, Carbon-rich Regions in the Solar Nebula from an Unusual Cometary Dust Particle*, *The Astrophysical Journal*, *848*, 113.

Defouilloy C., Nakashima D., Joswiak D. J., Brownlee D. E., Tenner T. J., and Kita N. T. (2017) *Origin of crystalline silicates from Comet 81P/Wild 2: Combined study on their oxygen isotopes and mineral chemistry*, *Earth and Planetary Science Letters*, *465*, 145–154.

Della Corte V., Rotundi A., Fulle M., Gruen E., Weissman P., Sordini R., Ferrari M., Ivanovski S., Lucarelli F., and Accolla M. (2015) *GIADA: Shining a light on the monitoring of the comet dust production from the nucleus of 67P/Churyumov-Gerasimenko*, *Astronomy & Astrophysics*, *583*, A13.

Dello Russo N., Vervack R., Kawakita H., Bonev B., Di Santi M., Gibb E., McKay A., Cochran A., Weaver H., Biver N., Crovisier J., Bockelee-Morvan D., Kobayashi H., Harris W., Roth N., Saki M., and Khan Y. (2021) in *AAS/Division for Planetary Sciences Meeting Abstracts*, vol. 53 of *AAS/Division for Planetary Sciences Meeting Abstracts*, p. 210.01.

Divine N. and Newburn R. L. (1988) in *Exploration of Halley's Comet* (M. Grewing, F. Praderie, and R. Reinhard, eds.), pp. 867–872, Springer, Berlin, Heidelberg.

Dobrica E., Engrand C., Duprat J., Gounelle M., Leroux H., Quirico E., and Rouzaud J. N. (2009) *Connection between micrometeorites and Wild 2 particles: From Antarctic snow to cometary ices*, *Meteoritics and Planetary Science*, *44*, 1643–1661.

Dobrică E., Engrand C., Quirico E., Montagnac G., and Duprat J. (2011) *Raman characterization of carbonaceous matter in CONCORDIA Antarctic micrometeorites*, *Meteoritics and Planetary Science*, *46*, 1363–1375.

Dobrică E., Engrand C., Leroux H., Rouzaud J. N., and Duprat J. (2012) *Transmission Electron Microscopy of CONCORDIA UltraCarbonaceous Antarctic MicroMeteorites (UCAMMs): Mineralogical properties*, *Geochim. Cosmochim. Acta*, *76*, 68–82.

Dollfus A. (1989) *Polarimetry of grains in the coma of P/Halley. II-Interpretation*, *Astronomy and Astrophysics*, *213*, 469–478.

Dollfus A., Bastien P., Le Borgne J.-F., Levasseur-Regourd A.-C., and Mukai T. (1988) *Optical polarimetry of P/Halley-Synthesis of the measurements in the continuum*, *Astronomy and Astrophysics*, *206*, 348–356.

Dorschner J., Begemann B., Henning T., Jaeger C., and Mutschke H. (1995) *Steps toward interstellar silicate mineralogy. II. Study of Mg-Fe-silicate glasses of variable composition.*, *Astron. Astrophys.*, *300*, 503.

Duprat J., Dobrică E., Engrand C., Aléon J., Marrocchi Y., Mostefaoui S., Meibom A., Leroux H., Rouzaud J. N., Gounelle M., and Robert F. (2010) *Extreme Deuterium Excesses in Ultracarbonaceous Micrometeorites from Central Antarctic Snow*, *Science*, *328*, 742.

Duprat J., Engrand C., Maurette M., Kurat G., Gounelle M., and Hammer C. (2007) *Micrometeorites from central antarctic snow: The concordia collection*, *Advances in Space Research*, *39*, 605–611.

Ellerbroek L. E., Gundlach B., Landeck A., Dominik C., Blum J., Merouane S., Hilchenbach M., Bentley M. S., Mannel T., John H., and van Veen H. A. (2017) *The footprint of cometary dust analogues – i. laboratory experiments of low-velocity impacts and comparison with rosetta data*, *Monthly Notices of the Royal Astronomical Society*, *469*, S204–S216.

Ellerbroek L. E., Gundlach B., Landeck A., Dominik C., Blum J., Merouane S., Hilchenbach M., John H., and van Veen H. A. (2019) *The footprint of cometary dust analogues – II. Morphology as a tracer of tensile strength and application to dust collection by the Rosetta spacecraft*, *Monthly Notices of the Royal Astronomical Society*, *486*, 3755–3765.

Ellis T. A. and Neff J. S. (1991) *Numerical simulation of the emission and motion of neutral and charged dust from P/Halley*, *Icarus*, *91*, 280–296.

Elsila J. E., Glavin D. P., and Dworkin J. P. (2009) *Cometary glycine detected in samples returned by Stardust*, *Meteoritics and Planetary Science*, *44*, 1323–1330.

Engrand C., Benzerara K., Leroux H., Duprat J., Dartois E., Bardin N., and Delauche L. (2015) *Carbonaceous Phases and Mineralogy of Ultracarbonaceous Antarctic Micrometeorites Identified by C- and N-XANES/STXM and TEM*, *Lunar and Planetary Science Conference*, p. 1902.

Epifani E., Colangeli L., Fulle M., Brucato J. R., Bussoletti E., De Sanctis M. C., Mennella V., Palomba E., Palumbo P., and Rotundi A. (2001) *ISOCAM Imaging of Comets 103P/Hartley 2 and 2P/Encke*, *Icarus*, *149*, 339–350.

Fabian D., Jäger C., Henning T., Dorschner J., and Mutschke H. (2000) *Steps toward interstellar silicate mineralogy. V. Thermal Evolution of Amorphous Magnesium Silicates and Silica*, *Astron. Astrophys.*, *364*, 282–292.

Feaga L., Sunshine J., Bonev B., Dello Russo N., Di Santi M., and Combi M. (2021) in *AAS/Division for Planetary Sciences Meeting Abstracts*, vol. 53 of *AAS/Division for Planetary Sciences Meeting Abstracts*, p. 208.02.

Finson M. J. and Probstein R. F. (1968a) *A theory of dust comets. I. Model and equations*, *The Astrophysical Journal*, *154*, 327–352.

Finson M. L. and Probstein R. F. (1968b) *A theory of dust comets. II. Results for Comet Arend-Roland*, *The Astrophysical Journal*, *154*, 353–380.

Floss C. and Haenecour P. (2016) *Presolar silicate grains: Abundances, isotopic and elemental compositions, and the effects of secondary processing*, *Geochemical Journal*, *50*, 3–25.

Floss C., Noguchi T., and Yada T. (2012) *Ultracarbonaceous Antarctic Micrometeorites: Origins and Relationships to Other Primitive Extraterrestrial Materials*, *Lunar and Planetary Science Conference*, 1217.

Floss C., Stadermann F. J., Kearsley A. T., Burchell M. J., and Ong W. J. (2013) *The abundance of presolar grains in comet 81p/wild 2*, *The Astrophysical Journal*, *763*, 140.

Flynn G. J., Bleuet P., Borg J., Bradley J. P., Brenker F. E., Brennan S., Bridges J., Brownlee D. E., Bullock E. S., Burghammer M., Clark B. C., Dai Z. R., Daghlian C. P., Djouadi Z., Fakra S., Ferroir T., Floss C., Franchi I. A., Gainsforth Z., Gallien J.-P., Gillet P., Grant P. G., Graham G. A., Green S. F., Grossemy F., Heck P. R., Herzog G. F., Hoppe P., Hörz F., Huth J., Ignatyev K., Ishii H. A., Janssens K., Joswiak D., Kearsley A. T., Khodja H., Lanzirotti A., Leitner J., Lemelle L., Leroux H., Luening K., MacPherson G. J., Marhas K. K., Marcus M. A., Matrajt G., Nakamura T., Nakamura-Messenger K., Nakano T., Newville M., Papanastassiou D. A., Pianetta P., Rao W., Riekel C., Rietmeijer F. J. M., Rost D., Schwandt C. S., See T. H., Sheffield-Parker J., Simionovici A., Sitnitsky I., Snead C. J., Stadermann F. J., Stephan T., Stroud R. M., Susini J., Suzuki Y., Sutton S. R., Taylor S., Teslich N., Troadec D., Tsou P., Tsuchiyama A., Uesugi K., Vekemans B., Vicenzi E. P., Vincze L., Westphal A. J., Wozniakiewicz P., Zinner E., and Zolensky M. E. (2006) *Elemental compositions of comet 81p/wild 2 samples collected by stardust*, *Science*, *314*, 1731–1735.

Flynn G. J., Durda D. D., Sandel L. E., Kreft J. W., and Strait M. M. (2009) *Dust production from the hypervelocity impact disruption of the murchison hydrous cm2 meteorite: Implications for the disruption of hydrous asteroids and the production of interplanetary dust*, *Planetary and Space Science*, *57*, 119–126.

Flynn G. J., Keller L. P., Feser M., Wirick S., and Jacobsen C. (2003) *The origin of organic matter in the solar system: evidence from the interplanetary dust particles*, *Geochimica et Cosmochimica Acta*, *67*, 4791–4806.

Flynn G. J., Wirick S., Northrup P. N., Douglas K. M., Keller L. P., Araki T., Abyanch M., and Kaulich B. (2020) in *Lunar and Planetary Science Conference*, Lunar and Planetary Science Conference, p. 1226.

Fomenkova M. and Chang S. (1994) in *Analysis of Interplanetary Dust, AIP Conf. Proc.* (M. Zolensky, T. Wilson, F. Rietmeijer, and G. J. Flynn, eds.), vol. 310, pp. 193–202, Amer. Inst. Physics Press, New YOrk.

Fomenkova M. N., Chang S., and Mukhin L. M. (1994) *Carbonaceous components in the comet Halley dust*, *Geochimica et Cosmochimica Acta*, *58*, 4503–4512.

Fomenkova M. N., Kerridge J. F., Marti K., and McFadden L. A. (1992) *Compositional trends in rock-forming elements of comet Halley dust*, *Science*, *258*, 266–269.

Fomenkova M. N. and Mendis D. A. (1992) *A note on the very small grains (Vsgs) observed at Halley comet*, *Astrophysics and Space Science*, *189*, 327–331.

Frank D. R., Westphal A. J., Zolensky M. E., Gainsforth Z., Butterworth A. L., Bastien R. K., Allen C., Anderson D., Ansari A., Bajt S., Bassim N., Bechtel H. A., Borg J., Brenker F. E., Bridges J., Brownlee D. E., Burchell M., Burghammer M., Changela H., Cloetens P., Davis A. M., Doll R., Floss C., Flynn G., Grün E., Heck P. R., Hillier J. K., Hoppe P., Hudson B., Huth J., Hvide B., Kearsley A., King A. J., Lai B., Leitner J., Lemelle L., Leroux H., Leonard A., Lettieri R., Marchant W., Nittler L. R., Ogliore R., Ong W. J., Postberg F., Price M. C., Sandford S. A., Tresseras J.-A. S., Schmitz S., Schoonjans T., Silversmit G., Simionovici A. S., Solé V. A., Srama R., Stephan T., Sterken V. J., Stodolna J., Stroud R. M., Sutton S., Trieloff M., Tsou P., Tsuchiyama A., Tyliszczak T., Vekemans B., Vincze L., Korff J. V., Wordsworth N., Zevin D., and dusters S. h. (2014) *Stardust interstellar preliminary examination ii: Curating the interstellar dust collector, picokeystones, and sources of impact tracks*, *Meteoritics and Planetary Science*, *49*, 1522–1547.

Frank D. R., Zolensky M. E., and Le L. (2014) *Olivine in terminal particles of Stardust aerogel tracks and analogous grains in chondrite matrix*, *Geochim. Cosmochim. Acta*, *142*, 240–259.

Frattin E., Cremonese G., Simioni E., Bertini I., Lazzarin M., Ott T., Drolshagen E., La Forgia F., Sierks H., Barbieri C., Lamy P., Rodrigo R., Koschny D., Rickman H., Keller H. U., Agarwal J., A'Hearn M. F., Barucci M. A., Bertaux J.-L., Da Deppo V., Davidsson B., Debei S., De Cecco M., Deller J., Ferrari S., Ferri F., Fornasier S., Fulle M., Gicquel A., Groussin O., Gutierrez P. J., Güttler C., Hofmann M., Hviid S. F., Ip W.-H., Jorda L., Knollenberg J., Kramm J.-R., Kührt E., Küppers M., Lara L. M., Lopez Moreno J. J., Lucchetti A., Marzari F., Massironi M., Mottola S., Naletto G., Oklay N., Pajola M., Penasa L., Shi X., Thomas N., Tubiana C., and Vincent J.-B. (2017) *Post-perihelion photometry of dust grains in the coma of 67P/ Churyumov–Gerasimenko*, *Monthly Notices of the Royal Astronomical Society*, *469*, S195–S203.

Fray N., Bardyn A., Cottin H., Baklouti D., Briois C., Colangeli L., Engrand C., Fischer H., Glasmachers A., Grün E., Haerendel G., Henkel H., Höfner H., Hornung K., Jessberger E. K., Koch A., Krüger H., Langevin Y., Lehto H., Lehto K., Le Roy L., Merouane S., Modica P., Orthous-Daunay F.-R., Paquette J., Raulin F., Rynö J., Schulz R., Silén J., Siljeström S., Steiger W., Stenzel O., Stephan T., Thirkell L., Thomas R., Torkar K., Varmuza K., Wanczek K.-P., Zaprudin B., Kissel J., and Hilchenbach M. (2016) *High-molecular-weight organic matter in the particles of comet 67p/churyumov-gerasimenko*, *Nature*, *538*, 72–74.

Fray N., Bardyn A., Cottin H., Baklouti D., Briois C., Engrand C., Fischer H., Hornung K., Isnard R., Langevin Y., Lehto H., Le Roy L., Mellado E. M., Merouane S., Modica P., Orthous-Daunay F.-R., Paquette J., Rynö J., Schulz R., Silén J., Siljeström S., Stenzel O., Thirkell L., Varmuza K., Zaprudin B., Kissel J., and Hilchenbach M. (2017) *Nitrogen-to-carbon atomic ratio measured by cosima in the particles of comet 67p/churyumov–gerasimenko*, *Monthly Notices of the Royal Astronomical Society*, *469*, S506–S516.

Fukuda K., Brownlee D. E., Joswiak D. J., Tenner T. J., Kimura M., and Kita N. T. (2021) *Correlated isotopic and chemical evidence for condensation origins of olivine in comet 81p/wild 2 and in aoas from cv and co chondrites*, *Geochimica et Cosmochimica Acta*, *293*, 544–574.

Fulle M. (1987) *A new approach to the Finson-Probstein method of interpreting cometary dust tails*, *Astronomy and Astrophysics*, *171*, 327–335.

Fulle M. (2004) in *Comets II*, pp. 565–575, Arizona University Press.

Fulle M., Altobelli N., Buratti B., Choukroun M., Fulchignoni M., Grün E., Taylor M., and Weissman P. (2016a) *Unexpected and significant findings in comet 67P/Churyumov–Gerasimenko: An interdisciplinary view*, *Monthly Notices of the Royal Astronomical Society*, *462*, S2–S8.

Fulle M. and Blum J. (2017) *Fractal dust constrains the collisional history of comets*, *Monthly Notices of the Royal Astronomical Society*, *469*, S39–S44.

Fulle M., Colangeli L., Mennella V., Rotundi A., and Bussoletti E. (1995) *The sensitivity of the size distribution to the grain dynamics: Simulation of the dust flux measured by Giotto at P/Halley*, *Astronomy and Astrophysics*, *304*, 622.

Fulle M., Corte V. D., Rotundi A., Weissman P., Juhasz A., Szego

K., Sordini R., Ferrari M., Ivanovski S., Lucarelli F., Accolla M., Merouane S., Zakharov V., Epifani E. M., Moreno J. J. L., Rodríguez J., Colangeli L., Palumbo P., Grün E., Hilchenbach M., Bussoletti E., Esposito F., Green S. F., Lamy P. L., McDonnell J. A. M., Mennella V., Molina A., Morales R., Moreno F., Ortiz J. L., Palomba E., Rodrigo R., Zarnecki J. C., Cosi M., Giovane F., Gustafson B., Herranz M. L., Jerónimo J. M., Leese M. R., Jiménez A. C. L., and Altobelli N. (2015) *Density and charge of pristine fluffy particles from Comet 67P/Churyumov-Gerasimenko*, *The Astrophysical Journal*, *802*, L12.

Fulle M., Della Corte V., Rotundi A., Green S. F., Accolla M., Colangeli L., Ferrari M., Ivanovski S., Sordini R., and Zakharov V. (2017) *The dust-to-ices ratio in comets and Kuiper belt objects*, *Monthly Notices of the Royal Astronomical Society*, *469*, S45–S49.

Fulle M., Della Corte V., Rotundi A., Rietmeijer F. J. M., Green S. F., Weissman P., Accolla M., Colangeli L., Ferrari M., Ivanovski S., Lopez-Moreno J. J., Epifani E. M., Morales R., Ortiz J. L., Palomba E., Palumbo P., Rodriguez J., Sordini R., and Zakharov V. (2016b) *Comet 67P/Churyumov–Gerasimenko preserved the pebbles that formed planetesimals*, *Monthly Notices of the Royal Astronomical Society*, *462*, S132.

Fulle M., Levasseur-Regourd A. C., McBride N., and Hadamcik E. (2000) *In situ dust measurements from within the coma of 1p/halley: First-order approximation with a dust dynamical model*, *The Astronomical Journal*, *119*, 1968.

Fulle M., Marzari F., Corte V. D., Fornasier S., Sierks H., Rotundi A., Barbieri C., Lamy P. L., Rodrigo R., Koschny D., Rickman H., Keller H. U., López-Moreno J. J., Accolla M., Agarwal J., A'Hearn M. F., Altobelli N., Barucci M. A., Bertaux J.-L., Bertini I., Bodewits D., Bussoletti E., Colangeli L., Cosi M., Cremonese G., Crifo J.-F., Deppo V. D., Davidsson B., Debei S., Cecco M. D., Esposito F., Ferrari M., Giovane F., Gustafson B., Green S. F., Groussin O., Grün E., Gutierrez P., Güttler C., Herranz M. L., Hviid S. F., Ip W., Ivanovski S. L., Jerónimo J. M., Jorda L., Knollenberg J., Kramm R., Kührt E., Küppers M., Lara L., Lazzarin M., Leese M. R., López-Jiménez A. C., Lucarelli F., Epifani E. M., McDonnell J. A. M., Mennella V., Molina A., Morales R., Moreno F., Mottola S., Naletto G., Oklay N., Ortiz J. L., Palomba E., Palumbo P., Perrin J.-M., Rietmeijer F. J. M., Rodríguez J., Sordini R., Thomas N., Tubiana C., Vincent J.-B., Weissman P., Wenzel K.-P., Zakharov V., and Zarnecki J. C. (2016c) *Evolution of the dust size distribution of comet 67p/churyumov–gerasimenko from 2.2 au to perihelion*, *The Astrophysical Journal*, *821*, 19.

Furusho R., Ikeda Y., Kinoshita D., Ip W.-H., Kawakita H., Kasuga T., Sato Y., Lin H.-C., Chang M.-S., Lin Z.-Y., and Watanabe J.-i. (2007) *Imaging polarimetry of Comet 9P/Tempel before and after the Deep Impact*, *Icarus*, *190*, 454–458.

Gainsforth Z., Brenker F. E., Simionovici A. S., Schmitz S., Burghammer M., Butterworth A. L., Cloetens P., Lemelle L., Tresserras J.-A. S., Schoonjans T., Silversmit G., Solé V. A., Vekemans B., Vincze L., Westphal A. J., Allen C., Anderson D., Ansari A., Bajt S., Bastien R. K., Bassim N., Bechtel H. A., Borg J., Bridges J., Brownlee D. E., Burchell M., Changela H., Davis A. M., Doll R., Floss C., Flynn G., Fougeray P., Frank D., Grün E., Heck P. R., Hillier J. K., Hoppe P., Hudson B., Huth J., Hvide B., Kearsley A., King A. J., Lai B., Leitner J., Leroux H., Leonard A., Lettieri R., Marchant W., Nittler L. R., Ogliore R., Ong W. J., Postberg F., Price M. C., Sandford S. A., Srama R., Stephan T., Sterken V., Stodolna J., Stroud R. M., Sutton S., Trieloff M., Tsou P., Tsuchiyama A., Tyliszczak T., Von Korff J., Zevin D., Zolensky M. E., and Stardust home dusters . (2014) *Stardust interstellar preliminary examination VIII: identification of crystalline material in two interstellar candidates*, *Meteoritics and Planetary Science*, *49*, 1645–1665.

Gainsforth Z., Butterworth A., Ogliore R., Westphal A., and Tyliszczak T. (2010) *Combined STEM/STXM Elemental Quantification for Cometary Particles*, *Microscopy and Microanalysis*, *16*, 922–923.

Gainsforth Z., Butterworth A. L., Jilly-Rehak C. E., Westphal A. J., Brownlee D. E., Joswiak D., Ogliore R. C., Zolensky M. E., Bechtel H. A., Ebel D. S., Huss G. R., Sandford S. A., and White A. J. (2016) *Possible GEMS and Ultra-Fine Grained Polyphase Units in Comet Wild 2*, *Lunar and Planetary Science Conference*, *47*, 2366.

Gainsforth Z., Butterworth A. L., Stodolna J., Westphal A. J., Huss G. R., Nagashima K., Ogliore R., Brownlee D. E., Joswiak D., Tyliszczak T., and Simionovici A. S. (2015) *Constraints on the formation environment of two chondrule-like igneous particles from comet 81P/Wild 2*, *Meteoritics and Planetary Sciences*, *50*, 976–1004.

Gainsforth Z., McLeod A. S., Butterworth A. L., Dominguez G., Basov D., Keilmann F., Thiemens M., Tyliszczak T., and Westphal A. J. (2013) *Caligula, a Stardust Sulfide-Silicate Assemblage Viewed Through SEM, NanoFTIR, and STXM*, *Lunar and Planetary Science Conference*, *44*, 2332.

Gardner E., Lehto H. J., Lehto K., Fray N., Bardyn A., Lönnberg T., Merouane S., Isnard R., Cottin H., Hilchenbach M., and the COSIMA team (2020) *The detection of solid phosphorus and fluorine in the dust from the coma of comet 67P/Churyumov–Gerasimenko*, *Monthly Notices of the Royal Astronomical Society*, *499*, 1870–1873

Gehrz R. D. and Ney E. P. (1992) *0.7- to 23-μm photometric observations of P/Halley 1986 III and six recent bright comets*, *Icarus*, *100*, 162–186.

Geiss J. and Gloeckler G. (1998) *Abundances of Deuterium and Helium-3 in the Protosolar Cloud*, *Space Sci. Rev.*, *84*, 239–250.

Glassmeier K.-H., Boehnhardt H., Koschny D., Kührt E., and Richter I. (2007) *The rosetta mission: Flying towards the origin of the solar system*, *Space Science Reviews*, *128*, 1–21.

Green S. F., McDonnell J. a. M., McBride N., Colwell M. T. S. H., Tuzzolino A. J., Economou T. E., Tsou P., Clark B. C., and Brownlee D. E. (2004) *The dust mass distribution of comet 81P/Wild 2*, *Journal of Geophysical Research: Planets*, *109*.

Groussin O., Attree N., Brouet Y., Ciarletti V., Davidsson B., Filacchione G., Fischer H.-H., Gundlach B., Knapmeyer M., and Knollenberg J. (2019) *The thermal, mechanical, structural, and dielectric properties of cometary nuclei after Rosetta*, *Space Science Reviews*, *215*, 1–51.

Guérin B., Engrand C., Le Guillou C., Leroux H., Duprat J., Dartois E., Bernard S., Benzerara K., Rojas J., Godard M., Delauche L., and Troadec D. (2020) *STEM and STXM-XANES Analysis of FIB Sections of Ultracarbonaceous Antarctic Micrometeorites (UCAMMs)*, *Lunar and Planetary Science Conference*, p. #2117.

Gundlach B., Schmidt K. P., Kreuzig C., Bischoff D., Rezaei F., Kothe S., Blum J., Grzesik B., and Stoll E. (2018) *The tensile strength of ice and dust aggregates and its dependence on particle properties*, *Monthly Notices of the Royal Astronomical Society*, *479*, 1273–1277.

Güttler C., Krause M., Geretshauser R. J., Speith R., and Blum J. (2009) *The physics of protoplanetesimal dust agglomerates. IV. Toward a dynamical collision model*, *701*, 130–141.

Güttler C., Mannel T., Rotundi A., Merouane S., Fulle M., Bockelée-Morvan D., Lasue J., Levasseur-Regourd A. C., Blum J., and Naletto G. (2019) *Synthesis of the morphological description of cometary dust at comet 67P/Churyumov-Gerasimenko*, *Astronomy & Astrophysics*, *630*, A24.

Guzik P., Drahus M., Rusek K., Waniak W., Cannizzaro G., and Pastor-Marazuela I. (2020) *Initial characterization of interstellar comet 2I/Borisov*, *Nature Astronomy*, *4*, 53–57.

Hadamcik E., Levasseur-Regourd A. C., Hines D. C., Sen A. K., Lasue J., and Renard J.-B. (2016) *Properties of dust particles in comets from photometric and polarimetric observations of 67P*, *Monthly Notices of the Royal Astronomical Society*, *462*, S507–S515.

Hadamcik E., Renard J.-B., Levasseur-Regourd A. C., and Lasue J. (2006) *Light scattering by fluffy particles with the PROGRA2 experiment: Mixtures of materials*, *Journal of Quantitative Spectroscopy and Radiative Transfer*, *100*, 143–156.

Hadamcik E., Renard J.-B., Rietmeijer F. J. M., Levasseur-Regourd A. C., Hill H. G. M., Karner J. M., and Nuth J. A. (2007) *Light scattering by fluffy Mg–Fe–SiO and C mixtures as cometary analogs (PROGRA2 experiment)*, *Icarus*, *190*, 660–671.

Hadamcik E., Sen A. K., Levasseur-Regourd A. C., Gupta R., and Lasue J. (2010) *Polarimetric observations of comet 67P/Churyumov-Gerasimenko during its 2008–2009 apparition*, *Astronomy & Astrophysics*, *517*, A86.

Hadraoui K., Cottin H., Ivanovski S. L., Zapf P., Altwegg K., Benilan Y., Biver N., Della Corte V., Fray N., Lasue J., Merouane S., Rotundi A., and Zakharov V. (2019) *Distributed glycine in comet 67p/churyumov-gerasimenko*, *A&A*, *630*, A32.

Hadraoui K., Cottin H., Ivanovski S. L., Zapf P., Altwegg K., Benilan Y., Biver N., Della Corte V., Fray N., Lasue J., Merouane S., Rotundi A., and Zakharov V. (2021) *Distributed glycine in comet 67p/churyumov-gerasimenko (corrigendum)*, *A&A*, *651*, C2.

Hanner M. S. (1983) in *Cometary Exploration, Volume 2*, vol. 2, pp. 1–22.

Hanner M. S. (2003) *The scattering properties of cometary dust*, *Journal of Quantitative Spectroscopy and Radiative Transfer*, *79*, 695–705.

Hanner M. S., Gehrz R. D., Harker D. E., Hayward T. L., Lynch D. K., Mason C. C., Russell R. W., Williams D. M., Wooden D. H., and Woodward C. E. (1997) *Thermal Emission From The Dust Coma Of Comet Hale-Bopp And The Composition Of The Silicate Grains*, *Earth Moon and Planets*, *79*, 247–264.

Hanner M. S., Giese R. H., Weiss K., and Zerull R. (1981) *On the definition of albedo and application to irregular particles*, *Astron. Astrophys.*, *104*, 42–46.

Hanner M. S., Knacke R., Sekanina Z., and Tokunaga A. T. (1985) *Dark grains in comet Crommelin*, *Astron. Astrophys.*, *152*, 177–181.

Hanner M. S. and Zolensky M. E. (2010) *The Mineralogy of Cometary Dust*, vol. 815, pp. 203–232.

Harker D. E. and Desch S. J. (2002) *Annealing of Silicate Dust by Nebular Shocks at 10 AU*, *Astrophys. J. Lett.*, *565*, L109–L112.

Harker D. E., Kelley M. S. P., Woodward C. E., and Wooden D. H. (2022) *Dust Properties of Comets Observed by Spitzer*.

Harker D. E., Wooden D. H., Woodward C. E., and Lisse C. M. (2002) *Grain Properties of Comet C/1995 O1 (Hale-Bopp)*, *Astrophys. J.*, *580*, 579–597.

Harker D. E., Woodward C. E., and Wooden D. H. (2005) *The Dust Grains from 9P/Tempel 1 Before and After the Encounter with Deep Impact*, *Science*, *310*, 278–280.

Harker D. E., Woodward C. E., Wooden D. H., Fisher R. S., and Trujillo C. A. (2007) *Gemini-N mid-IR observations of the dust properties of the ejecta excavated from Comet 9P/Tempel 1 during Deep Impact*, *Icarus*, *190*, 432–453.

Haser L., Oset S., and Bodewits D. (2020) *Intensity Distribution in the Heads of Comets*, *The Planetary Science Journal*, *1*, 83.

Hashizume K., Chaussidon M., Marty B., and Terada K. (2004) *Protosolar carbon isotopic composition: Implications for the origin of meteoritic organics*, *The Astrophysical Journal*, *600*, 480–484.

Hayward T. L., Hanner M. S., and Sekanina Z. (2000) *Thermal Infrared Imaging and Spectroscopy of Comet Hale-Bopp (C/1995 O1)*, *Astrophys. J.*, *538*, 428–455.

Heck P. R., Hoppe P., and Huth J. (2012) *Sulfur four isotope NanoSIMS analysis of comet-81P/Wild 2 dust in impact craters on aluminum foil C2037N from NASA's Stardust mission*, *Meteoritics and Planetary Science*, *47*, 649–659.

Henning T. and Mutschke H. (1997) *Low-temperature infrared properties of cosmic dust analogues.*, *Astronomy & Astrophysics*, *327*, 743–754.

Hilchenbach M., Fischer H., Langevin Y., Merouane S., Paquette J., Rynö J., Stenzel O., Briois C., Kissel J., Koch A., Schulz R., Silen J., Altobelli N., Baklouti D., Bardyn A., Cottin H., Engrand C., Fray N., Haerendel G., Henkel H., Höfner H., Hornung K., Lehto H., Mellado E. M., Modica P., Le Roy L., Siljeström S., Steiger W., Thirkell L., Thomas R., Torkar K., Varmuza K., Zaprudin B., and the COSIMA Team (2017) *Mechanical and electrostatic experiments with dust particles collected in the inner coma of comet 67P by COSIMA onboard Rosetta*, *Philosophical Transactions of the Royal Society of London A: Mathematical, Physical and Engineering Sciences*, *375*.

Hilchenbach M., Kissel J., Langevin Y., Briois C., Von Hoerner H., Koch A., Schulz R., Silén J., Altwegg K., and Colangeli L. (2016) *Comet 67P/Churyumov–Gerasimenko: Close-up on dust particle fragments*, *The Astrophysical journal letters*, *816*, L32.

Hofmeister A. M. and Speck A. K. (2003) in *Astrophysics of Dust* (A. N. Witt, ed.), p. 148.

Hoppe P., Strebel R., Eberhardt P., Amari S., and Lewis R. S. (2000) *Isotopic properties of silicon carbide X grains from the Murchison meteorite in the size range 0.5-1.5 μm*, *Meteoritics & Planetary Science*, *35*, 1157–1176.

Horányi M. (1996) *Charged dust dynamics in the solar system*, *Annual Review of Astronomy and Astrophysics*, *34*, 383–418.

Hornung K., Merouane S., Hilchenbach M., Langevin Y., Mellado E. M., Della Corte V., Kissel J., Engrand C., Schulz R., Ryno J., Silen J., and COSIMA Team (2016) *A first assessment of the strength of cometary particles collected in-situ by the COSIMA instrument onboard ROSETTA*, *Planet. Space Sci.*, *133*, 63–75.

Hörz F., Bastien R., Borg J., Bradley J. P., Bridges J. C., Brownlee D. E., Burchell M. J., Chi M., Cintala M. J., Dai Z. R., Djouadi Z., Dominguez G., Economou T. E., Fairey S. A. J., Floss C., Franchi I. A., Graham G. A., Green S. F., Heck P., Hoppe P., Huth J., Ishii H., Kearsley A. T., Kissel J., Leitner J., Leroux H., Marhas K., Messenger K., Schwandt C. S., See T. H., Snead C., Stadermann F. J., Stephan T., Stroud R., Teslich N., Trigo-Rodríguez J. M., Tuzzolino A. J., Troadec D., Tsou P., Warren J., Westphal A., Wozniakiewicz P., Wright I., and Zinner E. (2006) *Impact features on stardust: Implications for comet 81p/wild 2 dust*, *Science*, *314*, 1716–1719.

Hyland M. G., Fitzsimmons A., and Snodgrass C. (2019) *Near-UV and optical spectroscopy of comets using the ISIS spectrograph on the WHT*, *Monthly Notices of the Royal Astronomical Society*, *484*, 1347–1358.

Hynes K. and Gyngard F. (2009) in *40th Annual Lunar and Planetary Science Conference*, p. 1198.

Isa J., Rubin A. E., Marin-Carbonne J., McKeegan K. D., and Wasson J. T. (2011) in *42nd Annual Lunar and Planetary Science Conference*, Lunar and Planetary Science Conference, p. 2623.

Ishiguro M., Yang H., Usui F., Pyo J., Ueno M., Ootsubo T., Kwon S. M., and Mukai T. (2013) *High-resolution imaging of the gegenschein and the geometric albedo of interplanetary dust*, *The Astrophysical Journal*, *767*, 75.

Ishii H. A., Bradley J. P., Bechtel H. A., Brownlee D. E., Bustillo K. C., Ciston J., Cuzzi J. N., Floss C., and Joswiak D. J. (2018) *Multiple generations of grain aggregation in different environments preceded solar system body formation*, *Proceedings of the National Academy of Science*, *115*, 6608–6613.

Ishii H. A., Bradley J. P., Dai Z. R., Chi M., Kearsley A. T., Burchell M. J., Browning N. D., and Molster F. (2008) *Comparison of comet 81p/wild 2 dust with interplanetary dust from comets*, *Science*, *319*, 447–450.

Ishii H. A., Wozniakiewicz P. J., Kearsley A. T., Burchell M. J., Bradley J. P., Teslich N., Price M. C., and Cole M. J. (2011) *The question of GEMS in comet 81P/Wild 2: Stardust analogue impacts of fine-grained mineral aggregates*, *Meteoritics and Planetary Science Supplement*, *74*, 5213.

Isnard R., Bardyn A., Fray N., Briois C., Cottin H., Paquette J., Stenzel O., Alexander C., Baklouti D., Engrand C., Orthous-Daunay F. R., Siljeström S., Varmuza K., and Hilchenbach M. (2019) *H/C elemental ratio of the refractory organic matter in cometary particles of 67P/Churyumov-Gerasimenko*, *Astron. Astrophys.*, *630*, A27.

Jaeger C., Molster F. J., Dorschner J., Henning T., Mutschke H., and Waters L. B. F. M. (1998) *Steps toward interstellar silicate mineralogy. IV. The crystalline revolution*, *Astronomy and Astrophysics*, *339*, 904–916.

Jarosewich E. (1990) *Chemical analyses of meteorites: a compilation if stony and iron meteorite analyses*, *Meteoritics*, *25*, 33–337.

Jenniskens P., Baratta G. A., Kouchi A., Degroot M. S., Greenberg J. M., and Strazzulla G. (1993) *Carbon dust formation on interstellar grains*, *Astronomy and Astrophysics*, *273*, 583–600.

Jenniskens P. and Jenniskens P. M. M. (2006) *Meteor Showers and Their Parent Comets*, Cambridge University Press.

Jessberger E. K. (1999) *Rocky cometary particulates: their elemental, isotopic and mineralogical ingredients*, *Space Science Reviews*, *90*, 91–97.

Jessberger E. K., Christoforidis A., and Kissel J. (1988) *Aspects of the major element composition of halley's dust*, *Nature*, *332*, 691–695.

Jessberger E. K., Kissel J., Fechtig H., and Krueger F. R. (1986) in *Comet Nucleus Sample Return Mission* (O. Melita, ed.), vol. 249 of *ESA Special Publication*, pp. 27–30.

Joswiak D. J., Brownlee D. E., Matrajt G., Westphal A. J., and Snead C. J. (2009) *Kosmochloric ca-rich pyroxenes and feo-rich olivines (kool grains) and associated phases in stardust tracks and chondritic porous interplanetary dust particles: Possible precursors to feo-rich type ii chondrules in ordinary chondrites*, *Meteoritics and Planetary Science*, *44*, 1561–1588.

Joswiak D. J., Brownlee D. E., Matrajt G., Westphal A. J., Snead C. J., and Gainsforth Z. (2012) *Comprehensive examination of large mineral and rock fragments in Stardust tracks: Mineralogy, analogous extraterrestrial materials, and source regions*, *Meteoritics and Planetary Sciences*, *47*, 471–524.

Joswiak D. J., Brownlee D. E., Nguyen A. N., and Messenger S. (2017) *Refractory materials in comet samples*, *Meteoritics and Planetary Science*, *52*, 1612–1648.

Joswiak D. J., Nakashima D., Brownlee D. E., Matrajt G., Ushikubo T., Kita N. T., Messenger S., and Ito M. (2014) *Terminal particle from Stardust track 130: Probable Al-rich chondrule fragment from comet Wild 2*, *Geochimica et Cosmochimica Acta*, *144*, 277–298.

Juhász A., Bouwman J., Henning T., Acke B., van den Ancker M. E., Meeus G., Dominik C., Min M., Tielens A. G. G. M., and Waters L. B. F. M. (2010) *Dust Evolution in Protoplanetary Disks Around Herbig Ae/Be Stars—the Spitzer View*, *Astrophysical Journal*, *721*, 431–455.

Juhász A., Henning T., Bouwman J., Dullemond C. P., Pascucci I., and Apai D. (2009) *Do We Really Know the Dust? Systematics and Uncertainties of the Mid-Infrared Spectral Analysis Methods*, *Astrophys. J.*, *695*, 1024–1041.

Kadono T., Sugita S., Sako S., Ootsubo T., Honda M., Kawakita H., Miyata T., Furusho R., and Watanabe J. (2007) *The thickness and formation age of the surface layer on comet 9p/tempel 1*, *The Astrophysical Journal Letters*, *661*, L89.

Keller L. P., Bajt S., Baratta G. A., Borg J., Bradley J. P., Brownlee D. E., Busemann H., Brucato J. R., Burchell M., Colangeli L., d'Hendecourt L., Djouadi Z., Ferrini G., Flynn G., Franchi I. A., Fries M., Grady M. M., Graham G. A., Grossemy F., Kearsley A., Matrajt G., Nakamura-Messenger K., Mennella V., Nittler L., Palumbo M. E., Stadermann F. J., Tsou P., Rotundi A., Sandford S. A., Snead C., Steele A., Wooden D., and Zolensky M. (2006) *Infrared spectroscopy of comet 81P/Wild 2 samples returned by Stardust*, *Science*, *314*, 1728–1731.

Keller L. P. and Messenger S. (2011) *On the origins of GEMS grains*, *Geochimica et Cosmochimica Acta*, *75*, 5336–5365.

Keller L. P., Messenger S., and Bradley J. P. (2000) *Analysis of a deuterium-rich interplanetary dust particle (IDP) and implications for presolar material in IDPs*, *Journal of Geophysical Research: Space Physics*, *105*, 10397–10402.

Keller L. P., Messenger S., Flynn G. J., Clemett S., Wirick S., and Jacobsen C. (2004) *The nature of molecular cloud material in interplanetary dust*, *Geochim. Cosmochim. Acta*, *68*, 2577–2589.

Kelley M. S., Lindler D. J., Bodewits D., A'Hearn M. F., Lisse C. M., Kolokolova L., Kissel J., and Hermalyn B. (2013) *A distribution of large particles in the coma of comet 103P/Hartley 2*, *Icarus*, *222*, 634–652.

Kelley M. S. P., Harker D. E., Woodward C. E., and Wooden D. H. (2021) *Spitzer Space Telescope spectroscopy of comets, urn:nasa:pds:spitzer:spitzer-spec-comet::1.0, NASA Planetary Data System*.

Kerridge J. F., Mackay A. L., and Boynton W. V. (1979) *Magnetite in CI Carbonaceous Meteorites: Origin by Aqueous Activity on a Planetesimal Surface*, *Science*, *205*, 395–397.

Kikuchi S., Mikami Y., Mukai T., Mukai S., and Hough J. H. (1988) in *Exploration of Halley's Comet* (M. Grewing, F. Praderie, and R. Reinhard, eds.), pp. 689–692, Springer, Berlin, Heidelberg.

Kimura H., Kolokolova L., Li A., and Lebreton J. (2016) in *Light Scattering Reviews, Volume 11*, pp. 363–418, Springer.

Kimura H., Kolokolova L., and Mann I. (2003) *Optical properties of cometary dust. Constraints from numerical studies on light scattering by aggregate particles*, *Astron. Astrophys.*, *407*, L5–L8.

Kimura H., Kolokolova L., and Mann I. (2006) *Light scattering by cometary dust numerically simulated with aggregate particles consisting of identical spheres*, *Astronomy and Astrophysics*, *449*, 1243–1254.

Kiselev N., Rosenbush V., Levasseur-Regourd A. C., and Kolokolova L. (2015) in *Polarization of Stars and Planetary Systems*, Cambridge University Press.

Kiss C., Müller T. G., Kidger M., Mattisson P., and Marton G. (2015) *Comet C/2013 A1 (Siding Spring) as seen with the Herschel Space Observatory*, *Astron. Astrophys.*, *574*, L3.

Kissel J., Altwegg K., Clark B. C., Colangeli L., Cottin H., Czempiel S., Eibl J., Engrand C., Fehringer H. M., Feuerbacher B., Fomenkova M., Glasmachers A., Greenberg J. M., Grün E., Haerendel G., Henkel H., Hilchenbach M., von Hoerner H., Höfner H., Hornung K., Jessberger E. K., Koch A., Krüger H., Langevin Y., Parigger P., Raulin F., Rüdenauer F., Rynö J., Schmid E. R., Schulz R., Silén J., Steiger W., Stephan T., Thirkell L., Thomas R., Torkar K., Utterback N. G., Varmuza K., Wanczek K. P., Werther W., and Zscheeg H. (2007) *COSIMA - high resolution time-of-flight secondary ion mass spectrometer for the analysis of cometary dust particles onboard Rosetta*, *Space Science Reviews*, *128*, 823–867.

Kita N. T., Huberty J. M., Kozdon R., Beard B. L., and Valley J. W. (2011) *High-precision SIMS oxygen, sulfur and iron stable isotope analyses of geological materials: accuracy, surface topography and crystal orientation*, *Surface and Interface Analysis*, *43*, 427–431.

Klock W., Thomas K. L., McKay D. S., and Palme H. (1989) *Unusual olivine and pyroxene composition in interplanetary dust and unequilibrated ordinary chondrites*, *Nature*, *339*, 126–128.

Koike C., Chihara H., Tsuchiyama A., Suto H., Sogawa H., and Okuda H. (2003) *Compositional dependence of infrared absorption spectra of crystalline silicate. II. Natural and synthetic olivines*, *Astron. Astrophys.*, *399*, 1101–1107.

Koike C., Imai Y., Chihara H., Suto H., Murata K., Tsuchiyama A., Tachibana S., and Ohara S. (2010) *Effects of Forsterite Grain Shape on Infrared Spectra*, *Astrophys. J.*, *709*, 983–992.

Kolokolova L. (2015) *Polarimetry of stars and planetary systems*.

Kolokolova L., Hanner M. S., Levasseur-Regourd A.-C., and Gustafson B. Å. (2004) *Physical properties of cometary dust from light scattering and thermal emission*, *Comets II*, *577*, 184.

Kolokolova L., Kelley M., Kimura H., and Hoang T. (2022) *Interaction of electromagnetic radiation with the cometary dust*, *Comets III*.

Kolokolova L. and Kimura H. (2010) *Comet dust as a mixture of aggregates and solid particles: Model consistent with ground-based and space-mission results*, *Earth, planets and space*, *62*, 17–21.

Kolokolova L., Kimura H., Kiselev N., and Rosenbush V. (2007) *Two different evolutionary types of comets proved by polarimetric and infrared properties of their dust*, *Astron. Astrophys.*, *463*, 1189–1196.

Kulyk I., Korsun P., Lukyanyk I., Ivanova O., Afanasiev V., and Lara L. (2021) *Optical observations of near isotropic comet C/2006 OF2 (Broughton) at two different heliocentric distances*, *Icarus*, *355*, 114156.

Langevin Y., Hilchenbach M., Ligier N., Merouane S., Hornung K., Engrand C., Schulz R., Kissel J., Rynö J., and Eng P. (2016) *Typology of dust particles collected by the COSIMA mass spectrometer in the inner coma of 67P/Churyumov Gerasimenko*, *Icarus*, *271*, 76–97.

Langevin Y., Hilchenbach M., Vincendon M., Merouane S., Hornung K., Ligier N., Engrand C., Schulz R., Kissel J., and Rynö J. (2017) *Optical properties of cometary particles collected by the COSIMA mass spectrometer on-board Rosetta during the rendezvous phase around comet 67P/Churyumov-Gerasimenko*, *Mon. Not. R. Astron. Soc.*, *469*, S535–S549.

Lanzirotti A., Sutton S. R., Flynn G. J., Newville A., and Rao W. (2008) *Chemical composition and heterogeneity of Wild 2 cometary particles determined by synchrotron X-ray fluorescence*, *Meteoritics and Planetary Science*, *43*, 187–213.

Lasue J., Levasseur-Regourd A. C., Hadamcik E., and Alcouffe G. (2009) *Cometary dust properties retrieved from polarization observations: Application to C/1995 O1 Hale–Bopp and 1P/Halley*, *Icarus*, *199*, 129–144.

Lasue J., Maroger I., Botet R., Garnier P., Merouane S., Mannel T., Levasseur-Regourd A. C., and Bentley M. S. (2019) *Flattened loose particles from numerical simulations compared to particles collected by Rosetta*, *Astronomy & Astrophysics*, *630*, A28.

Lawler M. E. and Brownlee D. E. (1992) *CHON as a component of dust from comet Halley*, *Nature*, *359*, 810–812.

Leroux H., Cuvillier P., Zanda B., and Hewins R. H. (2015) *GEMS-like material in the matrix of the Paris meteorite and the early stages of alteration of CM chondrites*, *Geochim. Cosmochim. Acta*, *170*, 247–265.

Leroux H., Jacob D., Stodolna J., Nakamura-Messenger K., and Zolensky M. E. (2008) *Igneous ca-rich pyroxene in comet 81p/wild 2*, *American Mineralogist*, *93*, 1933–1936.

Levasseur-Regourd A.-C., Agarwal J., Cottin H., Engrand C., Flynn G., Fulle M., Gombosi T., Langevin Y., Lasue J., and Mannel T. (2018) *Cometary dust*, *Space science reviews*, *214*, 1–56.

Levasseur-Regourd A.-C., McBride N., Hadamcik E., and Fulle M. (1999) *Similarities between in situ measurements of local dust light scattering and dust flux impact data within the coma of 1P/Halley*, *Astronomy and Astrophysics*, *348*, 636–641.

Levasseur-Regourd A. C., Renard J.-B., Hadamcik E., Lasue J., Bertini I., and Fulle M. (2019) *Interpretation through experimental simulations of phase functions revealed by Rosetta in 67P/Churyumov-Gerasimenko dust coma*, *Astronomy & Astrophysics*, *630*, A20.

Li A. G. and Greenberg J. M. (1997) *A unified model of interstellar dust*, *Astronomy and Astrophysics*, *323*, 566–584.

Li J.-Y., Samarasinha N. H., Kelley M. S. P., Farnham T. L., A'Hearn M. F., Mutchler M. J., Lisse C. M., and Delamere W. A. (2014) *Constraining the Dust Coma Properties of Comet C/Siding Spring (2013 a1) at Large Heliocentric Distances*, *Astrophys. J. Lett.*, *797*, L8.

Lin Y., Amari S., and Pravdivtseva O. (2002) *Presolar grains from the qingzhen (EH3) meteorite*, *The Astrophysical Journal*, *575*, 257–263.

Lindsay S. S., Wooden D. H., Harker D. E., Kelley M. S., Woodward C. E., and Murphy J. R. (2013) *Absorption efficiencies of forsterite. i. discrete dipole approximation explorations in grain shape and size*, *Astrophysical Journal*, *766*, 54.

Lisse C. M., A'Hearn M. F., Farnham T. L., Groussin O., Meech K. J., Fink U., and Schleicher D. G. (2005) in *Deep Impact Mission: Looking Beneath the Surface of a Cometary Nucleus*

(C. T. Russell, ed.), pp. 161–192, Springer Netherlands, Dordrecht.

Lisse C. M., Kraemer K. E., Nuth J. A., Li A., and Joswiak D. (2007) *Comparison of the composition of the Tempel 1 ejecta to the dust in Comet C/Hale Bopp 1995 O1 and YSO HD 100546*, *Icarus*, *191*, 223–240.

Lisse C. M., VanCleve J., Adams A. C., A'Hearn M. F., Fernández Y. R., Farnham T. L., Armus L., Grillmair C. J., Ingalls J., Belton M. J. S., Groussin O., McFadden L. A., Meech K. J., Schultz P. H., Clark B. C., Feaga L. M., and Sunshine J. M. (2006) *Spitzer Spectral Observations of the Deep Impact Ejecta*, *Science*, *313*, 635–640.

LLera K., Burch J. L., Goldstein R., and Goetz C. (2020) *Simultaneous Observation of Negatively and Positively Charged Nanograins at Comet 67P/Churyumov-Gerasimenko*, *Geophysical Research Letters*, *47*, e2019GL086147, e2019GL086147 2019GL086147.

Lodders K. (2010) in *Principles and Perspectives in Cosmochemistry* (A. Goswami and B. E. Reddy, eds.), Astrophysics and Space Science Proceedings, pp. 379–417, Springer Berlin Heidelberg.

Love S. G. and Brownlee D. E. (1993) *A direct measurement of the terrestrial mass accretion rate of cosmic dust*, *Science*, *262*, 550–553.

Mannel T., Bentley M. S., Boakes P. D., Jeszenszky H., Ehrenfreund P., Engrand C., Koeberl C., Levasseur-Regourd A. C., Romstedt J., Schmied R., Torkar K., and Weber I. (2019) *Dust of comet 67P/Churyumov-Gerasimenko collected by Rosetta/MIDAS: classification and extension to the nanometer scale*, *Astron. Astrophys.*, *630*, A26.

Mannel T., Bentley M. S., Schmied R., Jeszenszky H., Levasseur-Regourd A. C., Romstedt J., and Torkar K. (2016) *Fractal cometary dust – a window into the early solar system*, *Monthly Notices of the Royal Astronomical Society*, *462*, S304–S311.

Matrajt G., Guan Y., Leshin L., Taylor S., Genge M., Joswiak D., and Brownlee D. E. (2005) in *Workshop on Dust in Planetary Systems*, p. abstract 4060, Kauai, Hawaii.

Matrajt G., Ito M., Wirick S., Messenger S., Brownlee D. E., Joswiak D., Flynn G., Sandford S., Snead C., and Westphal A. (2008) *Carbon investigation of two Stardust particles: A TEM, NanoSIMS, and XANES study*, *Meteoritics and Planetary Science*, *43*, 315–334.

Matrajt G., Messenger S., Brownlee D., and Joswiak D. (2012) *Diverse forms of primordial organic matter identified in interplanetary dust particles*, *Meteoritics and Planetary Science*, *47*, 525–549.

Matrajt G., Messenger S., Joswiak D., and Brownlee D. (2013) *Textures and isotopic compositions of carbonaceous materials in a and b-type stardust tracks: Track 130 (bidi), track 141 (coki) and track 80 (tule)*, *Geochimica et Cosmochimica Acta*, *117*, 65–79.

Matrajt G., Muñoz Caro G. M., Dartois E., D'Hendecourt L., Deboffle D., and Borg J. (2005) *FTIR analysis of the organics in IDPs: Comparison with the IR spectra of the diffuse interstellar medium*, *Astron. Astrophys.*, *433*, 979–995.

Matzel J. E. P., Ishii H. A., Joswiak D., Hutcheon I. D., Bradley J. P., Brownlee D., Weber P. K., Teslich N., Matrajt G., McKeegan K. D., and MacPherson G. J. (2010) *Constraints on the formation age of cometary material from the NASA Stardust mission*, *Science*, *328*, 483–486.

Maurette M. (2006) *Micrometeorites and the mysteries of our origins*, Advances in Astrobiology and Biogeophysics, Springer, Berlin Heidelberg New York.

Maurette M., Engrand C., Brack A., Kurat G., Leach S., and Perreau M. (1995) *Carbonaceous phases in antarctic micrometeorites and their mineralogical environment. their contribution to the possible role of micrometeorites as "chondritic chemical reactors" in atmospheres, waters and/or ices*, *Lunar and Planetary Science Conference*, *XXVI*, 913–914.

Maurette M., Hammer C., Brownlee D. E., Reeh N., and Thomsen H. H. (1986) *Placers of cosmic dust in the blue ice lakes of Greenland*, *Science*, *233*, 869–872.

Maurette M., Jéhano C., Robin E., and Hammer C. (1987) *Characteristics and mass distribution of extraterrestrial dust from the Greenland ice cap*, *Nature*, *328*, 699–702.

Maurette M., Olinger C., Michel-Levy M. C., Kurat G., Pourchet M., Brandstatter F., and Bourot-Denise M. (1991) *A collection of diverse micrometeorites recovered from 100 tonnes of Antarctic blue ice*, *Nature*, *351*, 44–47.

McDonnell J. A. M., Alexander W. M., Burton W. M., Bussoletti E., Clark D. H., Grard J. L., Gruen E., Hanner M. S., Sekanina Z., and Hughes D. W. (1986) *Dust density and mass distribution near comet Halley from Giotto observations*, *Nature*, *326*, 338–341.

McDonnell J. A. M., Alexander W. M., Burton W. M., Bussoletti E., Evans G. C., Evans S. T., Firth J. G., Grard R. J. L., Green S. F., and Grun E. (1987) in *Exploration of Halley's Comet*, pp. 719–741, Springer.

McDonnell J. a. M., McBride N., Beard R., Bussoletti E., Colangeli L., Eberhardt P., Firth J. G., Grard R., Green S. F., Greenberg J. M., Grün E., Hughes D. W., Keller H. U., Kissel J., Lindblad B. A., Mandeville J.-C., Perry C. H., Rembor K., Rickman H., Schwehm G. H., Turner R. F., Wallis M. K., and Zarnecki J. C. (1993) *Dust particle impacts during the Giotto encounter with comet Grigg–Skjellerup*, *Nature*, *362*, 732–734.

McKeegan K. D. (1987) *Ion microprobe measurements of H, C, O, Mg and Si isotopic abundances in individual interplanetary dust particles*, Ph.d. thesis, Washington Univ., St. Louis.

McKeegan K. D., Aléon J., Bradley J., Brownlee D., Busemann H., Butterworth A., Chaussidon M., Fallon S., Floss C., Gilmour J., Gounelle M., Graham G., Guan Y., Heck P. R., Hoppe P., Hutcheon I. D., Huth J., Ishii H., Ito M., Jacobsen S. B., Kearsley A., Leshin L. A., Liu M.-C., Lyon I., Marhas K., Marty B., Matrajt G., Meibom A., Messenger S., Mostefaoui S., Mukhopadhyay S., Nakamura-Messenger K., Nittler L., Palma R., Pepin R. O., Papanastassiou D. A., Robert F., Schlutter D., Snead C. J., Stadermann F. J., Stroud R., Tsou P., Westphal A., Young E. D., Ziegler K., Zimmermann L., and Zinner E. (2006) *Isotopic compositions of cometary matter returned by Stardust*, *Science*, *314*, 1724–1728.

McKeegan K. D., Walker R. M., and Zinner E. (1985) *Ion microprobe isotopic measurements of individual interplanetary dust particles*, *Geochimica et Cosmochimica Acta*, *49*, 1971–1987.

Meisner T., Wurm G., and Teiser J. (2012) *Experiments on centimeter-sized dust aggregates and their implications for planetesimal formation*, *Astronomy & Astrophysics*, *544*, A138.

Mendis D. A. and Horányi M. (2013) *Dusty Plasma Effects in Comets: Expectations for Rosetta*, *Reviews of Geophysics*, *51*, 53–75.

Merouane S., Djouadi Z., and Le Sergeant d'Hendecourt L. (2014) *Relations between Aliphatics and Silicate Components in 12 Stratospheric Particles Deduced from Vibrational Spectroscopy*, *The Astrophysical Journal*, *780*, 174.

Merouane S., Stenzel O., Hilchenbach M., Schulz R., Altobelli N., Fischer H., Hornung K., Kissel J., Langevin Y., Mellado E., Rynö J., and Zaprudin B. (2017) *Evolution of the physical properties of dust and cometary dust activity from 67P/Churyumov–Gerasimenko measured in situ by Rosetta/COSIMA*, *Monthly Notices of the Royal Astronomical Society*, *469*, S459–S474.

Merouane S., Zaprudin B., Stenzel O., Langevin Y., Altobelli N., Della Corte V., Fischer H., Fulle M., Hornung K., Silén J., Ligier N., Rotundi A., Ryno J., Schulz R., Hilchenbach M., Kissel J., and Cosima Team (2016) *Dust particle flux and size distribution in the coma of 67P/Churyumov-Gerasimenko measured in situ by the COSIMA instrument on board Rosetta*, *Astron. Astrophys.*, *596*, A87.

Messenger S. (2000) *Identification of molecular-cloud material in interplanetary dust particles*, *Nature*, *404*, 968–971.

Messenger S., Stadermann F. J., Floss C., Nittler L. R., and Mukhopadhyay S. (2003) *Isotopic signatures of presolar materials in interplanetary dust*, *Space Science Reviews*, *106*, 155–172.

Mikouchi T., Tachikawa O., Hagiya K., Ohsumi K., Suzuki Y., Uesugi K., Takeuchi A., and Zolensky M. E. (2007) *Mineralogy and Crystallography of Comet 81P/Wild 2 Particles*, *Lunar and Planetary Science Conference*, p. 1946.

Min M. (2005) *Optical properties of circumstellar and cometary grains*, Ph.D. thesis, FNWI: Sterrenkundig Instituut Anton Pannekoek, Postbus 19268, 1000 GG Amsterdam, The Netherlands.

Moreels G., Clairemidi J., Hermine P., Brechignac P., and Rousselot P. (1994) *Detection of a polycyclic aromatic molecule in comet P/Halley*, *Astronomy and Astrophysics*, *282*, 643–656.

Moreno F., Muñoz O., Vilaplana R., and Molina A. (2003) *Irregular Particles in Comet C/1995 O1 Hale-Bopp Inferred from its Mid-Infrared Spectrum*, *Astrophys. J.*, *595*, 522–530.

Moreno F., Muñoz O., Gutiérrez P. J., Lara L. M., Snodgrass C., Lin Z. Y., Della Corte V., Rotundi A., and Yagi M. (2017) *The dust environment of comet 67P/Churyumov–Gerasimenko: Results from Monte Carlo dust tail modelling applied to a large ground-based observation data set*, *Monthly Notices of the Royal Astronomical Society*, *469*, S186–S194.

Mukai T., Mukai S., and Kikuchi S. (1988) in *Exploration of Halley's Comet* (M. Grewing, F. Praderie, and R. Reinhard, eds.), pp. 650–652, Springer, Berlin, Heidelberg.

Muñoz Caro G. M., Matrajt G., Dartois E., Nuevo M., D'Hendecourt L., Deboffle D., Montagnac G., Chauvin N., Boukari C., and Le Du D. (2006) *Nature and evolution of the dominant carbonaceous matter in interplanetary dust particles: effects of irradiation and identification with a type of amorphous carbon*, *Astronomy and Astrophysics*, *459*, 147–159.

Nakamura T., Noguchi T., Ozono Y., Osawa T., and Nagao K. (2005) *Mineralogy of ultracarbonaceous large micrometeorites*, *Meteoritics and Planetary Science*, *40 Suppl*, #5046.

Nakamura T., Noguchi T., Tsuchiyama A., Ushikubo T., Kita N. T., Valley J. W., Zolensky M. E., Kakazu Y., Sakamoto K., Mashio E., Uesugi K., and Nakano T. (2008) *Chondrule-like objects in short-period comet 81p/wild 2*, *Science*, *321*, 1664–1667.

Nakamura-Messenger K., Clemett S. J., Messenger S., and Keller L. P. (2011) *Experimental aqueous alteration of cometary dust*, *Meteoritics and Planetary Science*, *46*, 843–856.

Nakamura-Messenger K., Keller L. P., Clemett S. J., Messenger S., and Ito M. (2011) *Nanometer-scale anatomy of entire Stardust tracks*, *Meteoritics and Planetary Science*, *46*, 1033–1051.

Nakamura-Messenger K., Keller L. P., Messenger S., Clemett S. J., Nguyen A. N., and Frank D. (2012) *Coordinated Analyses of Diverse Components in Whole Stardust Cometary Tracks*, *Lunar and Planetary Science Conference*, *43*, 2551.

Nakashima D., Ushikubo T., Joswiak D. J., Brownlee D. E., Matrajt G., Weisberg M. K., Zolensky M. E., and Kita N. T. (2012a) *Oxygen isotopes in crystalline silicates of comet wild 2: A comparison of oxygen isotope systematics between wild 2 particles and chondritic materials*, *Earth and Planetary Science Letters*, *357–358*, 355–365.

Nakashima D., Ushikubo T., Kita N. T., Weisberg M. K., Zolensky M. E., and Ebel D. S. (2015) *Late formation of a comet Wild 2 crystalline silicate particle, Pyxie, inferred from Al–Mg chronology of plagioclase*, *Earth and Planetary Science Letters*, *410*, 54–61.

Nakashima D., Ushikubo T., Zolensky M. E., and Kita N. T. (2012b) *High precision oxygen three-isotope analyses of anhydrous chondritic interplanetary dust particles*, *Meteoritics and Planetary Science*, *47*, 197–208.

Nguyen A. N., Berger E. L., Nakamura-Messenger K., Messenger S., and Keller L. P. (2017) *Coordinated mineralogical and isotopic analyses of a cosmic symplectite discovered in a comet 81P/Wild 2 sample*, *Meteoritics and Planetary Science*, *52*, 2004–2016.

Nguyen A. N., Brownlee D. E., and Joswiak D. J. (2020) *High presolar silicate abundance in giant cluster IDP U2-20GCA of probable cometary origin*.

Nguyen A. N., Stadermann F. J., Zinner E., Stroud R. M., Alexander C. M. O., and Nittler L. R. (2007) *Characterization of presolar silicate and oxide grains in primitive carbonaceous chondrites*, *The Astrophysical Journal*, *656*, 1223.

Nier A. O. and Schlutter D. J. (1993) *The thermal history of interplanetry dust particles collected in the earth's stratosphere*, *Meteoritics*, *28*, 675–681.

Nittler L. R. and Alexander C. M. (2003) *Automated isotopic measurements of micron-sized dust: application to meteoritic presolar silicon carbide*, *Geochimica et Cosmochimica Acta*, *67*, 4961–4980, a Special Issue Dedicated to Robert M Walker.

Nittler L. R., Stroud R. M., Trigo-Rodríguez J. M., De Gregorio B. T., Alexander C. M. O., Davidson J., Moyano-Cambero C. E., and Tanbakouei S. (2019) *A cometary building block in a primitive asteroidal meteorite*, *Nature Astronomy*.

Noguchi T., Ohashi N., Tsujimoto S., Mitsunari T., Bradley J. P., Nakamura T., Toh S., Stephan T., Iwata N., and Imae N. (2015) *Cometary dust in antarctic ice and snow: Past and present chondritic porous micrometeorites preserved on the earth's surface*, *Earth and Planetary Science Letters*, *410*, 1–11.

Ogliore R. C., Butterworth A., Gainsforth Z., Huss G. R., Nagashima K., Stodolna J., and Westphal A. J. (2012a) *Sulfur Isotope Measurements of a Stardust Fragment*, *Lunar and Planetary Science Conference*, *43*, 1670.

Ogliore R. C., Huss G. R., Nagashima K., Butterworth A. L., Gainsforth Z., Stodolna J., Westphal A. J., Joswiak D., and Tyliszczak T. (2012b) *Incorporation of a Late-forming Chondrule into Comet Wild 2*, *Astrophys. J. Lett.*, *745*, L19.

Ogliore R. C., Nagashima K., Huss G. R., Westphal A. J., Gainsforth Z., and Butterworth A. L. (2015) *Oxygen isotopic composition of coarse- and fine-grained material from comet 81P/Wild 2*, *Geochimica et Cosmochimica Acta*, *166*, 74–91.

Ootsubo T., Kawakita H., Shinnaka Y., Watanabe J.-i., and Honda M. (2020) *Unidentified infrared emission features in mid-infrared spectrum of comet 21P/Giacobini-Zinner*, *Icarus*, *338*, 113450.

Ott T., Drolshagen E., Koschny D., Güttler C., Tubiana C., Frattin E., Agarwal J., Sierks H., Bertini I., and Barbieri C. (2017) *Dust mass distribution around comet 67P/Churyumov–Gerasimenko determined via parallax measurements using Rosetta's OSIRIS cameras*, *Monthly Notices of the Royal Astronomical Society*, *469*, S276–S284.

Pajola M., Lucchetti A., Fulle M., Mottola S., Hamm M., Da Deppo V., Penasa L., Kovacs G., Massironi M., Shi X., Tubiana C., Güttler C., Oklay N., Vincent J. B., Toth I., Davidsson B., Naletto G., Sierks H., Barbieri C., Lamy P. L., Rodrigo R., Koschny D., Rickman H., Keller H. U., Agarwal J., A'Hearn M. F., Barucci M. A., Bertaux J. L., Bertini I., Cremonese G., Debei S., De Cecco M., Deller J., El Maarry M. R., Fornasier S., Frattin E., Gicquel A., Groussin O., Gutierrez P. J., Höfner S., Hofmann M., Hviid S. F., Ip W. H., Jorda L., Knollenberg J., Kramm J. R., Kührt E., Küppers M., Lara L. M., Lazzarin M., Moreno J. J. L., Marzari F., Michalik H., Preusker F., Scholten F., and Thomas N. (2017) *The pebbles/boulders size distributions on Sais: Rosetta's final landing site on comet 67P/Churyumov–Gerasimenko*, *Monthly Notices of the Royal Astronomical Society*, *469*, S636–S645.

Palma R. L., Pepin R. O., and Schlutter D. (2005) *Helium and Neon Isotopic Compositions from IDPs of Potentially Cometary Origin*, *Meteoritics and Planetary Science Supplement*, *40*, 5012.

Paquette J. A., Engrand C., Hilchenbach M., Fray N., Stenzel O. J., Silen J., Rynö J., Kissel J., and Team T. C. (2018) *The oxygen isotopic composition ($^{18}O/^{16}O$) in the dust of comet 67P/Churyumov-Gerasimenko measured by COSIMA on-board Rosetta*, *Monthly Notices of the Royal Astronomical Society*, *477*, 3836–3844.

Paquette J. A., Fray N., Bardyn A., Engrand C., Alexander C. M. O., Siljeström S., Cottin H., Merouane S., Isnard R., Stenzel O. J., Fischer H., Rynö J., Kissel J., and Hilchenbach M. (2021) *D/H in the refractory organics of comet 67P/Churyumov-Gerasimenko measured by Rosetta/COSIMA*, *Monthly Notices of the Royal Astronomical Society*, *504*, 4940–4951.

Paquette J. A., Hornung K., Stenzel O. J., Rynö J., Silen J., Kissel J., Hilchenbach M., and (2017) *The 34S/32S isotopic ratio measured in the dust of comet 67P/Churyumov–Gerasimenko by Rosetta/COSIMA*, *Monthly Notices of the Royal Astronomical Society*, *469*, S230–S237.

Poch O., Istiqomah I., Quirico E., Beck P., Schmitt B., Theulé P., Faure A., Hily-Blant P., Bonal L., Raponi A., Ciarniello M., Rousseau B., Potin S., Brissaud O., Flandinet L., Filacchione G., Pommerol A., Thomas N., Kappel D., Mennella V., Moroz L., Vinogradoff V., Arnold G., Erard S., Bockelée-Morvan D., Leyrat C., Capaccioni F., De Sanctis M. C., Longobardo A., Mancarella F., Palomba E., and Tosi F. (2020) *Ammonium salts are a reservoir of nitrogen on a cometary nucleus and possibly on some asteroids*, *Science*, *367*, aaw7462.

Pollack J. B., Hollenbach D., Beckwith S., Simonelli D. P., Roush T., and Fong W. (1994) *Composition and Radiative Properties of Grains in Molecular Clouds and Accretion Disks*, *The Astrophysical Journal*, *421*, 615.

Price M. C., Kearsley A. T., Burchell M. J., Hörz F., Borg J., Bridges J. C., Cole M. J., Floss C., Graham G., Green S. F., Hoppe P., Leroux H., Marhas K. K., Park N., Stroud R., Stadermann F. J., Telisch N., and Wozniakiewicz P. J. (2010) *Comet 81P/Wild 2: The size distribution of finer (sub-10 um) dust collected by the Stardust spacecraft*, *Meteoritics and Planetary Science*, *45*, 1409–1428.

Quirico E., Borg J., Raynal P.-I., Montagnac G., and D'Hendecourt L. (2005) *A micro-Raman survey of 10 IDPs and 6 carbonaceous chondrites*, *Planetary and Space Science*, *53*, 1443–1448.

Quirico E., Moroz L. V., Schmitt B., Arnold G., Faure M., Beck P., Bonal L., Ciarniello M., Capaccioni F., Filacchione G., Erard S., Leyrat C., Bockelée-Morvan D., Zinzi A., Palomba E., Drossart P., Tosi F., Capria M. T., De Sanctis M. C., Raponi A., Fonti S., Mancarella F., Orofino V., Barucci A., Blecka M. I., Carlson R., Despan D., Faure A., Fornasier S., Gudipati M. S., Longobardo A., Markus K., Mennella V., Merlin F., Piccioni G., Rousseau B., and Taylor F. (2016) *Refractory and semi-volatile organics at the surface of comet 67P/Churyumov-Gerasimenko: Insights from the VIRTIS/Rosetta imaging spectrometer*, *Icarus*, *272*, 32–47.

Reach W. T., Vaubaillon J., Lisse C. M., Holloway M., and Rho J. (2010) *Explosion of Comet 17P/Holmes as revealed by the Spitzer Space Telescope*, *Icarus*, *208*, 276–292.

Rietmeijer F. J. M. (1998) in *Planetary Materials* (J. J. Papike, ed.), vol. 36 of *Reviews in mineralogy*, pp. 2/1–2/95, Mineralogical Society of America, Washington DC.

Rinaldi G., Bockelée-Morvan D., Ciarniello M., Tozzi G. P., Capaccioni F., Ivanovski S. L., Filacchione G., Fink U., Doose L., Taylor F., Kappel D., Erard S., Leyrat C., Raponi A., D'Aversa E., Capria M. T., Longobardo A., Palomba E., Tosi F., Migliorini A., Rotundi A., Della Corte V., and Salatti M. (2018) *Summer outbursts in the coma of comet 67P/Churyumov-Gerasimenko as observed by Rosetta-VIRTIS*, *Mon. Not. R. Astron. Soc.*, *481*, 1235–1250.

Rinaldi G., Della Corte V., Fulle M., Capaccioni F., Rotundi A., Ivanovski S. L., Bockelée-Morvan D., Filacchione G., D'Aversa E., Capria M. T., Tozzi G. P., Erard S., Leyrat C., Palomba E., Longobardo A., Ciarniello M., Taylor F., Mottola S., and Salatti M. (2017) *Cometary coma dust size distribution from in situ IR spectra*, *Monthly Notices of the Royal Astronomical Society*, *469*, S598–S605.

Rojas J., Duprat J., Engrand C., Dartois E., Delauche L., Godard M., Gounelle M., Carrillo-Sánchez J., Pokorný P., and Plane J. (2021) *The micrometeorite flux at dome c (antarctica), monitoring the accretion of extraterrestrial dust on earth*, *Earth and Planetary Science Letters*, *560*, 116794.

Rojas J., Duprat J., Nittler L. R., Dartois E., Engrand C., Bardin N., Guerin B., Delauche L., Mostefaoui S., Remusat L., Stroud R. M., and Wu T.-D. (2022) *Probing the isotopic composition of cometary organic matter with ultracarbonaceous Antarctic micrometeorites : a NanoSIMS study*, *Lunar and Planetary Science Conference*, p. #1852.

Rosenbush V. K., Ivanova O. V., Kiselev N. N., Kolokolova L. O., and Afanasiev V. L. (2017) *Spatial variations of brightness, colour and polarization of dust in comet 67P/Churyumov–Gerasimenko*, *Monthly Notices of the Royal Astronomical Society*, *469*, S475–S491.

Rotundi A., Sierks H., Corte V. D., Fulle M., Gutierrez P. J., Lara L., Barbieri C., Lamy P. L., Rodrigo R., Koschny D., Rickman H., Keller H. U., López-Moreno J. J., Accolla M., Agarwal J., A'Hearn M. F., Altobelli N., Angrilli F., Barucci M. A., Bertaux J.-L., Bertini I., Bodewits D., Bussoletti E., Colangeli L., Cosi M., Cremonese G., Crifo J.-F., Deppo V. D., Davidsson B., Debei S., Cecco M. D., Esposito F., Ferrari M., Fornasier S., Giovane F., Gustafson B., Green S. F., Groussin O., Grün E., Güttler C., Herranz M. L., Hviid S. F., Ip W., Ivanovski S., Jerónimo J. M., Jorda L., Knollenberg J., Kramm R., Kührt E., Küppers M., Lazzarin M., Leese M. R., López-Jiménez A. C., Lucarelli F., Lowry S. C., Marzari F., Epifani E. M., McDonnell J. A. M., Mennella V., Michalik H., Molina A., Morales R., Moreno F., Mottola S., Naletto G., Oklay N., Ortiz J. L., Palomba E., Palumbo P., Perrin J.-M., Rodríguez J., Sabau L., Snodgrass C., Sordini R., Thomas N., Tubiana C., Vincent J.-B., Weissman P., Wenzel K.-P., Zakharov V., and Zarnecki J. C. (2015) *Dust measurements in the coma of comet 67P/Churyumov-Gerasimenko inbound to the Sun*, *Science*.

Rousseau B., Érard S., Beck P., Quirico É., Schmitt B., Brissaud O., Montes-Hernandez G., Capaccioni F., Filacchione G., Bockelée-Morvan D., Leyrat C., Ciarniello M., Raponi A., Kappel D., Arnold G., Moroz L. V., Palomba E., Tosi F., and Virtis Team (2018) *Laboratory simulations of the Vis-NIR spectra of comet 67P using sub-μm sized cosmochemical analogues*, *Icarus*, *306*, 306–318.

Rubin, M., Altwegg, K., Balsiger, H., Berthelier, J.-J., Bieler, A., Calmonte, U., Combi, M., De Keyser, J., Engrand, C., Fiethe, B., Fuselier, S. A., Gasc, S., Gombosi, T. I., Hansen, K. C., Hässig, M., Le Roy, L., Mezger, K., Tzou, C.-Y., Wampfler, S. F., and Wurz, P. (2017) *Evidence for depletion of heavy silicon isotopes at comet 67P/Churyumov-Gerasimenko*, *601*, A123.

Sandford S. A., Bajt S., Clemett S. J., Cody G. D., Cooper G., Degregorio B. T., de Vera V., Dworkin J. P., Elsila J. E., Flynn G. J., Glavin D. P., Lanzirotti A., Limero T., Martin M. P., Snead C. J., Spencer M. K., Stephan T., Westphal A., Wirick S., Zare R. N., and Zolensky M. E. (2010) *Assessment and control of organic and other contaminants associated with the Stardust sample return from comet 81P/Wild 2*, *Meteoritics and Planetary Science*, *45*, 406–433.

Schulze H., Kissel J., and Jessberger E. K. (1997) in *From Stardust to Planetesimals* (Y. J. Pendleton, ed.), vol. 122 of *Astronomical Society of the Pacific Conference Series*, p. 397.

Simon S. B., Joswiak D. J., Ishii H. A., Bradley J. P., Chi M., Grossman L., Aléon J., Brownlee D. E., Fallon S., Hutcheon I. D., Matrajt G., and McKeegan K. D. (2008) *A refractory inclusion returned by stardust from comet 81p/wild 2*, *Meteoritics and Planetary Science*, *43*, 1861–1877.

Stadermann F. J., Hoppe P., Floss C., Heck P. R., Horz F., Huth J., Kearsley A. T., Leitner J., Marhas K. K., McKeegan K. D., and Stephan T. (2008) *Stardust in stardust - the c, n, and o isotopic compositions of wild 2 cometary matter in al foil impacts*, *Meteoritics and Planetary Science*, *43*, 299–313.

Starkey N. A., Franchi I. A., and Alexander C. M. O. (2013) *A raman spectroscopic study of organic matter in interplanetary dust particles and meteorites using multiple wavelength laser excitation*, *Meteoritics and Planetary Science*, *48*, 1800–1822.

Stephan T. (2008) *Assessing the elemental composition of comet 81P/Wild 2 by analyzing dust collected by Stardust*, *Space Science Reviews*, *138*, 247–258.

Stephan T., Bose M., Boujibar A., Davis A., Dory C., Gyngard F., Hoppe P., Hynes K., Liu N., Nittler L. et al. (2020) *The presolar grain database reloaded-silicon carbide*, *Lunar and Planetary Science Conference*, p. 2140.

Stephan T., Rost D., Vicenzi E. P., Bullock E. S., Macpherson G. J., Westphal A. J., Snead C. J., Flynn G. J., Sandford S. A., and Zolensky M. E. (2008) *TOF-SIMS analysis of cometary matter in Stardust aerogel tracks*, *Meteoritics and Planetary Science*, *43*, 233–246.

Steyer T. R. (1974) *Infrared Optical Properties of Some Solids of Possible Interest in Astronomy and Atmospheric Physics.*, Ph.D. thesis, The University of Arizona.

Storrs A. D., Cochran A. L., and Barker E. S. (1992) *Spectrophotometry of the continuum in 18 comets*, *Icarus*, *98*, 163–178.

Sugita S., Ootsubo T., Kadono T., Honda M., Sako S., Miyata T., Sakon I., Yamashita T., Kawakita H., Fujiwara H., Fujiyoshi T., Takato N., Fuse T., Watanabe J., Furusho R., Hasegawa S., Kasuga T., Sekiguchi T., Kinoshita D., Meech K. J., Wooden D. H., Ip W. H., and A'Hearn M. F. (2005) *Subaru Telescope Observations of Deep Impact*, *Science*, *310*, 274–278.

Tamanai A., Alexander D. R., Ferguson J. W., and Sedlmayr E. (2003) in *Stellar Atmosphere Modeling* (I. Hubeny, D. Mihalas, and K. Werner, eds.), vol. 288 of *Astronomical Society of the Pacific Conference Series*, p. 365.

Tamanai A., Mutschke H., Blum J., Posch T., Koike C., and Ferguson J. W. (2009) *Morphological effects on IR band profiles. Experimental spectroscopic analysis with application to observed spectra of oxygen-rich AGB stars*, *Astron. Astrophys.*, *501*, 251–267.

Tazaki R., Tanaka H., Okuzumi S., Kataoka A., and Nomura H. (2016) *Light Scattering by Fractal Dust Aggregates. I. Angular Dependence of Scattering*, *Astrophys. J.*, *823*, 70.

Thomas K. L., Blanford G. E., Keller L. P., Klock W., and McKay D. S. (1993) *Carbon abundance and silicate mineralogy of anhydrous interplanetary dust particles*, *Geochim. Cosmochim. Acta*, *57*, 1551–1566.

Tokunaga A. T., Golisch W. F., Griep D. M., Kaminski C. D., and Hanner M. S. (1986) *The NASA infrared telescope facility comet Halley monitoring program. I. Preperihelion results.*, *Astron. J.*, *92*, 1183–1190.

Toppani A., Robert F., Libourel G., de Donato P., Barres O., D'Hendecourt L., and Ghanbaja J. (2005) *A 'dry' condensation origin for circumstellar carbonates*, *Nature*, *437*, 1121–1124.

Tozzi G. P., Lara L. M., Kolokolova L., Boehnhardt H., Licandro J., and Schulz R. (2004) *Sublimating components in the coma of comet C/2000 WM*$_1$ *(LINEAR)*, *Astron. Astrophys.*, *424*, 325–330.

Tozzi G.-P., Rinaldi G., Fink U., Doose L., Capaccioni F., Filacchione G., Bockelée-Morvan D., Erard S., Leyrat C., Arnold G., Blecka M., Capria M. T., Ciarniello M., Combi M., Faggi S., Irwin P., Migliorini A., Paolomba E., Piccioni G., and Tosi F. (2015) in *AAS/Division for Planetary Sciences Meeting Abstracts*, vol. 47 of *AAS/Division for Planetary Sciences Meeting Abstracts*, p. 503.07.

Trigo-Rodriguez J. M., Dominguez G., Burchell M. J., Hoerz F., and Llorca J. (2008) *Bulbous tracks arising from hypervelocity capture in aerogel*, *Meteoritics and Planetary Science*, *43*, 75–86.

Trigo-Rodríguez J. M. and Llorca J. (2006) *The strength of cometary meteoroids: Clues to the structure and evolution of comets*, *Monthly Notices of the Royal Astronomical Society*, *372*, 655–660.

Tuzzolino A. J., Economou T. E., Clark B. C., Tsou P., Brownlee D. E., Green S. F., McDonnell J. A. M., McBride N., and Colwell M. T. S. H. (2004) *Dust measurements in the coma of comet 81P/Wild 2 by the dust flux monitor instrument*, *Science*, *304*, 1776–1780.

Villalon K. L., Ishii H. A., Bradley J. P., Stephan T., and Davis A. M. (2016) in *Lunar and Planetary Science Conference*, vol. 47 of *Lunar and Planetary Science Conference*, p. 1796.

Warren J. L. and Zolensky M. E. (1994) in *Analysis of Interplanetary Dust, AIP Conf. Proc.* (M. Zolensky, T. Wilson, F. Rietmeijer, and G. J. Flynn, eds.), vol. 310, pp. 245–253, Amer. Inst. Physics Press, New York.

Westphal A. J., Bridges J. C., Brownlee D. E., Butterworth A. L., De Gregorio B. T., Dominguez G., Flynn G. J., Gainsforth Z., Ishii H. A., Joswiak D., Nittler L. R., Ogliore R. C., Palma R., Pepin R. O., Stephan T., and Zolensky M. E. (2017) *The future of Stardust science*, *Meteoritics and Planetary Science*, *52*, 1859–1898.

Wirick S., Flynn G. J., Keller L. P., Nakamura-Messenger K., Peltzer C., Jacobsen C., Sand ford S. A., and Zolensky M. E. (2009) *Organic matter from comet 81P/Wild 2, IDPs, and carbonaceous meteorites; similarities and differences*, *Meteoritics and Planetary Science*, *44*, 1611–1626.

Wooden D. H. (2002) *Comet Grains: Their IR Emission and Their Relation to ISm Grains*, *Earth Moon and Planets*, *89*, 247–287.

Wooden D. H., Butner H. M., Harker D. E., and Woodward C. E. (2000) *Mg-Rich Silicate Crystals in Comet Hale-Bopp: ISM Relics or Solar Nebula Condensates?*, *Icarus*, *143*, 126–137.

Wooden D. H., Harker D. E., Woodward C. E., Butner H. M., Koike C., Witteborn F. C., and McMurtry C. W. (1999) *Silicate Mineralogy of the Dust in the Inner Coma of Comet C/1995 01 (Hale-Bopp) Pre- and Postperihelion*, *Astrophys. J.*, *517*, 1034–1058.

Wooden D. H., Ishii H. A., and Zolensky M. E. (2017) *Cometary dust: the diversity of primitive refractory grains*, *Philosophical Transactions of the Royal Society of London A: Mathematical, Physical and Engineering Sciences*, *375*, 20160260.

Wooden D. H., Woodward C. E., and Harker D. E. (2004) *Discovery of crystalline silicates in comet c/2001 q4 (neat)*, *The Astrophysical Journal Letters*, *612*, L77–L80.

Wooden D. H., Woodward C. E., Harker D. E., and Kelley M. S. P. (2021) *Cometary Particles with Amorphous Carbon: A Large Carbon Reservoir and Aggregate Particles' Optical Properties Computed with DDSCAT*, *Lunar and Planetary Science Conference*, *52*, 2694.

Wooden D. H., Woodward C. E., Kelley M. S., Harker D. E., Geballe T. R., and Li A. (2011) in *EPSC-DPS Joint Meeting 2011*, vol. 2011, p. 1557.

Woodward C. E., Kelley M. S. P., Harker D. E., Ryan E. L., Wooden D. H., Sitko M. L., Russell R. W., Reach W. T., de Pater I., Kolokolova L., and Gehrz R. D. (2015) *SOFIA Infrared Spectrophotometry of Comet C/2012 K1 (Pan-STARRS)*, *Astrophys. J.*, *809*, 181.

Woodward C. E., Wooden D. H., Harker D. E., Kelley M. S. P., Russell R. W., and Kim D. L. (2021) *The Coma Dust of Comet C/2013 US_{10} (Catalina): A Window into Carbon in the Solar System*, *Planetary Science Journal*, *2*, 25.

Wozniakiewicz P. J., Ishii H. A., Kearsley A. T., Bradley J. P., Price M. C., Burchell M. J., Teslich N., and Cole M. J. (2015) *The survivability of phyllosilicates and carbonates impacting stardust al foils: Facilitating the search for cometary water*, *Meteoritics and Planetary Science*, *50*, 2003–2023.

Xing Z. and Hanner M. S. (1997) *Light scattering by aggregate particles.*, *Astron. Astrophys.*, *324*, 805–820.

Yabuta H., Noguchi T., Itoh S., Nakamura T., Miyake A., Tsujimoto S., Ohashi N., Sakamoto N., Hashiguchi M., ichi Abe K., Okubo A., Kilcoyne A. D., Tachibana S., Okazaki R., Terada K., Ebihara M., and Nagahara H. (2017) *Formation of an ultracarbonaceous Antarctic micrometeorite through minimal aqueous alteration in a small porous icy body*, *Geochimica et Cosmochimica Acta*, *214*, 172 – 190.

Zhang M., Defouilloy C., Joswiak D. J., Brownlee D. E., Nakashima D., Siron G., Kitajima K., and Kita N. T. (2021) *Oxygen isotope systematics of crystalline silicates in a giant cluster idp: A genetic link to wild 2 particles and primitive chondrite chondrules*, *Earth and Planetary Science Letters*, *564*, 116928.

Zinner E., McKeegan K. D., and Walker R. M. (1983) *Laboratory measurements of D/H ratios in interplanetary dust*, *Nature*, *305*, 119–121.

Zolensky M. E. (1987) *Refractory interplanetary dust particles*, *Science*, *237*, 1466–1468.

Zolensky M. E., Hewins R. H., Mittlefehldt D. W., Lindstrom M. M., Xiao X., and Lipschutz M. E. (1992) *Mineralogy, petrology and geochemistry of carbonaceous chondritic clasts in the lew 85300 polymict eucrite*, *Meteoritics*, *27*, 596–604.

Zolensky M. E., Krot A. N., and Benedix G. (2008) *Record of low-temperature alteration in asteroids*, *Reviews in Mineralogy and Geochemistry*, *68*, 429–462.

Zolensky M. E., Nakamura K., Weisberg M. K., Prinz M., Nakamura T., Ohsumi K., Saitow A., Mukai M., and Gounelle M. (2003) *A primitive dark inclusion with radiation-damaged silicates in the ningqiang carbonaceous chondrite*, *Meteoritics and Planetary Science*, *38*, 305–322.

Zolensky M. E., Zega T. J., Yano H., Wirick S., Westphal A. J., Weisberg M. K., Weber I., Warren J. L., Velbel M. A., Tsuchiyama A., Tsou P., Toppani A., Tomioka N., Tomeoka K., Teslich N., Taheri M., Susini J., Stroud R., Stephan T., Stadermann F. J., Snead C. J., Simon S. B., Simionovici A., See T. H., Robert F., Rietmeijer F. J. M., Rao W., Perronnet M. C., Papanastassiou D. A., Okudaira K., Ohsumi K., Ohnishi I., Nakamura-Messenger K., Nakamura T., Mostefaoui S., Mikouchi T., Meibom A., Matrajt G., Marcus M. A., Leroux H., Lemelle L., Le L., Lanzirotti A., Langenhorst F., Krot A. N., Keller L. P., Kearsley A. T., Joswiak D., Jacob D., Ishii H., Harvey R., Hagiya K., Grossman L., Grossman J. N., Graham G. A., Gounelle M., Gillet P., Genge M. J., Flynn G., Ferroir T., Fallon S., Ebel D. S., Dai Z. R., Cordier P., Clark B., Chi M., Butterworth A. L., Brownlee D. E., Bridges J. C., Brennan S., Brearley A., Bradley J. P., Bleuet P., Bland P. A., and Bastien R. (2006) *Mineralogy and petrology of comet 81P/Wild 2 nucleus samples*, *Science*, *314*, 1735–1739.

Zubko E., Shkuratov Y., and Videen G. (2015) *Effect of morphology on light scattering by agglomerates*, *Journal of Quantitative Spectroscopy and Radiative Transfer*, *150*, 42–54.

Zubko E., Videen G., Hines D. C., Shkuratov Y., Kaydash V., Muinonen K., Knight M. M., Sitko M. L., Lisse C. M., Mutchler M., Wooden D. H., Li J.-Y., and Kobayashi H. (2015) *Comet C/2012 S1 (ISON) coma composition at ~4 au from HST observations*, *Planet. Space Sci.*, *118*, 138–163.

This 2-column preprint was prepared with the AAS LaTeX macros v5.2.